QUASI-STATIC CRUSHING BEHAVIOR OF NOMEX® HONEYCOMB FILLED THIN-WALLED ALUMINUM TUBES

A Thesis Submitted to
the Graduate School of Engineering and Sciences of
İzmir Institute of Technology
in Partial Fulfillment of the Requirements for the Degree of

MASTER OF SCIENCE

in Materials Science and Engineering

by
Cem ÇAKIROĞLU

July 2008
İZMİR

We approve the thesis of **Cem ÇAKIROĞLU**

Prof. Dr. Mustafa GÜDEN
Supervisor

Assist. Prof. Dr. Alper TAŞDEMİRCİ
Co-Supervisor

Assist. Prof. Dr. O. Özgür EĞİLMEZ
Committee Member

Assist. Prof. Dr. Ebubekir ATAN
Committee Member

11 July 2008

Date

Prof. Dr. Mustafa GÜDEN
Head of the Materials Science and Engineering Department

Prof. Dr. Hasan BÖKE
Dean of the Graduate School of Engineering and Sciences

ACKNOWLEDGEMENTS

I would like to thank my advisor Prof.Dr. Mustafa Güden, my co-advisor Assist. Prof. Dr. Alper Taşdemirci, Assist.Prof.Dr.O.Özgür Eğilmez and Assist. Prof. Dr. Ebubekir Atan for their patience and guidance. Without their effort this thesis would have never been accomplished. I would like to thank Levent Aktay Çağrı Ergönenç , A.Kaan Toksoy and Sinan Yüksel for their encouragements during the writing session of this thesis.

Also I would like to thank Ceyda Tokel, Serkan Ötleş, Fırat Adıgüzel, Can Ali Güven,Tarık Dikbasan, Deniz Karsu and my family for their never ending support. It was a long road, now comes to an end with this beautiful work. Thank you.

ABSTRACT

QUASI-STATIC CRUSHING BEHAVIOR OF NOMEX® HONEYCOMB FILLED THIN-WALLED ALUMINUM TUBES

The experimental and numerical studies presented in this thesis were focused on the experimental and numerical quasi-static crushing behavior of Nomex® honeycomb filled thin-walled aluminum tubes. Nomex® honeycombs having different cell sizes (3.2, 4.8 and 6.4 mm) and the same density (48 kg/m^3) were used to fill thin walled aluminum tube, 25 mm in diameter and 0.29 mm in thickness. Compression tests were conducted at quasi-static the strain rates of 1.64 10^{-2}, 6.56 10^{-3} and 3.28 10^{-3} s^{-1}. The results showed that the honeycomb cell size had a strong effect on the crushing behavior. Decreasing cell size increased crushing loads and the specific absorbed energy values of empty tubes. The highest strengthening effect of filling was found in 3.2 mm cell size honeycomb filled tubes. Although no effects of 4.8 and 6.4 mm cell-size honeycomb filling on the deformation mode of tube was observed (mixed), 3.2 mm cell size honeycomb filling changed the deformation mode to mixed/concertina. The numerical model of empty tube, 6.4 mm cell size honeycomb and 6.4 mm cell size honeycomb filled tube were performed using LS-DYNA™ and ANSYS™ finite element analysis programs. To acquire maximum computational efficiency, a mesh optimization was done. The effect of the honeycomb cell wall thickness was also investigated numerically and shown to have a strong effect on the crushing behavior of honeycomb. The experimental and numerical studies conducted showed that 3.2 mm cell size Nomex® honeycomb might become an alternative to aluminum foam filler in thin walled tubes as long as the tube crushing load was comparable with honeycomb crushing load.

ÖZET

NOMEX® BALPETEĞİ İLE DOLDURULMUŞ İNCE DUVARLI ALÜMİNYUM TÜPLERİN YARI STATİK EZİLME DAVRANIŞLARI

Bu çalışma Nomex® bal peteği ile doldurulmuş ince duvarlı alüminyum tüplerin yarı statik ezilme davranışlarının nümerik ve deneysel olarak incelenmesini kapsamaktadır. 25 mm çapında ve 0.29 mm kalınlığındaki alüminyum tüpler 3 farklı hücre boyutuna (3,2, 4,8 ve 6,4 mm) ve aynı yoğunluğa sahip (48 kg/m^3) Nomex® bal petekleri ile doldurulmuştur. Basma testleri, 1.64 10^{-2}, 6.56 10^{-3} ve 3.28 10^{-3} s^{-1} yarı statik deformasyon hızlarında gerçekleştirilmiştir. Sonuçlar hücre boyutunun bal peteği ezilme davranışları üzerinde önemli bir etkisi olduğunu ve daha düşük hücre boyutlarında boş tüplerin ezilme yükününün ve spesifik sönümlenen enerji miktarlarının arttığını göstermiştir. En yüksek güçlendirme etkisi 3.2 mm bal peteği ile doldurulmuş tüplerde bulunmuştur. 4.8 ve 6.4 mm hücre boyutundaki bal peteği dolumunun boş tüpün deformasyon modu (karışık deformasyon) üzerinde etkisinin olmadığı ancak 3.2 mm hücre boyutundaki bal peteği dolumunun deformasyon modunu değiştirdiği (karışık/konsertina deformasyon) bulunmuştur. Boş tüp, 6.4 mm hücre boyutundaki bal peteği ve 6.4 mm hücre boyutundaki bal peteği ile doldurulmuş tüplerin nümerik modelleri LS-DYNA™ ve ANSYS™ sonlu eleman analiz programları kullanılarak oluşturulmuştur. Nümerik model eleman sayısı hesaplama verimliliği göz önüne alınarak optimize edilmiştir. Bal peteği hücre duvar kalınlığının etkisi ayrıca nümerik olarak incelenmiş ve bal peteği ezilme davranışları üzerinde önemli bir etkisinin olduğu bulunmuştur. Yapılan deneysel ve nümerik çalışmalar boş tüplerin doldurulmasında, 3.2 mm hücre boyutundaki Nomex® bal peteğinin, tüp ezilme yükünün bal peteği ezilme yükü ile karşılaştırılabileceği durumlarda, alüminyum köpüklere alternatif bir dolgu malzemesi olabileceğini göstermiştir.

TABLE OF CONTENTS

LIST OF FIGURES ix
LIST OF TABLES xiv
NOMENCLATURE xv

CHAPTER 1. INTRODUCTION 1

CHAPTER 2. LITERATURE REVIEW 3

2.1. Honeycombs and Material Properties 3
2.2. The Crushing Behavior of Tubes 4
2.3. Terminologies Used in Crush Analysis 4
2.4. Crushing Behavior of Empty Tubes: Numerical and Experimental Analysis 7
2.5. Crushing Behavior of Foam Filled Tubes 14
2.6. Crushing Behavior of Honeycomb and Honeycomb Filled Tubes 16

CHAPTER 3. MATERIALS & EXPERIMENTAL SECTION 20

3.1. Nomex® Aramid Paper Honeycomb Filler Material 20
3.2. Empty and Nomex® Honeycomb Filled Tubes 23

CHAPTER 4. RESULTS 31

4.1. Compression Behavior of Honeycomb Filler 31
4.2. The Deformation of Honeycomb Filler 34
4.3. The Deformation Behavior of Empty and Nomex® Honeycomb Filled Tubes 38
4.3.1 The Deformation Behavior of Empty Tubes 38
4.3.2 The Deformation Behavior and Mechanism of Honeycomb Filled Tubes 42
4.4. Effect of Honeycomb Filling On the Average Crush Load, Specific Absorbed Energy and Stroke Efficiency 47
4.5. The Interaction Effect 54

CHAPTER 5. NUMERICAL ANALYSIS 57

5.1. Numerical Modeling of Empty Tube, Honeycomb Filler and Honeycomb Filled Tubes 57

5.2. The Mesh Optimization 58

5.2.1 The Mesh Optimization of Empty Tubes 58

5.2.2 The Mesh Optimization of Honeycomb Filler 60

5.2.3 The Mesh Optimization of Honeycomb Filled Tubes 61

5.3. The Comparison between Experimental and Numerical Results 63

5.4. The Effect of Honeycomb Cell Wall Thickness Variation 70

CHAPTER 6. DISCUSSION 73

6.1. The Average Crushing Loads and Deformation Modes of the Empty Tubes 73

6.2. The Average Crushing Loads and Deformation Modes of the Honeycomb and Honeycomb filled tubes 74

6.3. The Strengthening Effect and Specific Absorbed Energy 76

CHAPTER 7. CONCLUSIONS 77

REFERENCES 78

APPENDICES

APPENDIX A. Mean Crushing Load and Strength of Honeycombs……82

APPENDIX B .Mean Crushing Loads of Empty Tubes……83

APPENDIX C. The Mean Crushing Loads of Honeycomb Filled Tubes……88

APPENDIX D. Result Tables……..89

LIST OF FIGURES

Figure ..... **Page**

Figure 2.1. (a) aluminum, (b) aramid paper honeycomb and (c) honeycomb cell structure 3
Figure 2.2. Terminology used in the crush analysis 7
Figure 2.3. The collapse mode of deformation chart of HT30 Al alloys as function of L/D and t/D 8
Figure 2.4. Load-displacement curve of an aluminum deep drawn tube (3003-H14) of 20 mm in outside diameter, 50 mm in length and 0.9 mm in wall thickness 9
Figure 2.5. Alexander's concertina deformation mode model..... 10
Figure 2.6. The Axial crushing model for a cylindrical tube by Gupta and Abbas 12
Figure 2.7. The interaction effect in Al foam filled Al tubes..... 16
Figure 2.8. Effects of number of elements on the stress-strain curves of honeycomb..... 17
Figure 3.1. Nomex® honeycombs cells; cell size (a) 4.8 (b) 3.2 and (c) 6.4 mm 21
Figure 3.2. L and W directions of the honeycomb sheet 21
Figure 3.3. The SHIMADZU AG-I testing machine 23
Figure 3.4. The empty tubes; (a) as-received, (b) after cutting and (c) the cutting apparatus that was used to drill the honeycomb sheets 24
Figure 3.5. (a) Double layer honeycomb and (b) circular double layer honeycomb after drilling 25
Figure 3.6. Filling the empty Al tube with honeycomb filler 25
Figure 3.7. Filled Al tubes 26
Figure 4.1. The compression stress-strain curves of Nomex® honeycomb samples (cell size 4.8 mm, deformed at 1.64×10^{-2} s^{-1}) 31
Figure 4.2. Stress-strain curves of (a) 3.2 and (b) 6.4 mm cell size Nomex® honeycombs 32
Figure 4.3. The typical stress-strain curves of 3.2, 4.8 and 6.4 mm cell size honeycombs 33

Figure 4.4. Deformed 3.2 mm cell size Nomex® honeycomb sample: (a) top and (b) side view 35
Figure 4.5. Deformed 4.8 mm cell size Nomex® honeycomb sample; (a) top and (b) side view 35
Figure 4.6. Deformed 6.4 mm cell size Nomex® honeycomb sample; (a) top and (b) side view 35
Figure 4.7. The load-strain curves of (a) 3.2 (b) 4.8 and (c) 6.4 mm cell size double and single layer honeycomb samples 37
Figure 4.8. Typical load-displacement curve of empty aluminum tube ($1.64x10^{-2}$ s^{-1}) 38
Figure 4.9. Pictures of tube deformation in concertina mode: (a) front, (b) back and (c) side views 39
Figure 4.10. Pictures of tube deformation in mixed mode: (a) front, (b) back and (c) side views 39
Figure 4.11. Pictures of tube deformation in diamond mode: (a) front, (b) back and (c) side views 39
Figure 4.12. The effect of loading rate on load-displacement curve of empty tube 40
Figure 4.13. The load displacement curve for empty tubes compressed at the strain rate of $1.64x10^{-2}(s^{-1})$ 40
Figure 4.14. Load-displacement curves of (a) 3.2 mm (b) 4.8 mm and (c) 6.4 mm cell size honeycomb filled tubes 43
Figure 4.15. Deformed 3.2 mm cell size honeycomb filled tubes (a) top view, (b) cross-section and (c) side view 43
Figure 4.16. Deformed 4.8 mm cell size honeycomb filled tubes (a) top view, (b) cross-section and (c) side view 43
Figure 4.17. Deformed 6.4 mm cell size honeycomb filled tubes (a) top view (b) cross-section and (c) side view 44
Figure 4.18. Typical Load-displacement curves of the honeycomb filled and empty tubes ; (a) 3.2 mm, (b) 4.8 mm and (c) 6.4 mm cell size honeycomb 45

Figure 4.19. The load-displacement curves of filled tubes at different deformation rates (a) 3.2 mm cell size (b) 4.8 mm cell size (c) 6.4 mm cell size honeycomb filled tubes 46
Figure 4.20. Effect of honeycomb filling on the average crushing loads of (a) 3.2, (b) 4.8 and (c) 6.4 mm honeycomb (b) filled tubes ($1.64x10^{-2}$ s^{-1}) 48
Figure 4.21. (a) Pa and (b) P_{max} vs. honeycomb cell size 49
Figure 4.22. SE vs. honeycomb cell size 50
Figure 4.23. The comparison between the SAE's of (a) 3.2 , (b) 4.8 and (c) 6.4 mm honeycomb filled tubes and (b) empty tube ($1.64x10^{-2}$ s^{-1}) 52
Figure 4.24. SAE at stroke efficiency versus honeycomb cell size graphics 52
Figure 4.25. The total efficiency and corresponding stroke efficiency values for the filled tubes (a) 3.2 mm, (b) 4.8 mm and (c)6.4 mm honeycomb filled tubes 53
Figure 4.26. Variation of TE with honeycomb cell size at stroke efficiency 54
Figure 4.27. The interaction effect in (a) 3.2 mm cell size (b) 4,8 mm cell size (c) 6.4 mm cell size honeycomb filled tubes 55
Figure 4.28. Partially compressed honeycombs between tubes (a) 3.2 mm cell size honeycomb filled and (b) 6.4 mm cell size honeycomb filled tube (c) 4.8 mm cell size honeycomb filled tube 56
Figure 5.1. The Numerical and experimental load displacement curves of empty tubes with different meshes consist of (a)1600, (b) 3200 and (c) 6400 elements 59
Figure 5.2. The Numerical and experimental load displacement curves of honeycomb filler with 6.4 mm cell size (a)3x20, (b) 6x20 and (c) 12x20 elements (at each wall of the honeycomb) 61
Figure 5.3. The Numerical and experimental load displacement curves of honeycomb filled tubes with (a) 40x40-3x20, (b) 40x80-6x20 and (c) 50x128-12x20 elements 62

Figure 5.4. The deformation mechanism of empty tubes at 0%, 20%, 40%, 60%, 80% percent strains (left to right). (a) simulation (b) experimental 63
Figure 5.5. The load displacement curve of empty tubes and comparison between the experimental and simulation results 64
Figure 5.6. The Specific absorbed energy versus displacement graph for the empty tubes and comparison between the experimental and simulation results 64
Figure 5.7. The deformation mechanism of 6.4 mm honeycomb filler (a) double layer (b) single layer honeycomb at 0%, 20%, 40%, 60%, 80% percent strains (left to right)..... 65
Figure 5.8. The load displacement curve of single layer 6.4 mm cell size honeycomb and comparison between the experimental and simulation results 66
Figure 5.9. The Specific absorbed energy versus displacement graph for the 6.4 mm cell size honeycombs and comparison between the experimental and simulation results 66
Figure 5.10. The deformation mechanism of 6.4 mm cell size honeycomb filled tubes (a) experimental (b) numerical simulation at 0%, 20%, 40%, 60%, 80% percent strains..... 67
Figure 5.11. The load displacement curve of 6.4 mm cell size honeycomb filled tubes and comparison between the experimental and simulation results..... 68
Figure 5.12. The Specific absorbed energy versus displacement graph for the 6.4 mm cell size honeycomb filled tubes and comparison between the experimental and simulation results 68
Figure 5.13. The triggering mechanism starts in honeycomb filled tubes (a) at glued sections (b) upper end of the tube (c) simulation (upper end) 69
Figure 5.14. The Load displacement curves of 6.4 mm cell size honeycombs with different cell wall thickness (a)0.09, 0.12 and 0.15 mm (b) comparison between (c)experimental data..... 71

Figure 5.15. The Load displacement curves of 6.4 mm cell size honeycomb filled tubes with different honeycomb cell wall thickness (a) 0.09, 0.12 and 0.15 mm (a)comparison between experimental data..... 72
Figure 6.1. Figure 6.1 The effect of mesh size on the deformation of 6.4 mm cell size Nomex® honeycombs, (a) 3x20 (b) 6x20 (c) 12x20 elements on each wall of the honeycomb 75
Figure 6.2. The simulation of interaction effect in 6.4 mm cell size honeycomb filled tube 76

LIST OF TABLES

Table **Page**

Table 3.1. The compression and plate shear strength and elastic modulus values of Nomex® honeycombs according to their cell size 20
Table 3.2. Tested empty and filled tubes: coding as following; A: 6.4 mm cell size, B: 4.8 mm cell size and C: 3.2 mm cell size honeycombs 27
Table 3.3. Tested Nomex® honeycomb samples: coding as following; A: 6.4 mm cell size, B: 4.8 mm cell size and C: 3.2 mm cell size honeycombs 29
Table 4.1. Calculated and experimental mean crushing loads and strength values of honeycombs 37
Table 4.2. The average crushing loads and deformation modes with analytical, experimental results 41
Table 5.1. The experimental and the numerical deformation parameters of empty tube, filler and filled tube 69

NOMENCLATURE

A_E	Crush force efficiency
C	Strengthening effect of honeycomb filling
D	Diameter
D_C	Deformation capacity
E	Absorbed energy
H_F	Fold length
l	Total length of the deformation element
m_{hc}	Mass of the deformation element
m_t	Total mass of the deformation element
m_{tube}	Mass of the deformation element
N	Number of folds
P_a	Average crushing load
P_{max}	Maximum deformation load
P_m	Average crushing load of honeycomb
P_{nh}	Average crushing force of honeycomb filled tube
P_{ae}	Average crushing load of the empty tube
R	Radius of tube
SAE	Specific absorbed energy
S_E	Stroke efficiency
t	Thickness of the tube
t_h	Thickness of the honeycomb cell wall
T_E	Total crush efficiency
ρ	Honeycomb density
ρ_t	Tube material density
σ_0	Yield stress
σ_h	Mean crushing strength of honeycomb

CHAPTER 1

INTRODUCTION

Starting with Alexander's research in 1960's, the crash behavior of columnar structures including thin-walled circular and rectangular tubes was studied nearly in a time period of over 50 years. In the last decade the columnar structures started to be filled with light weight material cores. The reason of filling is to create weight and cost effective alternatives for crash absorbing systems or structures. Filling the structures with light weight materials increases the absorbed energy in a thin walled column and are preferred to the column wall thickening when the weight is taken into consideration. The absorbed energy of the filled columns is higher than the summation of the absorbed energies of empty tube and filler material alone. This phenomenon is known as the interaction effect. The columnar structures have a high variety of usage areas in energy absorbing structures including bumpers and crash boxes and main frames of automobiles, platforms and building frames in civil engineering applications.

In the filling of thin-walled aluminum tubes, light weight materials are usually used with two different classes of cores, namely foams and honeycombs. Honeycombs are extensively used as energy absorbers in real world applications. Because of their geometry and structure, they are very light materials. Their most common usage area is aero plane, and aerospace technology. These materials are excellent weight efficient materials due to their strength and energy absorption capacities. In the industry several types of honeycombs are used. Aluminum, sheet steel, aramid paper, thermoplastics and polymers are the most common materials that are used in honeycomb manufacturing. Many studies of honeycomb crush behavior and its energy absorption effects as a filler material have been investigated and in addition to these previous works, this study is aimed to determine the strengthening effect of honeycomb filling in thin walled aluminum circular tubes and support the results with numerical simulations.

In this study, the aramid paper based Nomex® honeycomb was used in three different cell-sizes as the filler material of filling thin walled aluminum tubes, with a constant wall thickness and diameter.

The variations of cell size, compression strain rate and adhesive addition's effect on deformation mode, specific absorbed energy, average crushing load, stroke efficiency and the interaction effect were investigated. The specific absorbed energy of filled tubes was compared according to cell-size and also with the empty tubes. The deformation mechanisms were investigated for tubes, honeycombs and for filled tubes at different strain rates to observe the possible deformation mechanism changes. According to support the experimental results the numerical analysis of empty tubes and 6.4 mm cell-sized honeycombs were made and a comparison was made between the experimental, analytical and numerical results.

CHAPTER 2

LITERATURE REVIEW

2.1. Honeycombs and Material Properties

Honeycombs are the light-weight materials used in various kinds of engineering applications including light-weight energy absorbing structures such as sandwich panels, special fire protective suits and etc. Honeycomb structures can be constructed from any material; however the current interest focuses on the honeycomb structures made from aluminum (Figure 2.1.a) and aramid paper (Figure 2.1.b). A honeycomb has a standard hexagonal geometry which can be characterized by the cell wall thickness (t), cell width (b), minor diameter of the cell (D) and height of the cells (2H) (Figure 2.1.c). The hexagonal cell arrangement leads to highly anisotropic material properties through T, L and W directions. T, L and W refer to through thickness, width and length of the honeycomb plate, respectively.

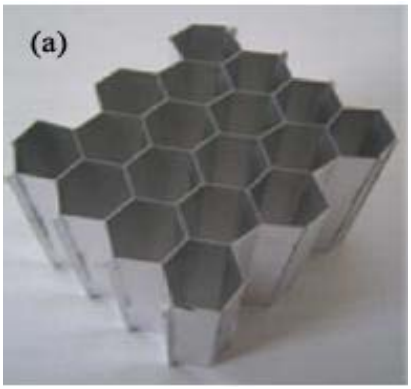

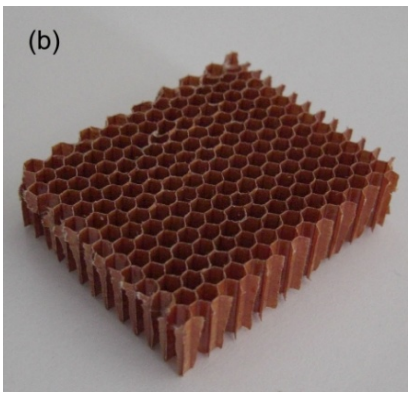

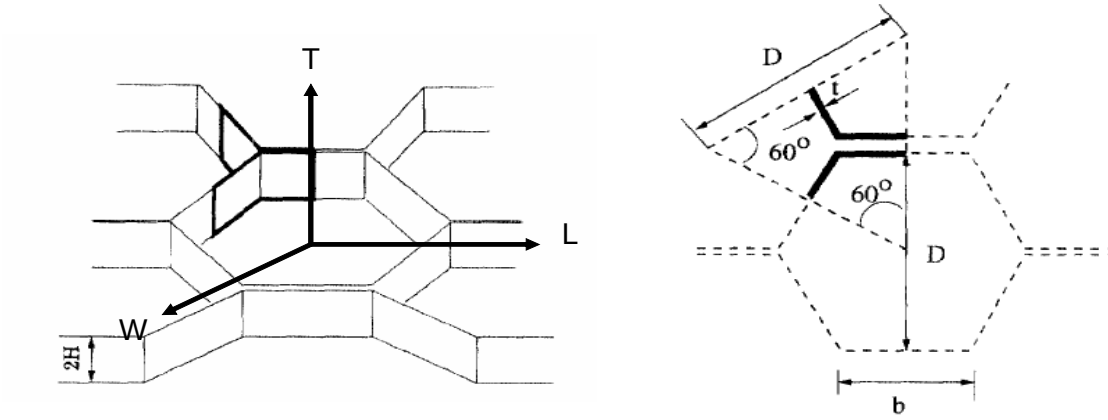

(c)

Figure 2.1.(a) aluminum, (b) aramid paper honeycomb and (c) honeycomb cell structure (Source: Santosa and Wierzbicki 1998)

Nomex® is a flame resistant meta-aramid material manufactured by DuPont Company in the 1970's. Due to its material characteristics, Nomex® is an aromatic nylon, the meta-variant of the para-aramid Kevlar. It is marketed both in fiber and sheet form and used in applications where resistance to heat and flame is required. The application areas of Nomex® paper encompass a variety of range. The paper form is used in electrical laminates such as circuit boards and transformer cores, in designing fire fighting equipments and in the race drivers. In honeycomb form, it is used in protective pressure suits due to its water immersion near vacuum and fire resistance properties and as core materials in sandwich panels, passenger seats and passenger cabin frames of airplanes due its light-weight and fire resistant properties.

2.2. The Crushing Behavior of Tubes

The crushing behavior of thin walled tubes has been studied over 50 years. For the last decade, the studies were also extended to numeric and finite element analysis. The numerical tools are helpful to predict the crushing behavior of tubes with different geometrical parameters, which may greatly reduce the number and the cost of experimentation. In the first part of this section the terminologies used the crash analysis of columnar structures will be given.

2.3. Terminologies Used In Crush Analysis

Consider the typical uniaxial compression load-displacement curve of a columnar structure given in Figure 2.2.a. Initially, the column deforms elastically until about a peak load (region I); thereafter, the structure plastically collapses as the folds form progressively (region II) and finally, folds are compressed together in the densification region; hence, the load values increases sharply in this region. In region II, the collapse mode in the form of progressive folding lead to a nearly constant load, providing energy absorption at a constant load. The total absorbed energy (E) of the crushed column is calculated from the area under the load-displacement curve given in Figure 2.2.a as;

$$E(\delta) = \int_0^{\delta} P d\delta \tag{2.1}$$

where δ and P are the displacement and load, respectively. The corresponding average or mean crushing load (P_a) is calculated by dividing the absorbed energy to the displacement as,

$$P_a(\delta) = \frac{E(\delta)}{\delta} \tag{2.2}$$

The specific absorbed energy per unit mass (SAE) shown in Figure 2.2.b is calculated using the following relation,

$$SAE = \frac{\int_0^{\delta} P d\delta}{m_t} \tag{2.3}$$

where m_t is the total mass of the crushing element, which includes the weight of column, filler and bonding material between wall and filler in the filled tubes. The crush force efficiency (A_E), which is the ratio between average load and the maximum load (P_{max}) is calculated using the following relations

$$A_E = \frac{P_a(\delta)}{P_{\max}(\delta)} = \frac{E(\delta)}{P_{\max}(\delta)\delta} \tag{2.4}$$

Total efficiency (T_E), defined as the ratio between total energy absorption and energy absorption at the maximum load, is shown in Figure 2.2.c and expressed as,

$$T_E = \frac{E(\delta)}{P_{\max}(\delta)l} \tag{2.5}$$

where l is the length of the column. ≤ the stroke.

The stroke efficiency (S_E), which is the maximum displacement (δ_{max}) divided by the total length of the crushing element, is

$$S_E = \frac{\delta_{\max}}{l} \tag{2.6}$$

The deformation capacity (D_C) which is the displacement divided by the initial length is,

$$D_C = \frac{\delta}{l} \tag{2.7}$$

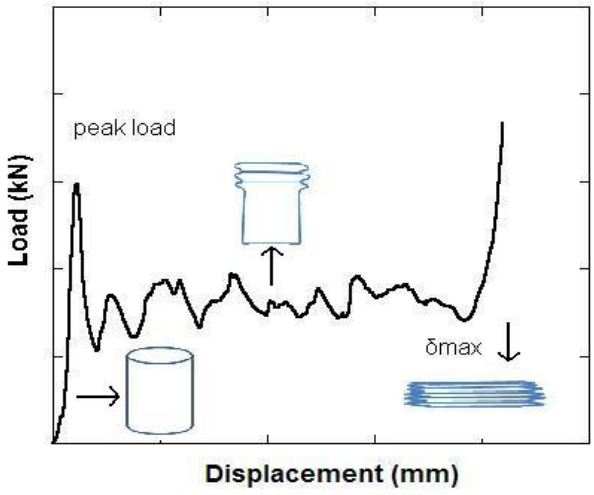

(a)

Figure 2.2. Terminology used in the crush analysis

(cont. on next page)

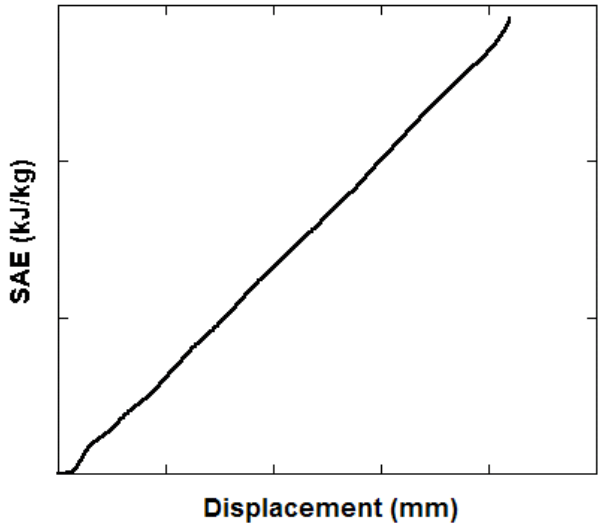

(b)

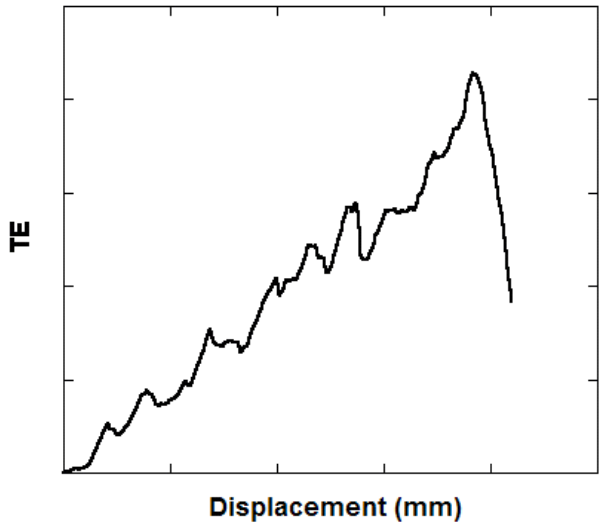

(c)

Figure 2.2. (cont.) Terminology used in the crush analysis

2.4. Crushing Behavior of Empty Tubes: Numerical and Experimental Analysis

Four main crushing modes of circular tubes under axial compressive loads are so far identified (Guillow, et al. 2001). These are (i) progressive axisymmetric: concertina mode, (ii) progressive non-symmetric: diamond mode, (iii) mixed mode: axisymmetric mode followed by non-symmetric mode and (iv) Euler or global buckling. Tubes with low D/t ratios and elastic perfectly plastic materials generally exhibit concertina mode

of deformation, on the other hand tubes with high D/t ratios and strain hardening materials exhibit diamond mode of deformation (Singace and Sobky 2001). Mixed mode is generally observed following the first couple of axisymmetric mode of folding. Euler buckling occurs in the tubes of high L/D ratios. The type of deformation mode depends on the geometrical as well as the material parameters. The concertina mode of deformation of HT30 Al alloy tubes was for example found, when D/t ratios varied between 10 and 90 and L/D ratios between 1 and 5 (Andrews, et al. 1983) (Figure 2.3). Diamond mode became dominant at D/t ratios higher than 90 as seen in Figure 2.3 Due to non-symmetric folding, the fold length (the total length of the fold section) increases in diamond mode as compared with concertina mode. Because of increased fold length and the promotion of the global bending, diamond mode of deformation is usually regarded as the lower mode of deformation as compared with concertina mode.

In addition, the experimental deformation and load-displacement curves of tubes were affected by several other factors including the folding parameter (ratio of internal folding to fold length) , load eccentricities, cut-off and grooving on the tube wall (Han, et al. 2007), foam-filling (Seitzberger, et al. 1997), (Santosa, et al. 2000) and any disturbances in the periodicity of folding.

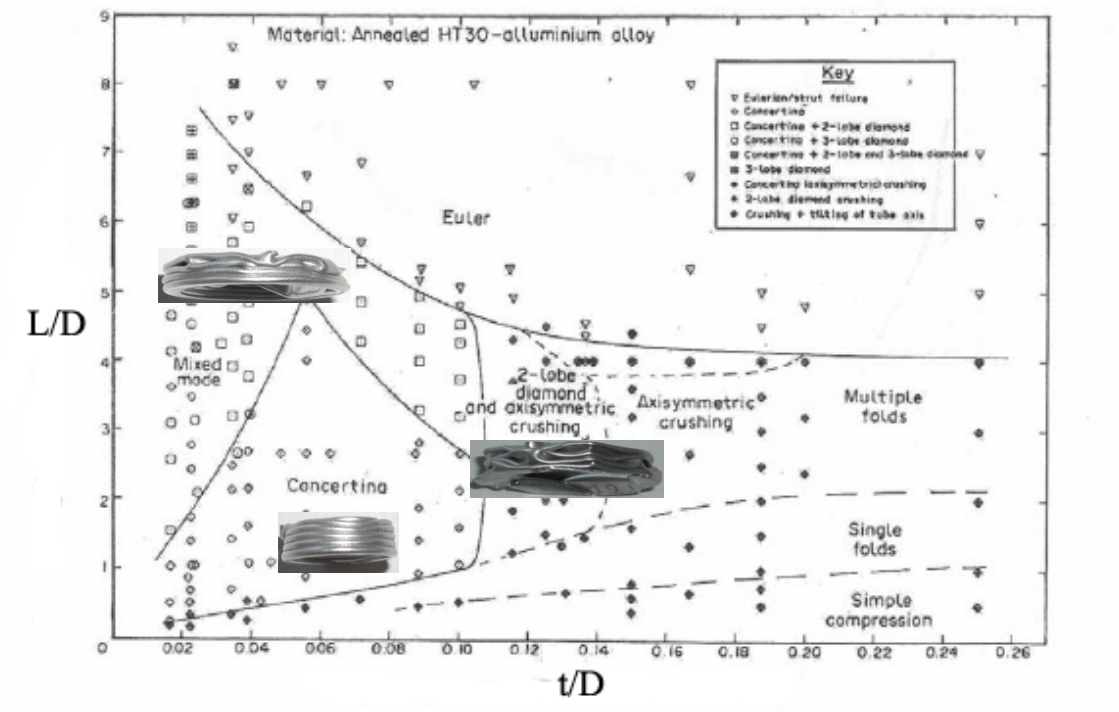

Figure 2.3. The collapse mode of deformation chart of HT30 Al alloys as function of L/D and t/D (Source: Andrews, et al. 1983)

The load-displacement curve of a 3003-H14 circular tube is shown in Figure 2.4 for an example for the deformation sequence involved in folding of tubes under uniaxial compressive loads. The load-displacement curve in Figure 2.4 shows characteristics of the tube crushing: a relatively high initial peak-load followed by a sharp decline in load values, and a gradual increase in the peak-load values following the initial peak-load as the displacement increases. The deformation sequence consists of inward and outward bending of the tube wall. Following the maximum initial peak-load (A), the tube wall bends outward and meanwhile the load values decrease until the point B in Figure 2.4; thereafter, the load values increase until the point C. During the inward folding of the tube wall over the first fold, the load values decrease once again (D in Figure 2.4). When the inner wall of the first fold comes into contact, the load values increase until point E, where outward folding starts to form over the first fold. When the outer knee of the second fold comes into contact with the first fold, the load values increase again from the point F in Figure 2.4. This sequence of tube wall deformation repeats as the third, fourth and fifth folds form, except the inner and outer fold formation (point C and D respectively) starts at the same point in the fourth and fifth folds. The distance between the peak-loads is the fold length as depicted in Figure 2.4.

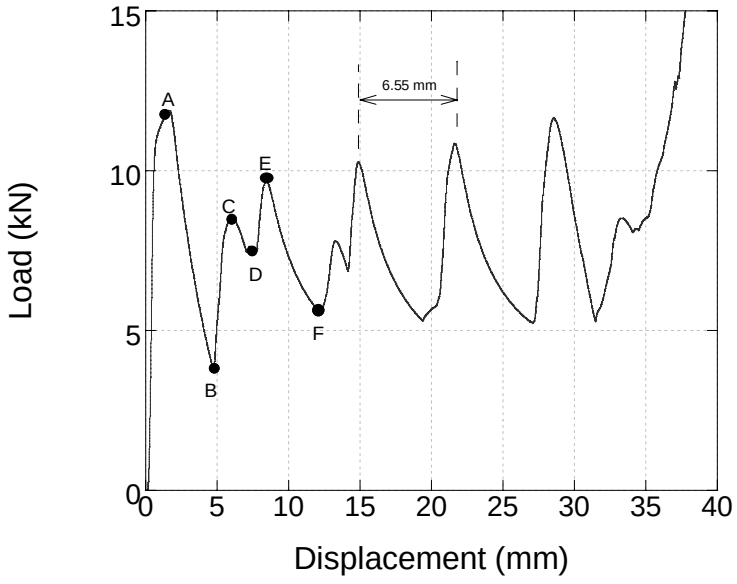

Figure 2.4. Load-displacement curve of an aluminum deep drawn tube (3003-H14) of 20 mm in outside diameter, 50 mm in length and 0.9 mm in wall thickness (Source : Tasdemirci 2008)

The first analytic study to formulate the crushing behavior of cylindrical thin-walled tubes was shown by Alexander (1960). He developed a simple model for the concertina mode of deformation using metal tubes with D/t ratios varying between 29 and 89, by considering the formation of four plastic hinges as shown in Figure 2.6. Note that in Alexander's model the inward folding of the tube wall is excluded in the analysis. The average crushing load for concertina mode of deformation in the model was given as,

$$P_a \cong 6\sigma_0 t(Dt)^{1/2} \tag{2.8}$$

In above equations σ_0 is the yield strength of the tube material, t is the thickness and D represents the diameter of the tube. The plastic half-wavelength H (half of the fold length) shown in Figure 2.5 is given by the following equation,

$$H = C\sqrt{Dt} \tag{2.9}$$

where C is a constant.

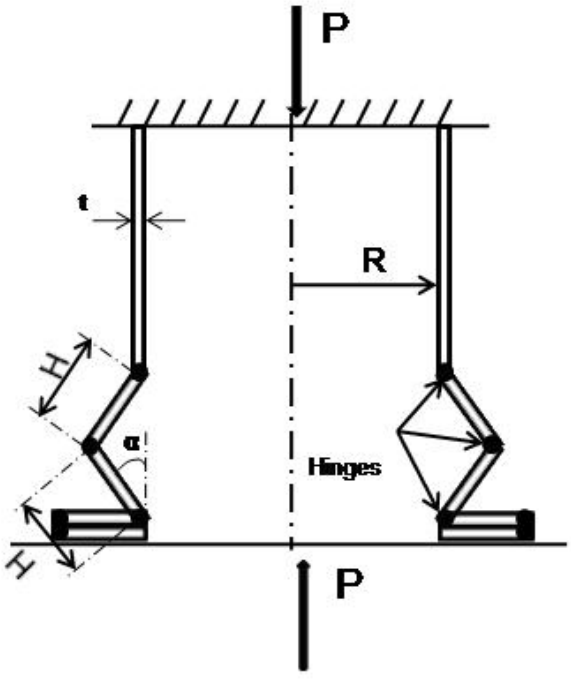

Figure 2.5 Alexander's concertina deformation mode model

(Source : Alexander 1960)

Abramowicz and Jones (1986) analytically analyzed concertina and diamond mode of deformation. The following equations were proposed for the average crushing force of concertina and diamond mode of deformations, respectively.

$$P_a = \frac{\sigma_0 \sqrt{Dt} + 3.44t}{0.86 - 0.568\sqrt{t/D}} \tag{2.10}$$

and

$$P_a = 86.14(D/t)^{0.33} \sigma_0 (t^2/4) \tag{2.11}$$

and

$$P_a = \sigma_0 t(6(Dt)^{1/2} + 3.44t) \tag{2.12}$$

Singace and Elbosky (1995) investigated the concertina and diamond mode of deformation and determined the eccentricity factor (m), which is the ratio of inward folding to outward folding, in both concertina and diamond mode of deformations and found the value of m as 0.65 for both types of deformation. The following equations were proposed by the same authors for the average axial crushing force of concertina and diamond mode of deformation, respectively

$$P_a = (\sigma_0 t^2/2\sqrt{3})22.27\sqrt{D/t} + 5.632 \tag{2.13}$$

and

$$P_a = \sigma_0 t^2 (7.874(R/t)^{1/2} + 1.408) \tag{2.14}$$

Gupta and Abbas (2000) developed a mathematical model for determining eccentricity factor m by considering with or without change of the thickness of the tube in the fold section. The model used in the analysis is shown in Figure 2.6. In this figure

mH and (1-H)m refer to inward and outward folding, respectively. The average crushing load was given in terms of the fold length as,

$$P_a = \pi\sigma_0 t[kt(\frac{\pi D}{h} + 2 - 4m) + h(rm^2 + (1-m)^2)] \quad (2.15)$$

Where the W_b, W_c and h was the energy dissipated in plastic bending in the formation of a fold, energy dissipated in circumferential deformation of a fold and the half fold length respectively.

k is defined as a parameter.

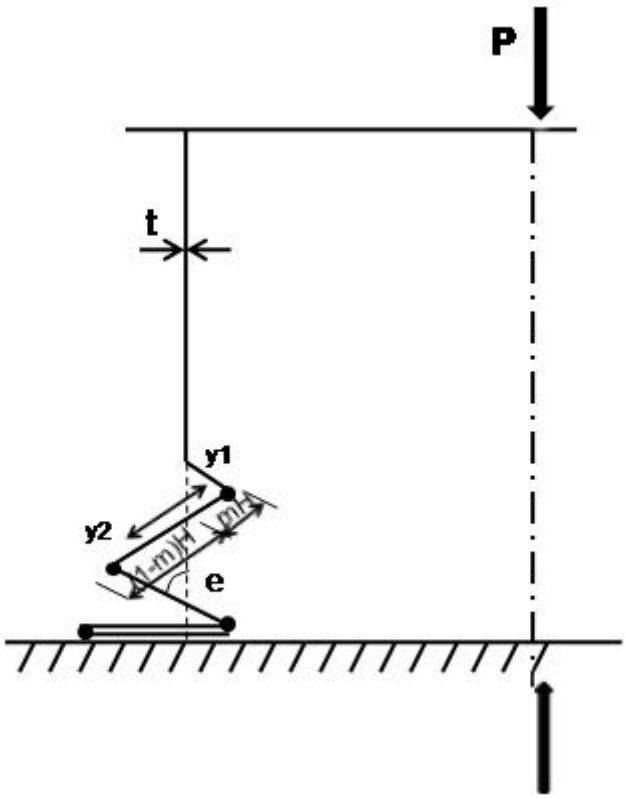

Figure 2.6. The Axial crushing model for a cylindrical tube
(Source : Gupta and Abbas 2000)

Pugsley and Macaulay (1960) studied the diamond mode of deformation of thin walled tubes with high D/t ratios. Based on the deformation energy resulting from the bending and shear of the folds, the following equation was proposed,

$$P_a = \sigma_0 t(10.05t + 0.38D) \tag{2.16}$$

Pugsley (1979) proposed a modified model of Alexander's plastic hinge analysis for the diamond mode of deformation based on n numbers of diamond folds as,

$$P_a = 2.286n^2\sigma_0 t^2 \tag{2.17}$$

The value of the n depends on the D/t ratio of the tube. Wierzbicki (1988) proposed an approximate expression for the average crushing load of the diamond mode of deformation as,

$$P_a = 18.15\sigma_0 t^2 (D/t)^{1/3} \tag{2.18}$$

and

$$P_a = 11.22\sigma_0 t^2 (R/t)^{1/2} \tag{2.19}$$

for concertina mode of deformation

$$P_a = 7.933\sigma_0 t^2 (D/t)^{1/2} \tag{2.20}$$

Guillow et al. (2001) defined the average crushing load of circular thin walled tubes as

$$P_a = \sigma_0 (t^2/4)72.3(D/t)^{0.32} \tag{2.21}$$

Singlace and Sobky (2001) studied the effect of end-constraints on the crushing behavior of mild steel and aluminum alloy tubes of relatively low D/t ratios subjected to axial crushing.

The partially constrained tubes were found to deform in concertina or diamond mode depending on D/t ratio. Mixed mode of deformation generally occurred when the tubes were constrained at both ends. It was proposed in the same study that the deformation mode and the absorbed energy of the crushing tubes could be controlled by

applying end constraints. Abramowicz and Jones (1986) studied the transition of the axially crushed tubes from the Euler bending mode to the non-symmetrical buckling mode under dynamic and static loadings. The transition point was found to depend on the tube length, material type, strain rate and the end condition.

2.5. Crushing Behavior of Foam filled tubes

The ultimate goal of light-weight material filling of columnar structures is to increase the specific energy absorption. One of the first investigations on the foam filling of tubes was by Thornton (1980). It was shown that although polyurethane foam filling increased the specific absorbed energy of the filled tube, it was not effective in increasing the specific absorbed energy over that of wall thickening of empty tube (the equal mass of empty tube). Hanssen et al. (1999) investigated static and dynamic crushing of circular aluminum extrusions with aluminum foam filler. It was shown in the same study that the filled tube showed higher crushing loads over that empty and foam alone as shown in Figure 2.7, which is known as interaction effect. The interaction may be partly due to the resistance of filler to the inward and/or outward folding of tube wall and partly due to the interfacial friction stress between foam and tube wall. The use of adhesive can contribute to the specific energy absorption of tube by two mechanisms, namely, increased load transfer from tube wall to the foam core and peeling of the adhesive. The latter mechanism occurs mainly due to the outward folding of the tube. The foam filling generally increases the number of folds formed and decreases the fold lengths in the metal tubes. Hannsen et al. (2000) developed an equation for the average crushing load of foam filled (P_{af}) columns by including contributions of the average crushing load of empty tube (P_{ae}), foam plateau stress (σ_{pl}) and interaction effect. The equation was found to be well agreed with experimental results and is given as

$$P_{af} = P_{ae} + \sigma_{pl} b^2 + C_{avg} \sqrt{\sigma_{pl} \sigma_y}\, bt \qquad (2.22)$$

where $C_{avg,}$, b are the dimensionless constant which is directly related to the interaction effect, tube width respectively. The second term of the right hand side of the equation 2.18 accounts for the axial compression of the foam and the last term for the interaction

effect. Santosa et al. (1998) noted that the bonding between filler and tube wall increased the average crushing load of filled tube over the unbounded filled tube when appropriate tube geometry and foam density were chosen. In this study, the filled tubes were moddeled using using PAM-CRASH. The model was created by the mesh generator program HYPERMESH. The column wall (aluminum) was modeled with Belytschko-Tsay-4 node thin shell element and the foam core (HYDRO and MEPURA aluminum foam) was modeled with an 8-node solid element. No triggering imperfection was used in the model. Based on finite element modeling results the same authors proposed the following equation for the average crushing load of foam-filled square tubes,

$$P_{af} = P_{ae} + C\sigma_{pl} b^2 \tag{2.23}$$

The constant C in equation .2.19 is considered *strengthening coefficient* of foam filling. The values of C for foam-filled single tubes were shown to be 1.8 and 2.8 for the unbounded and bounded cases, respectively. Kavi et al. (2006) studied the energy absorption characteristics of foam filled thin walled aluminum tubes. The foam filling was found to change the deformation mode of the tube from diamond (empty tube) into concertina, regardless the foam type and the foam density used. An interaction effect between the filler material and the empty tube was found. However, the foam filling was found not efficient in increasing the specific energy absorption than tube wall thickening. The strengthening coefficient of the foam filled tubes was found 1.7. Toksoy and Guden (2005) investigated the crushing behavior of polystyrene foam filled thin walled aluminum tubes with diameters of 16 mm and 25 mm. The foam filling changed the deformation mode from diamond to concertina mode in 25 mm diameter tubes. The strengthening coefficient was found around 1 for the concertina mode of deformation and higher than unity for the diamond mode of deformation.

In concertina mode the tubes were observed to deform independently from the filler, whilst in diamond mode of deformation the foam filler was detected to be compressed between the folds, leading to a higher strengthening coefficient.

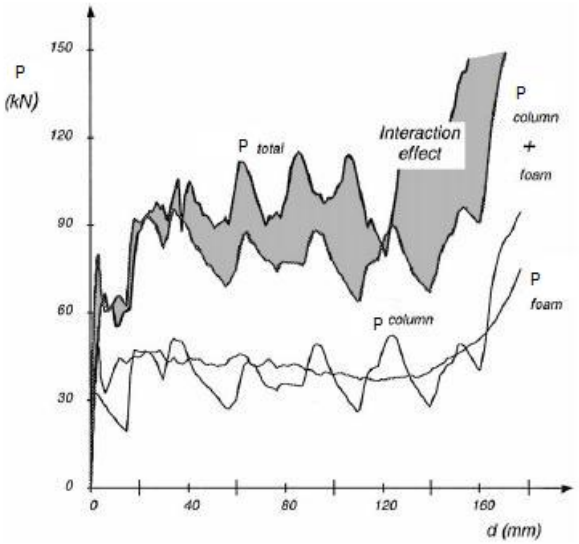

Figure 2.7. The interaction effect in Al foam filled Al tubes
(Source : Hanssen, et al. 1999)

2.6. Crushing Behavior of Honeycomb and Honeycomb Filled Tubes

Wierzbicki and Abramowicz (1983) proposed the following equation for the average crushing load of honeycomb structure based on the cell model shown in Figure 2.1.c;

$$P_{a,h} = 8.61\sigma_0 t^{5/3} b^{1/3} = 7.17\sigma_0 t^{5/3} D^{1/3} \tag{2.24}$$

By considering the area of the basic folding element (dark sections in Figure 2.1.c), which is $\frac{\sqrt{3}}{4} D^2$, the crushing strength of the honeycomb was proposed as

$$\sigma_h = 16.55\sigma_0 (t/D)^{5/3} = 3.22\sigma_0 (\rho_h / \rho_s)^{5/3} \tag{2.25}$$

where ρ_h and ρ_s are the density of the honeycomb and the density of the solid material respectively.

Chawla et al. (2003) investigated the crushing behavior of honeycomb structures using PAM-CRASH finite element analysis program. The finite element model was

created in IDEAS software. For the modeling section, 6 x 80 elements (6 elements along the thickness and 80 elements along the ribbon direction) per cell gave good results in the analysis, while 6 x 60 elements gave sufficient results without introducing large errors (Figure 2.8). A comparison was made between the materials models of elastic-perfectly plastic and elastic plastic. Two material models gave similar stress-strain behavior. It was concluded that the compressive strength depended on only the yield strength of the basic material.

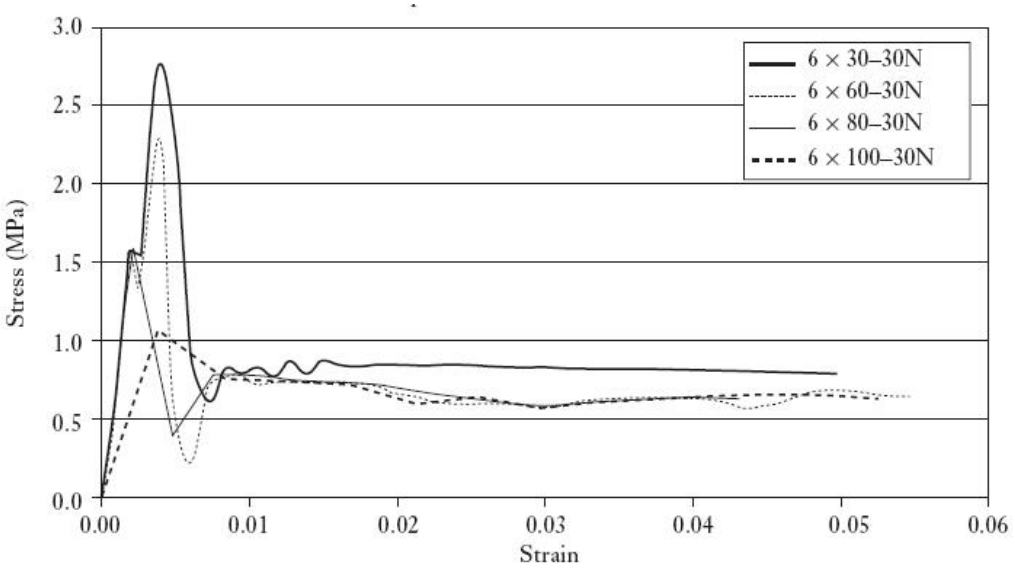

Figure 2.8. Effects of number of elements on the stress-strain curves of honeycomb (Source : Chawla, et al. 2003)

Aktay and Johnson (2007) modeled Nomex® honeycomb crush behavior using PAM-CRASH. Two standard modeling techniques were used: micromechanical and homogenized model. In the micromechanical model, Belytychko-Tsay–4 node thin shell elements were used to characterize each honeycomb shell. For the representation of Nomex® and aluminum honeycomb, were modeled using elastic-plastic isotropic thin shell material model.

They compared the numerical modeling techniques of semi-adaptive coupling technique and the element elimination technique and observed that both techniques gave approximate results with the experiments, but semi-adaptive coupling technique was found more CPU efficient. Wu and Jiang (1996) studied the axial crush behavior of 5052-H38 and 5056-H38 aluminum honeycombs. A unit cell model was developed for

honeycomb crushing. The effect of number of cells on the crushing behavior of the honeycomb was also investigated. It was shown that decreasing number of cells, cell size and core height and using stiffer core material increased energy absorption. Aminanda et al. (2005) studied the deformation modes of honeycombs made of aluminum, Nomex® and the drawing paper. The fold shape was found different in all three types of core materials. It was further proposed that the compression load was essentially carried by the vertical edges of the hexagonal cells of honeycomb.

Santosa and Wierzbicki (1997) studied the crash behavior of box columns filled with aluminum foam and honeycomb. The mean crushing load of the honeycomb filled columns were formulated as;

$$P_{m,honeycomb} = 14\sigma_0 t^{5/3} b^{1/3} + b^2 \sigma_h \tag{2.26}$$

In above equation, the first term is the crushing load of square box column with the cross-section of b x b. The strengthening coefficient of the honeycomb was taken as 1 as no interaction effect was found between the honeycomb filler and the tube wall. The specific energy absorption of honeycomb foam filled box column and box column with a effective crushing distance of 2/3(2H) were given sequentially as;

$$S.A.E_{h.comb} = \frac{39.15\sigma_0 (t/b)^{5/3} + 3\sigma_h}{16\rho_c (t/b) + 4\rho_h} \tag{2.27}$$

and

$$S.A.E_{box} = 2.45(\frac{\sigma_0}{\rho_c})(t/b)^{2/3} \tag{2.28}$$

where c and h refer to column and honeycomb. In terms of total column weight (m_t), SAEs were given sequentially as;

$$S.A.E_{h.comb} = \frac{3.1 + 97.4(m_t - 0.4)^{5/3}}{m_t} \tag{2.29}$$

and

$$S.A.E_{box} = 14.4 m_t^{2/3} \tag{2.30}$$

The specific absorbed energy was shown by the same authors to depend on the density of the filler. The results have shown that the aluminum honeycomb filling was more weight efficient than aluminum foam filling although aluminum foam resulted in higher average crushing loads. Zarei and Kröger (2006) performed quasi-static tests on aluminum honeycomb and honeycomb filled square and circular aluminum tubes. The crush response of the honeycomb filled sections was further modeled using LS-DYNA software. The tube walls were modeled with Belytschko-Tsay thin shell elements and the honeycomb filler with solid elements. The contact between the rigid body and the specimen was modeled using node to surface algorithm with a friction coefficient of 0.2. Results have shown that filled tubes deformed in a more stable manner; the specific absorbed energy increased over that of the empty tubes and the honeycomb filling of the tubes became energetically more efficient than tube wall thickening. It was also shown that increasing honeycomb density increased the interaction effect.

The aim of this thesis is the further investigation of the energy absorption behavior of honeycomb (aramid paper) filled thin-walled circular tubes. For that, honeycomb plates with three different cell sizes were used to fill aluminum tubes in order to determine the effect of cell size on the crushing performances of filled tubes. The results were also compared with the same Al circular tubes, those filled with Al closed-cell foam filler. The deformation of the empty and filled tubes were further modeled using LSDYNA software in order to support the experimental results and form a solid foundation to model complex shaped structures filled with honeycomb.

CHAPTER 3

MATERIALS & EXPERIMENTAL SECTION

3.1. Nomex® Aramid Paper Honeycomb Filler Material

The dimensions of three Nomex® honeycomb sheets, which were received from DuPont, were 1.27x60x120 cm with the cell-sizes of 3.2, 4.8 and 6.4 mm. The cells of three different cell sizes of honeycombs are shown sequentially in Figures 3.1.a, 3.1. b and 3.1.c. Although, the cell size of the honeycombs was different, the densities were the same, 48 kg/m^3. The honeycomb cell-wall thickness was measured using a digital micrometer and found to be varying between 0.08 and 0.15 mm with an average cell-wall thickness of 0.13 mm. At least 50 measurements were made for each honeycomb sheet and the results were averaged.

The honeycomb structures consist of hexagonal cells made of cell walls (Figure 3.1). The cell walls are glued to each other with the help of ribbons in the aramid paper's surface. Table 3.1 lists the mechanical properties of three honeycombs provided by the supplier. The mechanical properties in this table are through length (L) and width (W) directions, normal and parallel to the cells (Figure 3.2). As seen in this table, the honeycombs show strong anisotropy in mechanical behavior as the mechanical properties are higher through L direction.

Table 3.1. The compression and plate shear strength and elastic modulus values of Nomex® honeycombs according to their cell size

Product Designation			Compression	Plate Shear			
			Bare	L-Direction		W-Direction	
cell size-density			Strength	Strength	Modulus	Strength	Modulus
mm	kg/m^3	(μm)	(MPa)	(MPa)	(MPa)	(MPa)	(MPa)
			min type	min type	min type	min type	min type
ECA 3.2	48	(51)	1.90 - 2.10	1.16 -1.32	38 – 48	0.62 - 0.72	24 – 30
ECA 4.8	48	(51)	2.60 - 2.85	0.98 -1.14	34 – 40	0.56 - 0.66	22 – 28
ECA 6.4	48	(51)	0.80 – 1.06	0.54 -0.76	22 - 32	0.30 - 0.40	12 – 20

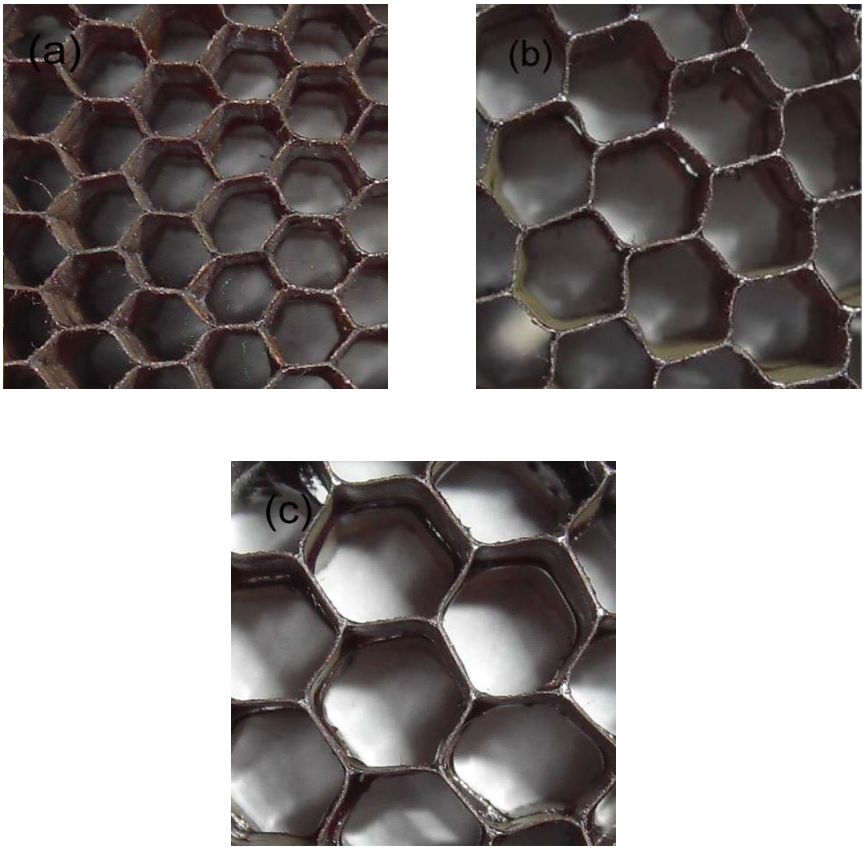

Figure 3.1. Nomex® honeycombs cells; cell size (a) 4.8, (b) 3.2 and (c) 6.4 mm

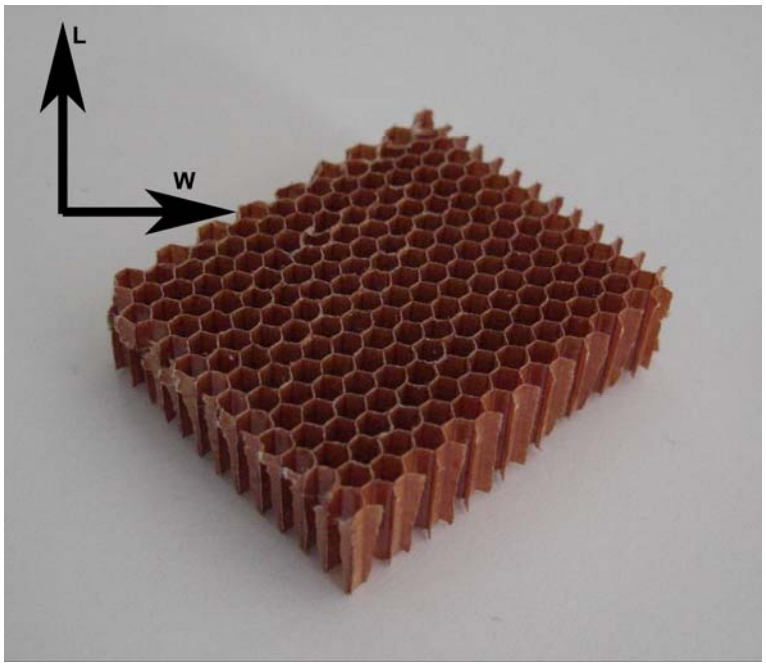

Figure 3.2. L and W directions of the honeycomb sheet

The crushing behavior of honeycombs was determined through compression testing on the cylindrical samples of L/D=1 (length/diameter) with 25.4 mm in diameter and square cross-section samples of 5x5x1.27 cm using the SHIMADZU AG-I testing machine (Figure 3.3). The compression tests were applied parallel to L directions of the samples with the cross-head speeds of 25, 10 and 5 mm min^{-1}, which corresponds to the strain rates of 1.64 10^{-2} s^{-1}, $6.56x10^{-3}$ s^{-1} and $3.28x10^{-3}$ s^{-1}, respectively. In a separate testing program, two layers of honeycomb samples were glued to each other using an epoxy based bond and these glued samples were tested (compression) at the same strain rates. During compression testing, the deformations of the samples were video recorded. The average crushing loads and Specific Absorbed Energies of the tested samples were calculated using following equations:

$$P_a = \frac{\int P d\delta}{\delta} \tag{3.1}$$

and

$$SAE = \frac{\int P d\delta}{m_t} \tag{3.2}$$

In the calculations of the average crushing loads the initial region of the load-displacement curves corresponding to the region of initial peak-load were excluded as this region may be affected by the end surfaces of the honeycombs and interfacial forces between compression test plates and end surfaces.

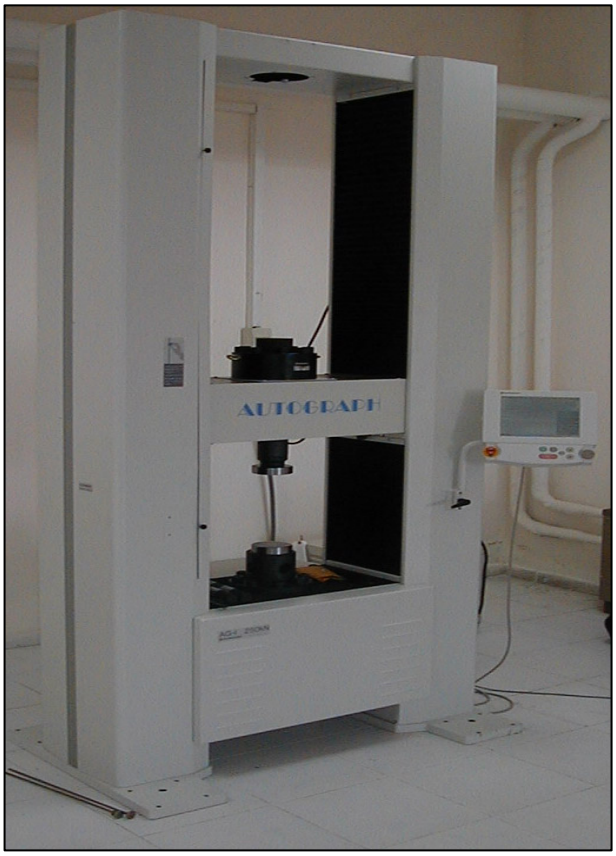

Figure 3.3. The SHIMADZU AG-I testing machine

3.2. Empty and Nomex® Honeycomb Filled Tubes

The thin walled aluminum tubes produced by METALUM Company of Turkey were received 25 mm in diameter and 50 mm in length with a wall thickness of 0.29 mm (Figure 3.4.a). The length of the tubes was reduced to 25.4 mm (2 times of the thickness of the honeycomb sheets) using PRESI MECATOME T255/300 saw. The cutting speed was set to 3200 rpm and water was used as the cutting fluid. After cutting, the tube ends were grinded using BUEHLER PHONIX Beta grinding machine with a turning speed of 300 rpm. Grinding was performed sequentially using silicon carbide grinding paper of P120, P320 and P600. A special metal block, which accommodated a 25 mm hole at the center, was used to accommodate tubes, providing flat surfaces of the tubes during grinding. Figure 3.4.b shows a cut and grinded tube sample. The quasi-static compression tests were applied to the empty tubes at the cross-head speeds of 25, 10 and 5 $mm.min^{-1}$ in both axial and lateral directions.

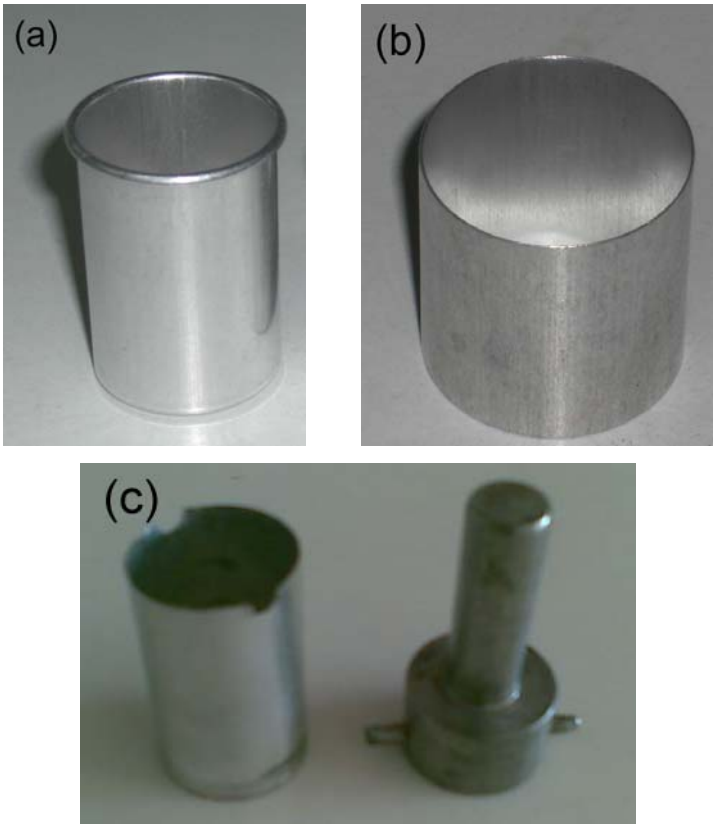

Figure 3.4. The empty tubes; (a) as-received, (b) after cutting process and (c) the cutting apparatus that was used to drill the honeycomb sheets

The honeycomb thickness and the tube length were matched by doubling the thickness of honeycomb sheets. The same type of honeycombs was glued to each other by using a Bison^{TM} type epoxy. The epoxy was applied as a thin layer onto a clean and smooth glass surface, and then each layer of honeycombs surfaces was covered with glue. During bonding, no pressure was applied to the honeycomb layers. The honeycomb layers were carefully glued and the cells fitted each other in a perfect order in order to avoid undesirable middle section buckling. The double layer of honeycomb (Figure 3.5.a) was drilled with a CHIN 16 Speed Drill Press using a special cutting head (Figure 3.4.c). In order to eliminate the possibility of tearing in honeycomb sheets, the cutting speed was kept low (120 rpm). In the filling of tubes, the circular double layer honeycombs (Figure 3.5.b) side surfaces were fist covered with an epoxy based bonding agent and then placed gently inside the empty tube (Figure 3.6). After curing of the epoxy bond (5 minutes), the excess epoxy was cleaned carefully with acetone.

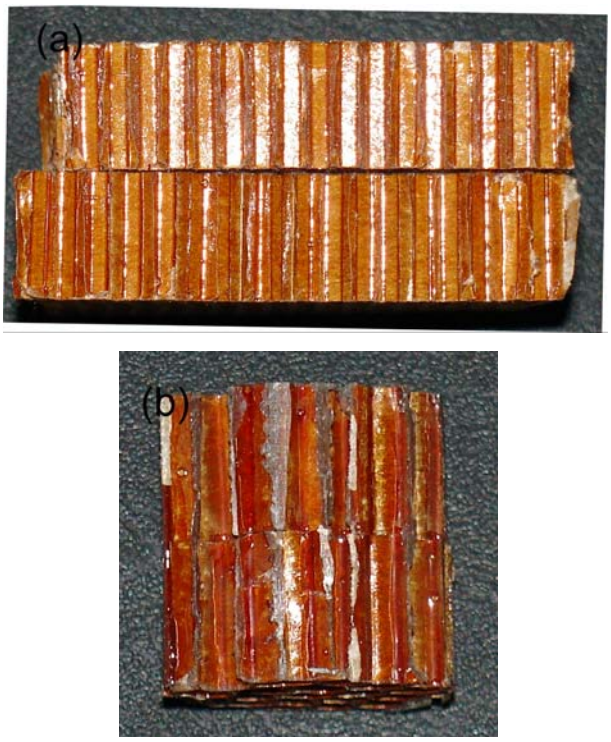

Figure 3.5. (a) Double layer honeycomb and (b) circular double layer honeycomb after drilling

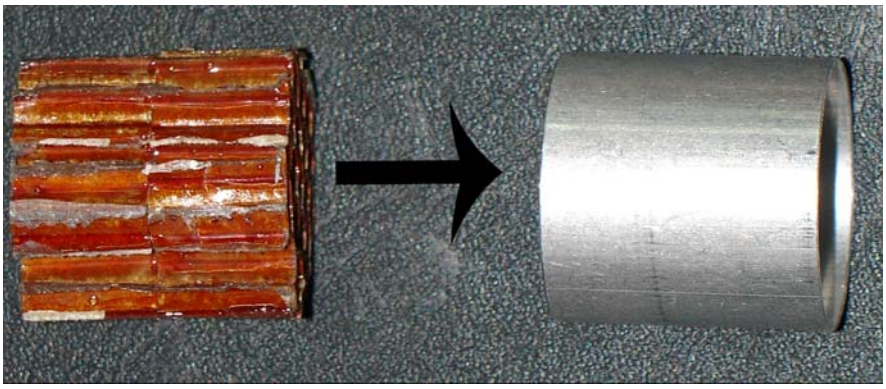

Figure 3.6. Filling the empty Al tube with a honeycomb filler

Using the above procedure, 21 filled Al tube test samples were prepared for each type of honeycomb filler. The weights of the tubes and honeycomb fillers were measured before and after filling so that the weight of the epoxy layer was calculated for each filled tube. A group of prepared test specimens are shown in Figure 3.7.

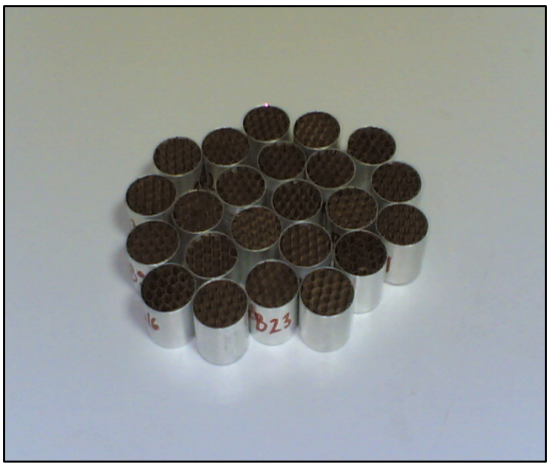

Figure 3.7. Filled Al tubes

The same cross-head speeds and strain rates were also used in the testing of the filled tubes, 1.64 10^{-2} s^{-1}, 6.56 10^{-3} s^{-1} and 3.28 10^{-3} s^{-1}. The strain rates applied and geometrical parameters of empty and filled tubes and honeycomb filler are listed in Table 3.2 and Table 3.3, respectively. Compression tests were also performed through the lateral direction of the empty and filled tubes in order to determine the effect of filling to the lateral loadings.

Table 3.2. Tested empty and filled tubes: coding as following; A: 6.4 mm cell size, B: 4.8 mm cell size and C: 3.2 mm cell size honeycombs

Tube type	Strain rate	Test Direction	Number of specimens tested	Diameter (mm)	Length (mm)
Empty tube	$1.64\ 10^{-2}\ s^{-1}$	Axial	9	25	25.4
Empty tube	$6.56\ 10^{-3}\ s^{-1}$	Axial	3	25	25.4
Empty tube	$3.28\ 10^{-3}\ s^{-1}$	Axial	3	25	25.4
Empty tube	$1.64\ 10^{-2}\ s^{-1}$	Lateral	1	25	25.4
Filled tube A type	$1.64\ 10^{-2}\ s^{-1}$	Axial	6	25	25.4
Filled tube A type	$6.56\ 10^{-3}\ s^{-1}$	Axial	3	25	25.4
Filled tube A type	$3.28\ 10^{-3}\ s^{-1}$	Axial	3	25	25.4
Filled tube A type	$1.64\ 10^{-2}\ s^{-1}$	Lateral	1	25	25.4
Filled tube B type	$1.64\ 10^{-2}\ s^{-1}$	Axial	6	25	25.4
Filled tube B type	$6.56\ 10^{-3}\ s^{-1}$	Axial	3	25	25.4
Filled tube B type	$3.28\ 10^{-3}\ s^{-1}$	Axial	3	25	25.4
Filled tube B type	$1.64\ 10^{-2}\ s^{-1}$	Lateral	1	25	25.4

(cont. on next page)

Table 3.2.(cont.) Tested empty and filled tubes: coding as following ; A: 6.4 mm cell size, B: 4.8 mm cell size and C : 3.2 mm cell size honeycombs

Tube type	Strain rate	Test Direction	Number of specimens tested	Diameter	Length
Filled tube C type	$1.64\ 10^{-2}\ s^{-1}$	Axial	6	25	25.4
Filled tube C type	$6.56\ 10^{-3}\ s^{-1}$	Axial	3	25	25.4
Filled tube C type	$3.28\ 10^{-3}\ s^{-1}$	Axial	3	25	25.4
Filled tube C type	$1.64\ 10^{-2}\ s^{-1}$	Lateral	1	25	25.4

Table 3.3. Tested Nomex® honeycomb samples: coding as following; A: 6.4 mm cell size B: 4.8 mm cell size and C: 3.2 mm cell size honeycombs

Honeycomb type	Strain rate (s^{-1})	Test Direction	Number of specimens tested	Cross-section (mm^2)	Honeycomb thickness (mm)
Type A (6.4 mm cell size)	$1.64\ 10^{-2}\ s^{-1}$	Axial	3	Circular (D= 25)	12.7
Type A (6.4 mm cell size)	$1.64\ 10^{-2}\ s^{-1}$	Axial	1	Rectangular L=50 W=50	12.7
Type A (6.4 mm cell size)	$1.64\ 10^{-2}\ s^{-1}$	Axial	3	Circular (D= 25)	25.4
Type B (4.8 mm cell size)	$1.64\ 10^{-2}\ s^{-1}$	Axial	3	Circular (D= 25)	12.7
Type B (4.8 mm cell size)	$1.64\ 10^{-2}\ s^{-1}$	Axial	1	Rectangular L=50 W=50	12.7
Type B (4.8 mm cell size)	$1.64\ 10^{-2}\ s^{-1}$	Axial	3	Circular (D= 25)	25.4

(cont. on next page)

Table 3.3. (cont.)Tested Nomex® honeycomb samples: coding as following; A: 6.4 mm cell size B: 4.8 mm cell size and C: 3.2 mm cell size honeycombs

Honeycomb type	Strain rate (s^{-1})	Test Direction	Number of specimens tested	Cross-section (mm^2)	Honeycomb thickness (mm)
Type C (3.2 mm cell size)	$1.64\ 10^{-2}\ s^{-1}$	Axial	3	Circular (D= 25)	12.7
Type C (3.2 mm cell size)	$1.64\ 10^{-2}\ s^{-1}$	Axial	1	Rectangular L=50 W=50	12.7
Type C (3.2 mm cell size)	$1.64\ 10^{-2}\ s^{-1}$	Axial	3	Circular (D= 25)	25.4

CHAPTER 4

RESULTS

4.1. Compression Behavior of Honeycomb Filler

The Nomex® honeycomb has a typical compression stress-strain curve comprising three different deformation regions. These are the linear elastic, plateau and densification regions as shown in Figure 4.1 for 4.8 mm cell size honeycomb sample. Cellular materials made from metals or polymers such as aluminum closed-cell foams and hollow spheres show the similar deformation regions sequentially. In the linear elastic region the stress increases until a maximum peak value which is known as the collapse or peak stress as shown in Figure 4.1. Following the linear elastic region, the stress values decrease abruptly to a plateau stress. In the plateau region the stress values oscillate around the plateau stress as the cells fold progressively. The plateau region continues until about the densification strain, after which the stress increases sharply as the folded cells are compressed together.

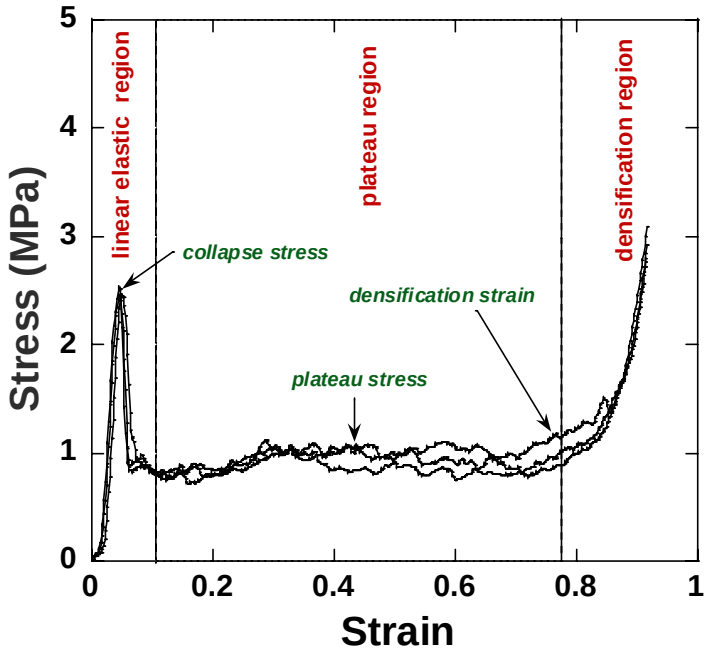

Figure 4.1. The compression stress-strain curves of Nomex® honeycomb samples (cell size 4.8 mm, deformed at 1.64×10^{-2} s^{-1})

In all tested honeycomb samples, the initial peak load and the following deformation regions stated are detected. It is also noted in Figure 4.1 that the stress values between individual tests slightly differs from each other. The differences in stress values however increase particularly at the later stages of the plateau region near the densification strain. Figures 4.2.a and 4.2.b show sequentially the compression stress-strain curves of 3.2 and 6.4 mm cell size honeycomb samples. The same deformation regions are also noted in these figures, showing globally the similar deformation sequences in different cell size honeycomb samples.

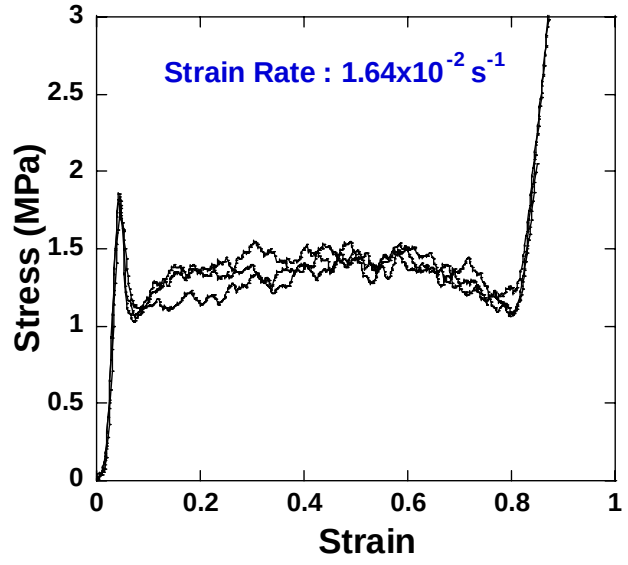

(a)

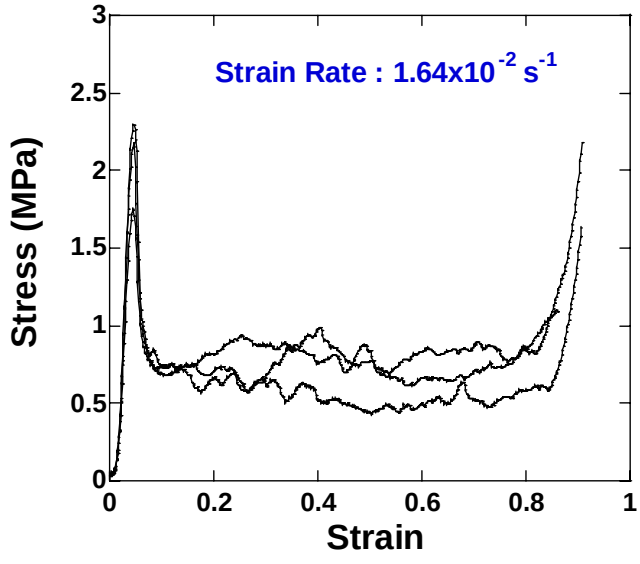

(b)

Figure 4.2. Stress-strain curves of (a) 3.2 and (b) 6.4 mm cell size Nomex® honeycombs.

The typical stress-strain curves of three different cell size honeycombs are shown together in Figure 4.3 for comparison. The effects of cell size on the stress-strain curves are as follows; as the cell size increases (a) plateau stress decreases and (b) densification strain slightly increases. As is clear from Figure 4.3 the increase in the cell size results in a decrease in the average crushing loads. In a honeycomb structure, an increase in the numbers of cells which means a decrease in the cell-size in a constant area, results in increase in the average crushing force. It is also noted in Figure 4.3 that 4.8 mm cell size honeycomb shows the highest peak load and 6.4 mm cell size honeycomb the lowest peak load. The peak stress corresponds to the buckling of the common edge of three honeycomb cells. The peak load is expected to be affected by the thickness of the cells, as well as the resin material used to bond the cells. In order to get equal densities from different cell size honeycombs, different types of resins are generally used and each resin may affect the material properties differently.

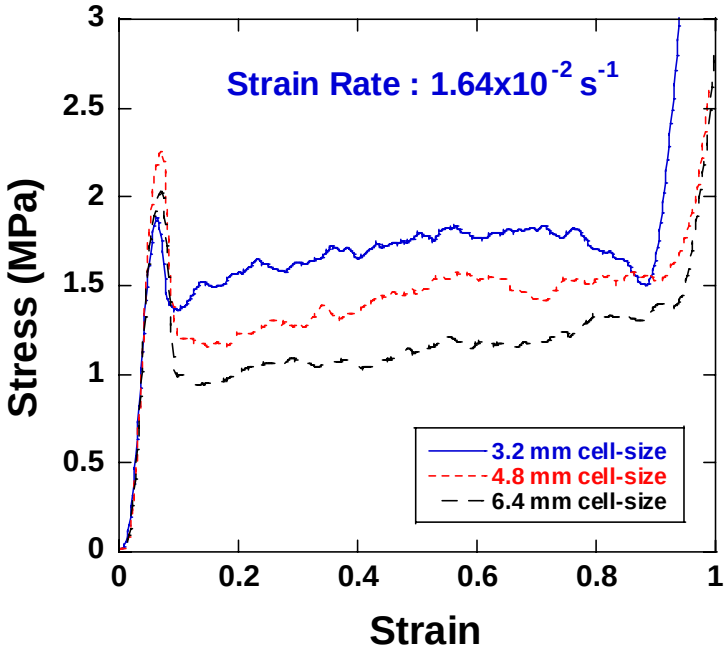

Figure 4.3. The typical stress-strain curves of 3.2, 4.8 and 6.4 mm cell size honeycombs

4.2. The Deformation of Honeycomb Filler

For the Nomex® honeycomb structures compressed in the thickness direction, the deformation mechanism started with the bending of the cell walls which gives linear elastic deformation. Beyond a critical strain the cells collapse by plastic yielding, creep or brittle fracture depending on the nature of the cell wall resin type for all three types of honeycombs. The collapsing of cell walls ended with the opposing cell walls began to contact each other and the structure densified and its stiffness increased rapidly. In case of Nomex® honeycombs the crush response consists three phases : the elastic buckling of cell walls followed by a plastic buckling, debonding fracture at the cell interfaces and the fracture of the resin layer due to the resin type.

The deformed top and side views of a 3.2 mm cell size honeycomb sample are shown sequentially in Figures 4.4.a and 4.4.b. The sample deformed until about the strains above the densification strain and gives valuable information about the deformation mechanism involved. The folding of the cells in the form of local buckling as in the case of circular tubes is presumably started following the initial maximum load, triggering from one of the free ends. The folding progresses gradually as the vertical edges of the sample start deform in the plateau region. Interpenetrating local tears and local separations are observed on the vertical edge. In the plateau region, honeycomb may deform either symmetrically or non-symmetrically. In 3.2 mm cell size honeycomb, as shown in Figure 4.4.b, the folding is progressive and symmetrically occurring without breaking the cell walls but some local tears take place on the vertical edges. Figures 4.5.a and 4.5.b show sequentially, the deformed top and side views of a 4.8 mm cell size honeycomb sample. As is seen in these pictures, the deformation is partly non-symmetrical and the tearing of vertical edges and the brittle fracture of the cell walls occur. Resulting from non symmetrical deformation and vertical edge tearing, continuous plastic fold formation as in 3.2 mm cell size sample is not observed. It is further noted that, the deformation character of 6.4 mm cell size filler is the same with that of 4.8 mm honeycomb filler. The cell walls tear (Figure 4.6.a) and the deformation continues with the fracture of the phenolic resin layer (Figure 4.6.b).

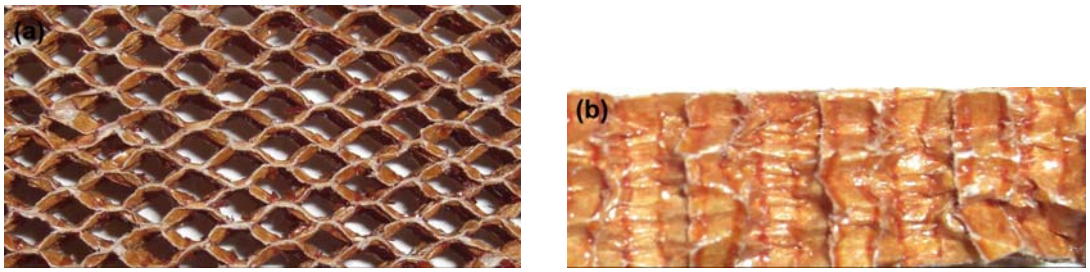

Figure 4.4. Deformed 3.2 mm cell size Nomex® honeycomb sample: (a) top and (b) side view

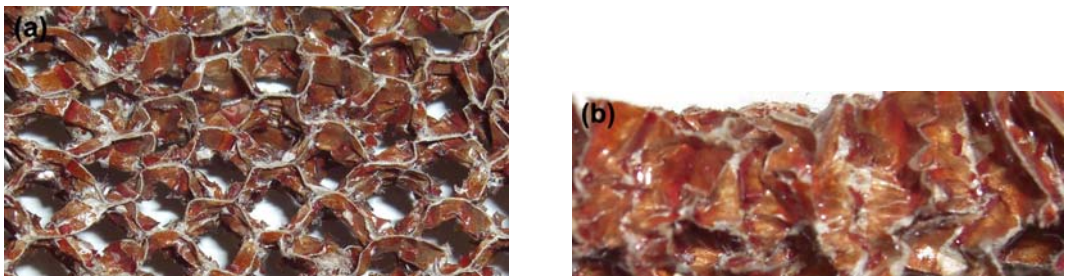

Figure 4.5. Deformed 4.8 mm cell size Nomex® honeycomb sample; (a) top and (b) side view

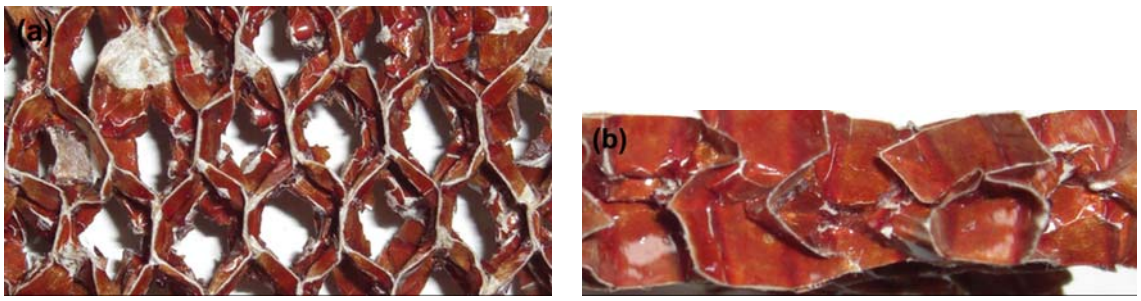

Figure 4.6. Deformed 6.4 mm cell size Nomex® honeycomb sample; (a) top and (b) side view

The uniform deformation and symmetrical folding mechanism are expected to result in higher energy absorption than non-symmetrical folding. Further, the tearing of the cell-walls tends to decrease the energy absorption. The dissipated energy is mainly absorbed by the vertical edges through the formation of plastic hinges and the compatibility zones in the honeycomb cell walls. In testing double layer honeycomb samples (two layers stick with epoxy), the bond section was separated in few samples; therefore, the cell collapse started from the mid-section.

The load-strain graphs of 3.2, 4.8 and 6.4 mm cell size honeycomb double and single layer honeycomb samples are shown in Figure 4.7.a-c, respectively. The effects of bond layer on load displacement curves of honeycomb samples shown in Figure 4.7.a-c are as follow: in double layer samples the load values in the plateau region and the peak load values are lower than those of single layer honeycomb samples. The reduced peak load values in double layer samples simply may arise from the fold triggering in the bonded region of the honeycomb layers. The cell wall collapse in 6.4 and 3.2 mm cell size honeycomb double layer samples starts in the bonded section, while in 4.8 mm cell size samples the triggering is very much similar with that of single layer samples, leading to similar load values.

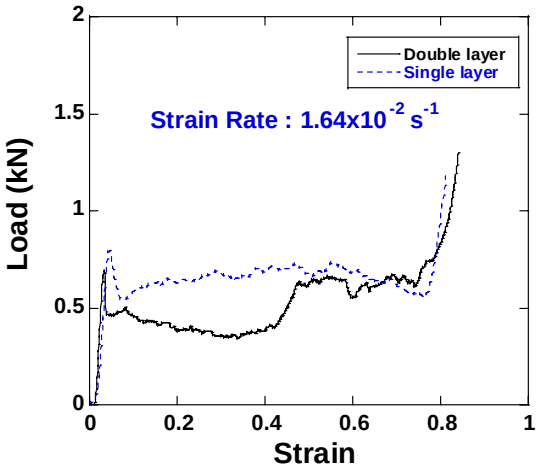

(a)

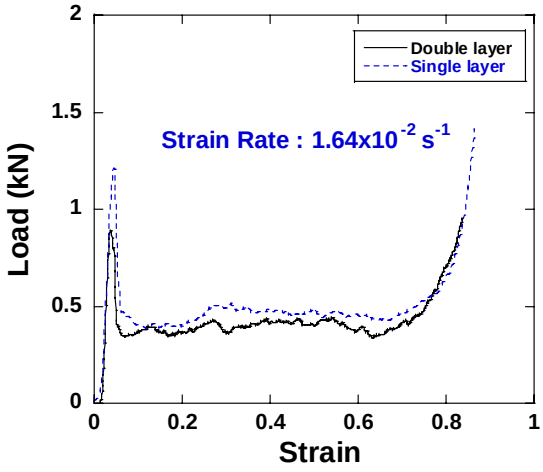

(b)

Figure 4.7. The load-strain curves of (a) 3.2 (b) 4.8 and (c) 6.4 mm cell size double and single layer honeycomb samples

(cont. on next page)

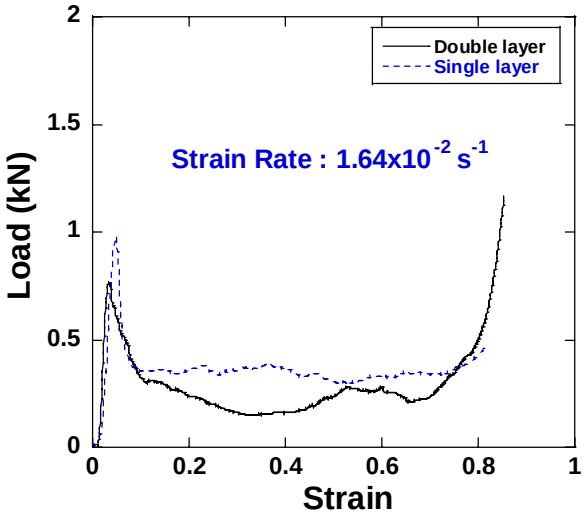

(c)

Figure 4.7. (cont.) The load-strain curves of (a) 3.2 (b) 4.8 and (c) 6.4 mm cell size double and single layer honeycomb samples

The average plateau loads of honeycombs are calculated from the plateau region and found 0.692, 0.503 and 0.370 (kN) for 3.2, 4.8 and 6.4 cell size honeycombs. The crushing loads and strength of honeycombs are also calculated using Equation 2.24 and 25 respectively and tabulated in Table 4.1. Equation 2.24 gives the similar crushing load values with experiments. The details of the crushing load and strength calculations of honeycombs are given in Appendix A.

Table 4.1. Calculated and experimental mean crushing loads and strength values of honeycombs.

Honeycomb cell size (mm)	**Mean crushing load (KN) (Equation 2.24)**	**Mean crushing load (kN) (Experimental)**	**Crushing Strength (MPa) (Equation 2.25)**	**Crushing Strength (MPa) (Experimental)**
3.2	0.717	0.692 0.532*	5.38	4.1
4.8	0.546	0.503 0.428*	2.7	2.741
6.4	0.362	0.370 0.3*	1.69	1.8

* Double layer samples

4.3. The Deformation Behavior of Empty and Nomex® Honeycomb Filled Tubes

4.3.1. The Deformation Behavior of Empty Tubes

The empty tubes deformed dominantly in mixed mode within the studied strain rate regime, while few samples deformed in concertina and diamond mode. The folding starts from of the ends of the tube in axisymmetric mode and is reverted into asymmetric mode after axisymmetric fold formation. The typical load-displacement curve of the empty tube is shown in Figure 4.8. The densification starts after 20 mm, corresponding to 80% deformation and total 3-4 fold are formed as marked in Figure 4.8. Deformed tube samples front, back and side views are shown sequentially for concertina, mixed and diamond mode of deformation in Figures 4.9, 4.10 and 4.11, respectively.

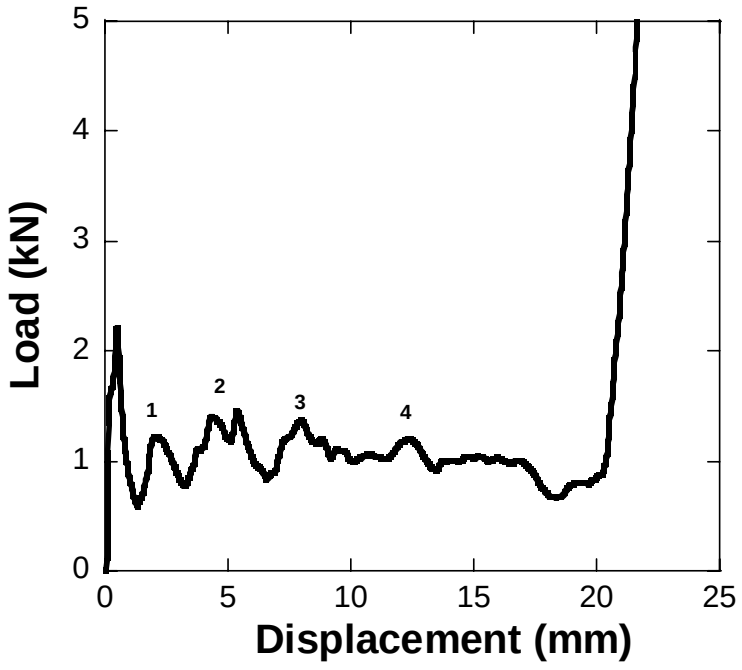

Figure 4.8. Typical load-displacement curve of empty aluminum tube ($1.64x10^{-2}$ s^{-1})

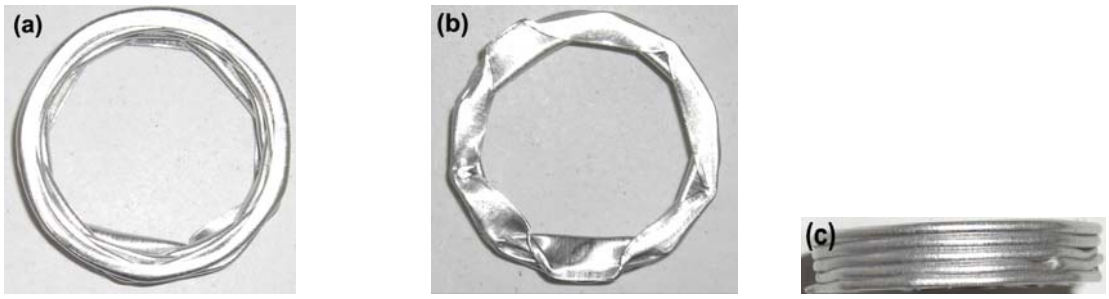

Figure 4.9. Pictures of tube deformation in concertina mode: (a) front, (b) back and (c) side views.

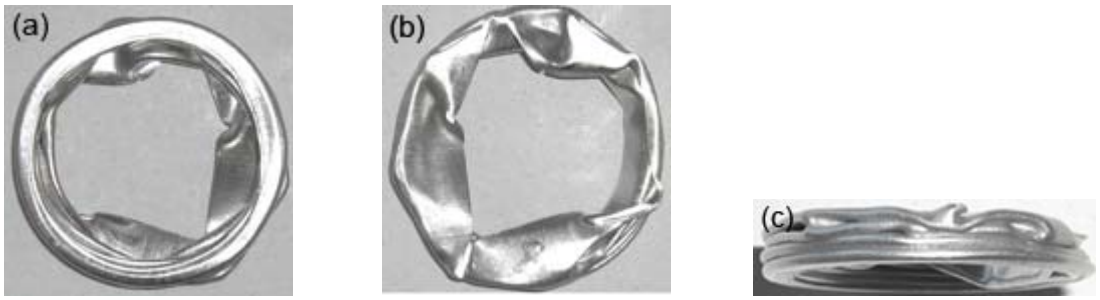

Figure 4.10. Pictures of tube deformation in mixed mode: (a) front, (b) back and (c) side views.

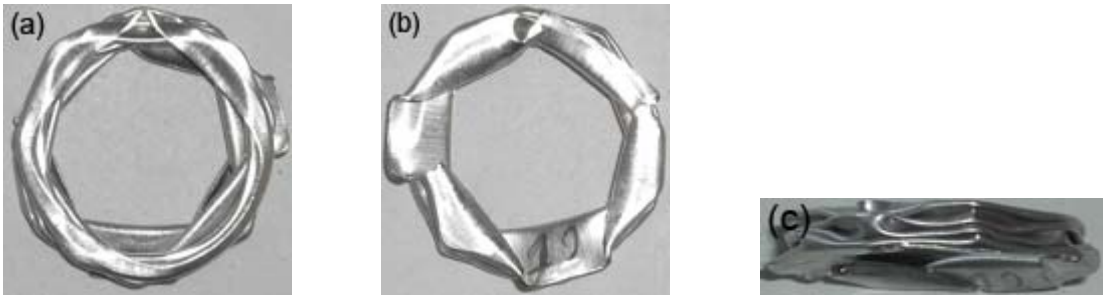

Figure 4.11. Pictures of tube deformation in diamond mode: (a) front, (b) back and (c) side views.

The effect of deformation rate (cross-head speed) on the empty tube load-displacement curves are shown in Figure 4.12. When considered the scattering of the load values, the tubes are found to show no significant differences in load values at strain rates of 6.56×10^{-3}, 3.28×10^{-3} and 1.64×10^{-2} s^{-1}. The variation of the load values of the Al tubes between the individual tests at a loading rate of 1.64×10^{-3} s^{-1} are shown in Figure 4.13. The average crushing loads of empty tubes are calculated and the results were averaged. An average load of 1.108 (kN) is calculated for the empty tube.

The average crushing loads of empty tube are also calculated using analytical approaches in the literature. The results of calculations are tabulated in Table 4.2. The details of calculations are further given in Appendix B. Table 4.2 shows that Pugsley's and Wierzbicki's approaches of diamond mode of deformation give the average crushing loads comparable with that of experiment. The fold lengths of the empty tubes are found 2.833, 3.1 and 3.24 mm for the strain rates of $1.64x10^{-2}$, $6.56x10^{-3}$ and $3.28x10^{-3}s^{-1}$ which corresponds to the cross-head speed of 25, 10 and 5 mm/min respectively.

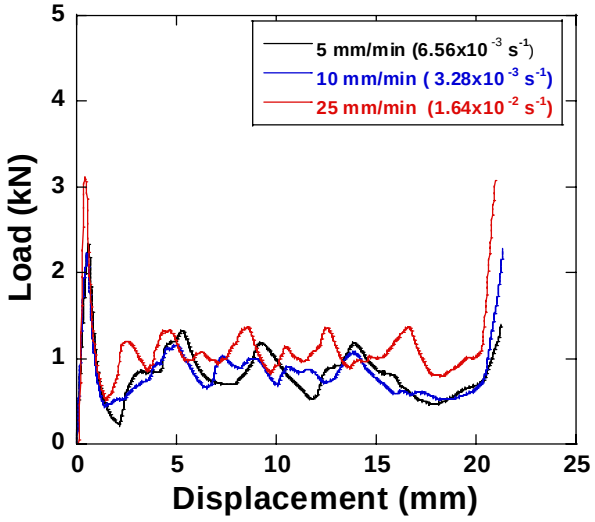

Figure 4.12. The effect of loading rate on load-displacement curve of empty tube

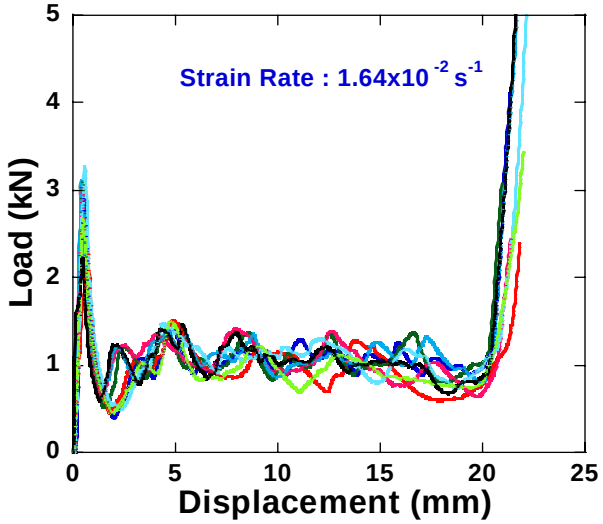

Figure 4.13. The load displacement curve for empty tubes compressed at the strain rate of $1.64x10^{-2}(s^{-1})$

Table 4.2. The average crushing loads and deformation modes with analytical, experimental results

Approach	Formulation of P_a	Deformation Mode	Analytical Results
Alexander	$6\sigma_0 t(Dt)^{1/2}$	Concertina	**0.726 kN**
Abramowicz & Jones	$\sigma_0 t(6(Dt)^{1/2}+3.44t)$	Concertina	**0.804 kN**
Abramowicz & Jones	$86.14(D/t)^{0.33}\sigma_0(t^2/4)$	Concertina	**1.286 kN**
Abramowicz & Jones	$\dfrac{\sigma_0\sqrt{Dt}+3.44t}{0.86-0.568\sqrt{t/D}}$	Diamond	**1.008 kN**
Pugsley & Macaulay	$\sigma_0 t(10.05t+0.38D)$	Diamond	**0.573 kN**
Pugsley	$2.286n^2\sigma_0 t^2$	Diamond	**1.148 kN**
Wierzbicki	$18.15\sigma_0 t^2(D/t)^{1/3}$	Diamond	**1.098 kN**
Wierzbicki	$11.22\sigma_0 t^2(R/t)^{1/2}$	Diamond	**1.006 kN**
Wierzbicki	$7.933\sigma_0 t^2(D/t)^{1/2}$	Concertina	**1.007 kN**
Singace	$P_a=\sigma_0 t^2(7.874(R/t)^{1/2}+1.4$	Diamond	**0.725 kN**
Singace	$(\sigma_0 t^2/2\sqrt{3})22.27\sqrt{D/t}+5.6$	Concertina	**0.833 kN**
Guillow	$\sigma_0(t^2/4)72.3(D/t)^{0.32}$	Diamond	**1.33**

(The experimental average crushing load is found as 1.108 kN)

4.3.2. The Deformation Behavior of Honeycomb Filled Tubes

The load-displacement curves of 3.2, 4.8 and 6.4 mm cell size honeycomb filled Al tubes deformed at $1.64x10^{-2}s^{-1}$ strain rate are sequentially shown in Figure 4.14.a-c, respectively. In 3.2 mm cell size honeycomb filled tubes the deformation mode changes from diamond/mixed to concertina/mixed mode of deformation (Figure 4.15), while honeycomb filling with 6.4 mm and 4.8 mm cell size is found not to affect the deformation mode of empty tube as shown in Figure 4.16 and Figure 4.17.

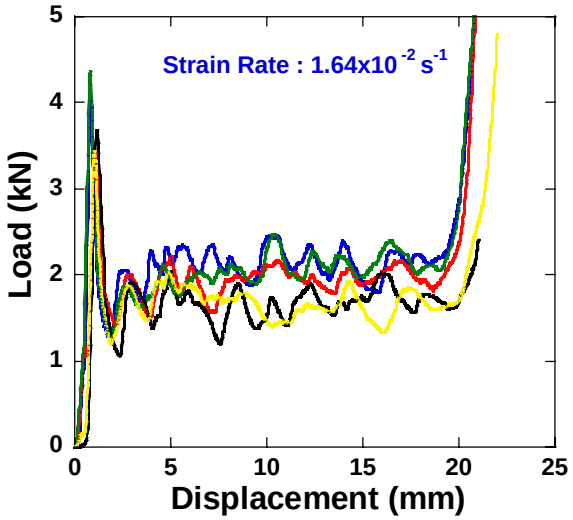

(a)

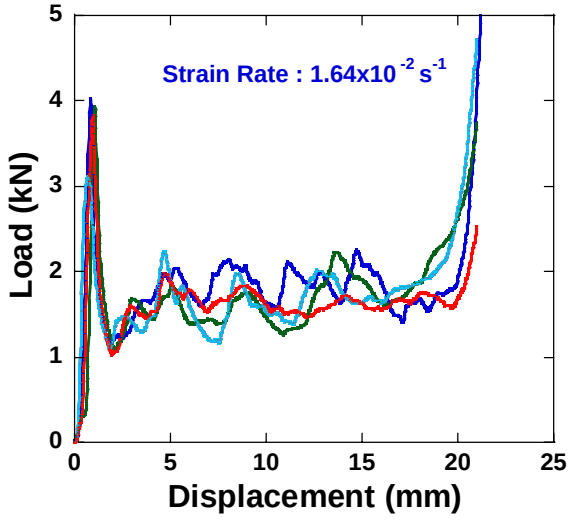

(b)

Figure 4.14. Load-displacement curves of (a) 3.2 mm (b) 4.8 mm and (c) 6.4 mm cell size honeycomb filled tubes

(cont. on text page)

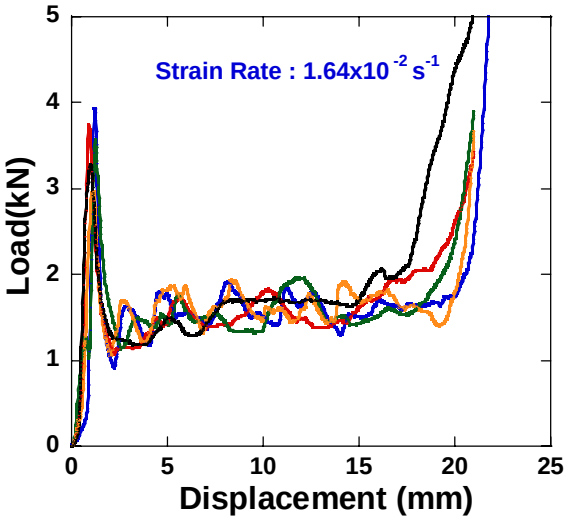

(c)

Figure 4.14. (cont.)Load-displacement curves of (a) 3.2 mm (b) 4.8 mm and (c) 6.4 mm cell size honeycomb filled tubes

Figure 4.15. Deformed 3.2 mm cell size honeycomb filled tubes (a) top view, (b) cross-section and (c) side view

Figure 4.16. Deformed 4.8 mm cell size honeycomb filled tubes (a) top view, (b) cross-section and (c) side view

Figure 4.17. Deformed 6.4 mm cell size honeycomb filled tubes (a) top view (b) cross-section and (c) side view

Figures 4.18.a-c show sequentially the typical load-displacement curves 3.2, 4.8 and 6.4 mm honeycomb filled Al tubes together with empty tube load-displacement curve. As is seen in these figures, honeycomb filling increases peak load values and plateau stress values and decreases the densification strain. The fold length is found to increase as the cell size increases. The fold lengths are calculated for each type of the specimens. In 3.2 mm cell-size honeycomb filled samples deformed at $1.64x10^{-2}s^{-1}$ strain rate, the fold length is 2.524 mm and in the samples deformed at $6.56x10^{-3}s^{-1}$ it is 3.273 mm. The average fold length at $3.28x10^{-3}s^{-1}$ strain rate is calculated 3.275 mm. The average fold lengths are 2.813 mm for the 4.8 mm cell size honeycomb filled tubes deformed at $1.64x10^{-2}s^{-1}$ strain rate while the fold length is 3.128 mm and 3.397 mm for $6.56x10^{-3}s^{-1}$ and $3.28x10^{-3}$ s^{-1} respectively. The average fold lengths of 6.4 mm cell-size honeycomb filled tubes are sequentially 2.953 mm, 3.410 mm and 3.702 mm for $1.64x10^{-2}s^{-1}$, $6.56x10^{-3}s^{-1}$ and $3.28x10^{-3}s^{-1}$ strain rates respectively. The effect of deformation rate on the load-displacement curves of 3.2, 4.8 and 6.4 mm cell size honeycomb filled tubes are shown in Figures 4.19.a-c, respectively.

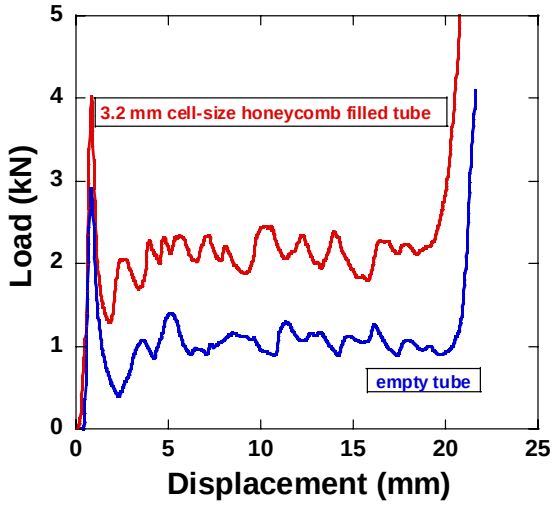

(a)

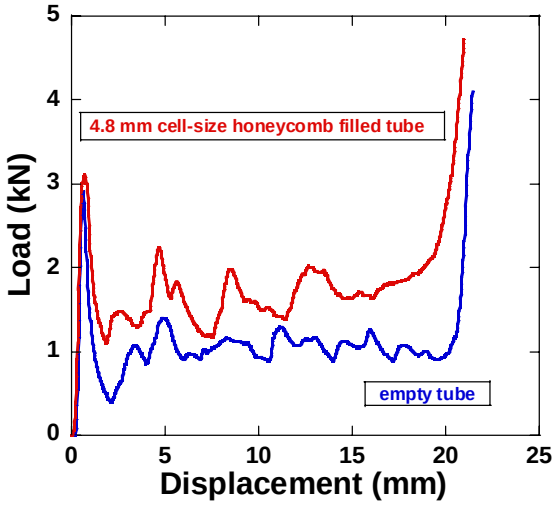

(b)

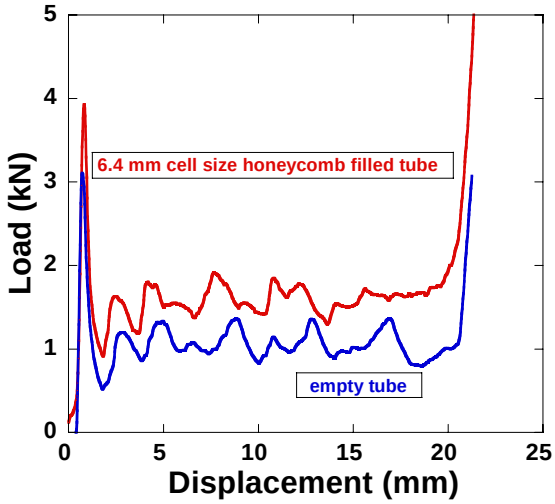

(c)

Figure 4.18. Typical Load-displacement curves of the honeycomb filled and empty tubes; (a) 3.2 mm, (b) 4.8 mm and (c) 6.4 mm cell size honeycomb

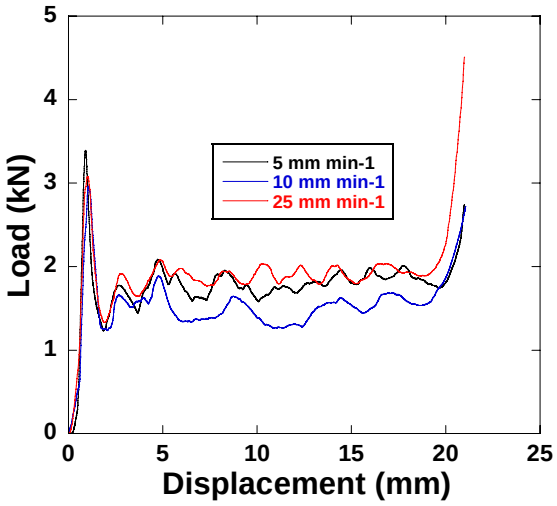

(a)

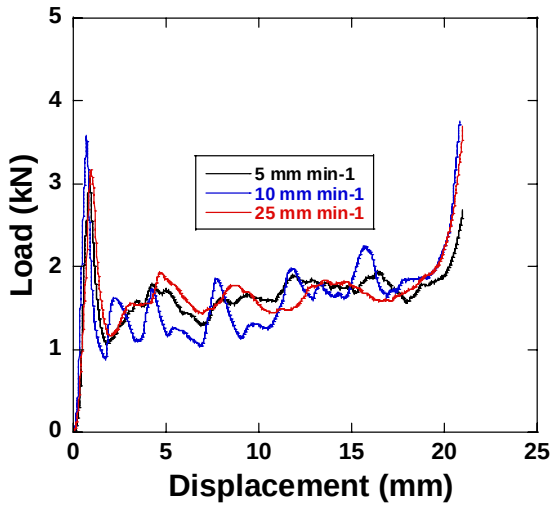

(b)

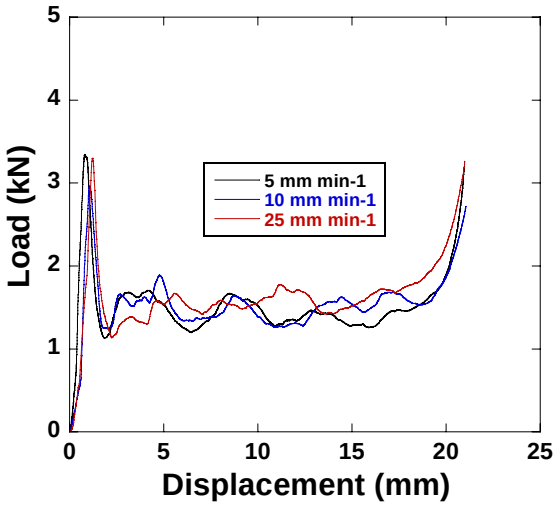

(c)

Figure 4.19. The load-displacement curves of filled tubes at different deformation rates (a) 3.2 mm (b) 4.8 mm (c) 6.4 mm cell size honeycomb filled tubes

4.4. Effect of Honeycomb Filling On the Average Crush Load, Specific Absorbed Energy and Stroke Efficiency

Figure 20.a-c shows sequentially the effect of honeycomb filling on the average crushing loads of empty tubes for 3.2, 4.8 and 6.4 mm honeycomb filling. The average crushing loads increases with decreasing honeycomb cell size as seen in Figure 4. 21.a Although the average crushing load of empty tube is pretty much constant in the plateau region, the average crushing loads of filled tubes increase slightly in the plateau region with increasing displacement. It is further noted that, honeycomb filling decreases the differences between the initial average crushing peak load and average crushing loads in the plateau region, leading to more homogenous deformation of the tube. The highest average crushing load and maximum load are found in 3.2 mm cell-size honeycomb filled tube as shown in Figure 4.21.a and 4.21.b, respectively. The average crushing loads, maximum load, SE and the other important crush properties of the filled tubes are further listed in Appendix C.

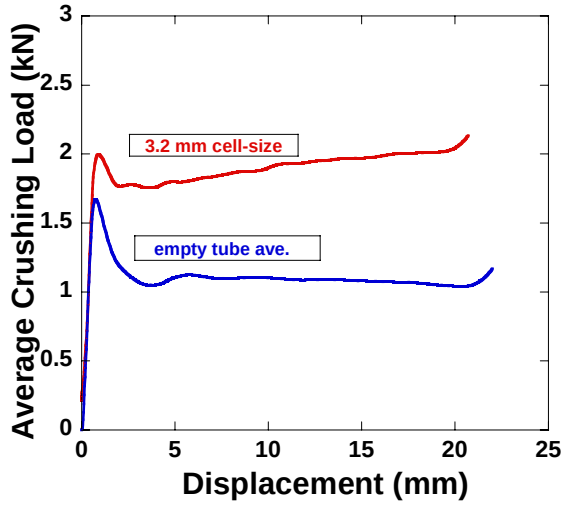

(a)

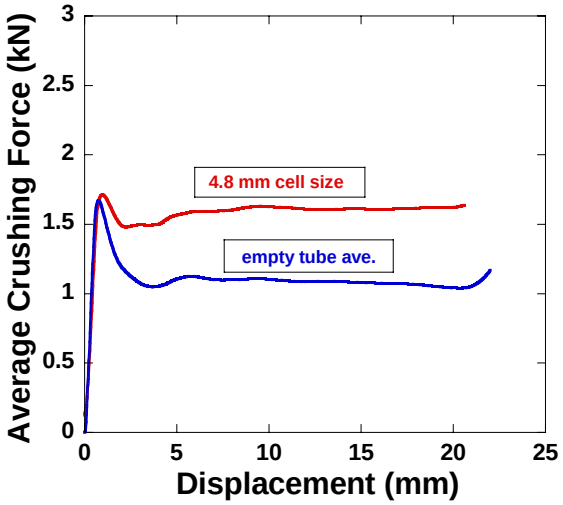

(b)

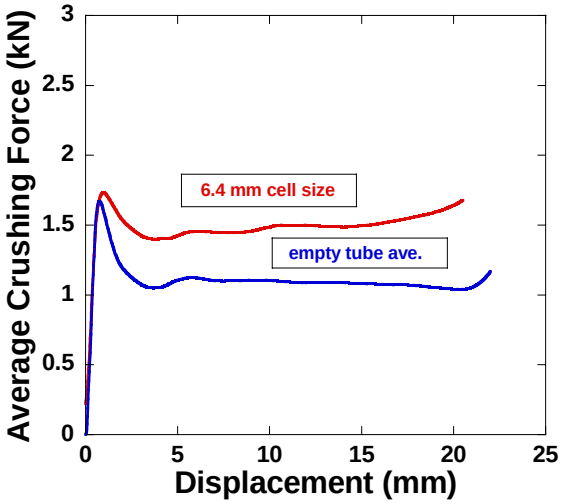

(c)

Figure 4.20. Effect of honeycomb filling on the average crushing loads of (a) 3.2, (b) 4.8 and (c) 6.4 mm honeycomb filled tubes (1.64×10^{-2} s^{-1})

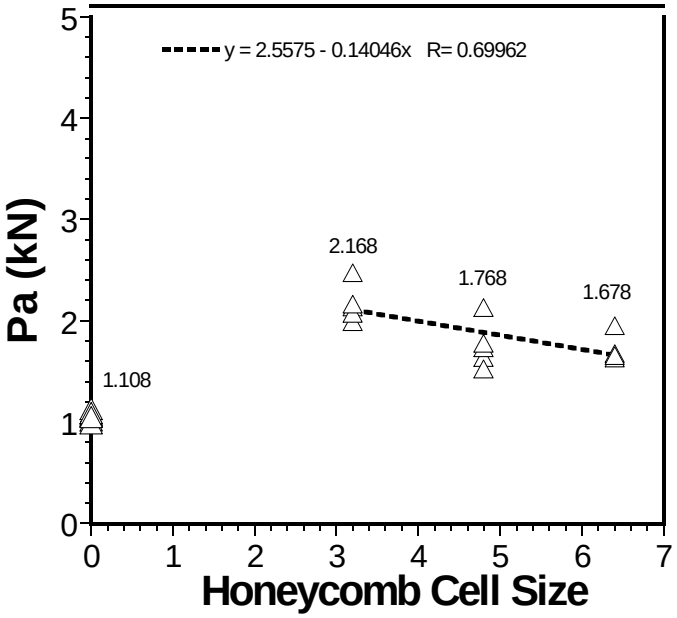

(a)

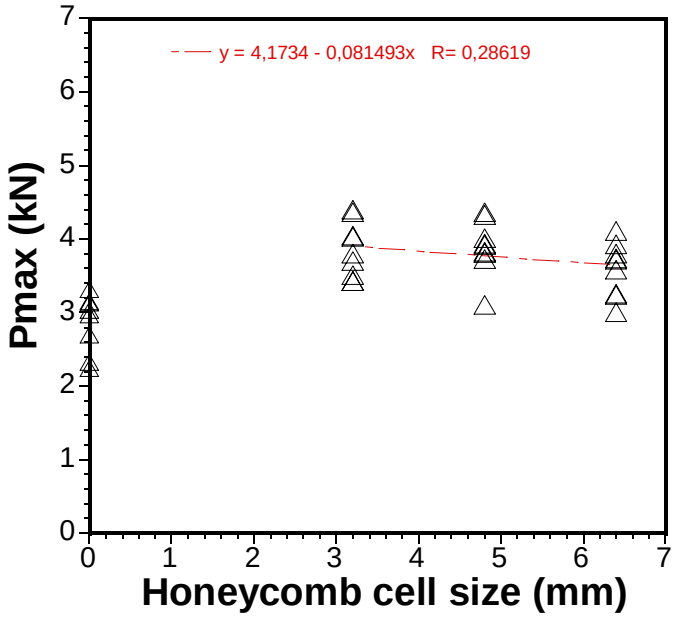

(b)

Figure 4.21. (a) Pa and (b) P_{max} vs. honeycomb cell size

The stroke efficiencies of the filled tubes and empty tubes are almost the same as depicted in Figure 4.22. The stroke efficiencies are determined as 0.75, 0.73 and 0.73 for the 3.2, 4.8 and 6.4 mm cell-size honeycomb filled tubes and 0.75 for empty tubes.

The specific absorbed energy -displacement curves are shown in Figures 4.23.a-d for 3.2, 4.8 and 6.4 mm cell size honeycomb filled tubes and empty tubes, respectively. 3.2 mm cell size honeycomb filled tubes results in the highest SAE values at 50% displacement and at the stroke efficiency (Figure 4. 24). The SAE values of filled and empty tubes at 50% and at stroke efficiency deformations are further listed in Appendix C.

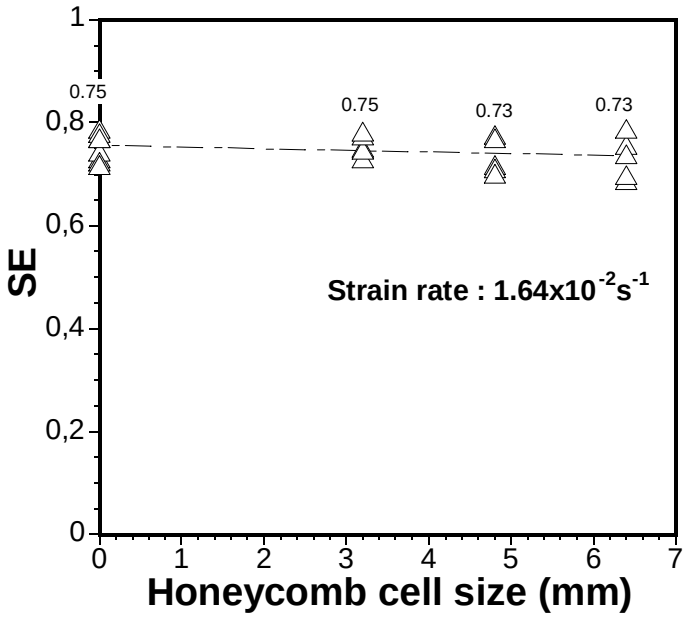

Figure 4.22. SE vs. honeycomb cell size

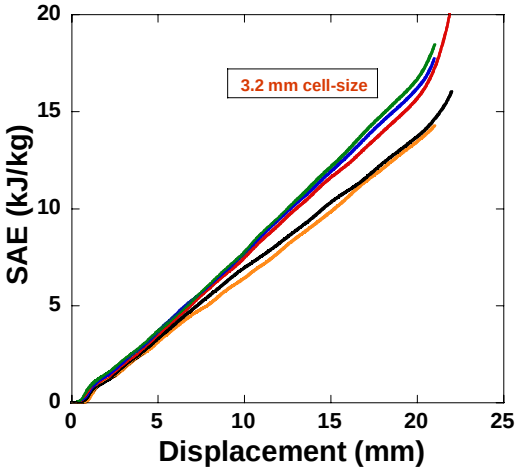

(a)

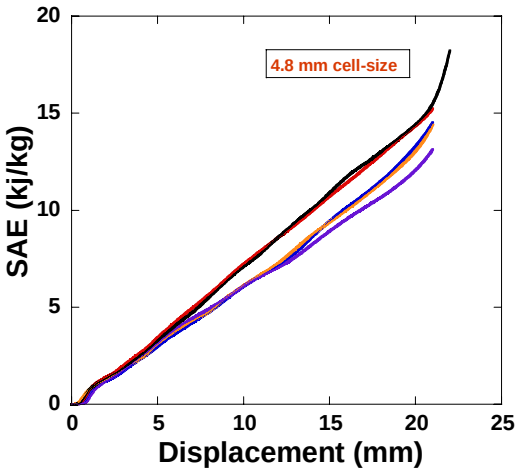

(b)

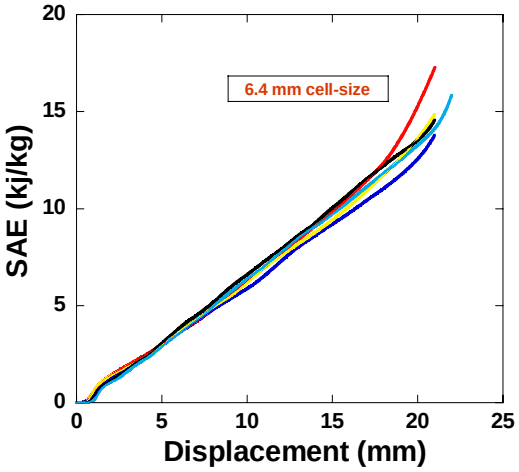

(c)

Figure 4.23. The comparison between the SAE's of (a) 3.2, (b) 4.8 and (c) 6.4 mm honeycomb filled tubes and (b) empty tube (1.64×10^{-2} s^{-1})

(cont. on next page)

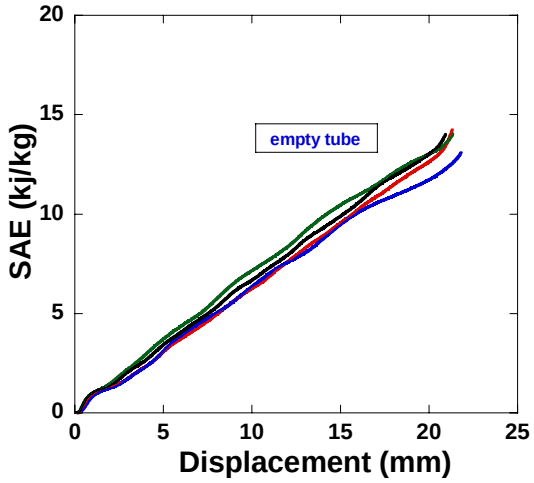

(d)

Figure 4.23. (cont.)The comparison between the SAE's of (a) 3.2, (b) 4.8 and (c) 6.4 mm honeycomb filled tubes and (b) empty tube ($1.64x10^{-2}$ s^{-1})

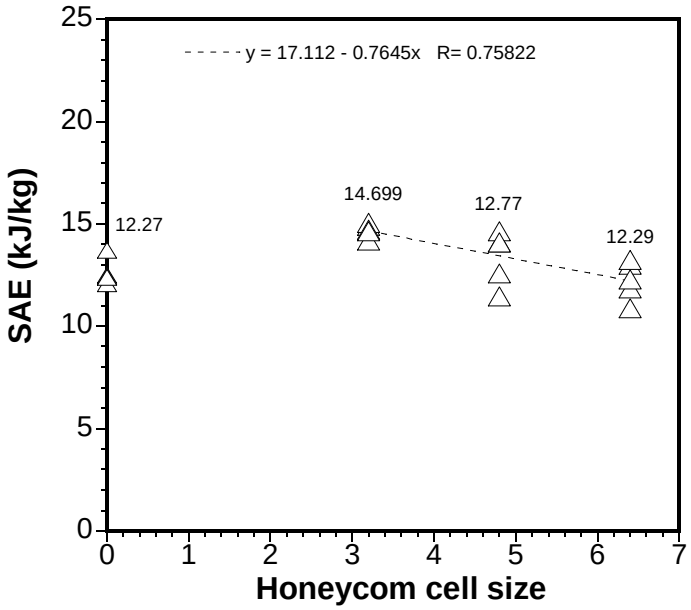

Figure 4.24. SAE at stroke efficiency versus honeycomb cell size

The variations of TE with displacement are shown in Figure 4.25.a-c. for 3.2, 4.8 and 6.4 mm honeycomb filled tubes. TE values of 4.8 and 6.4 mm honeycomb filled tubes show variation while TE values of 3.2 mm honeycomb filled tubes show relatively small scattering, proving a more stable crushing in small size honeycomb filling of tubes (Figure 4.26). On the average, the highest TE is found in 3.2 mm honeycomb filled tubes.

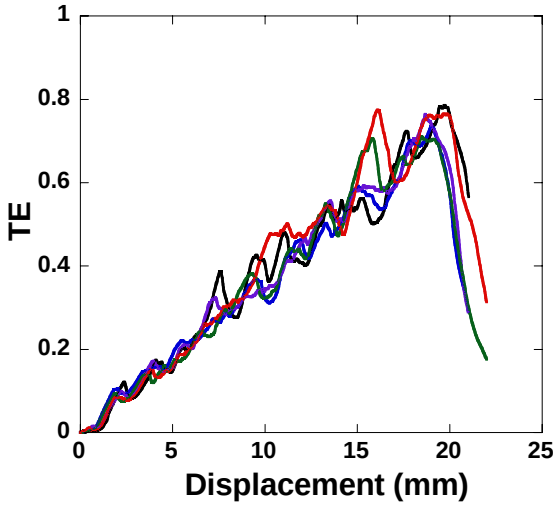

(a)

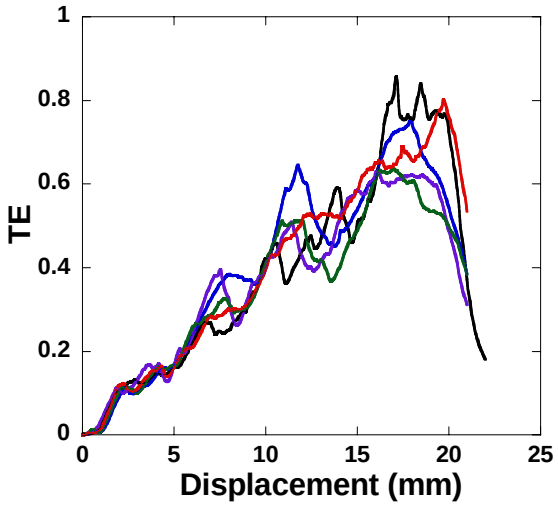

(b)

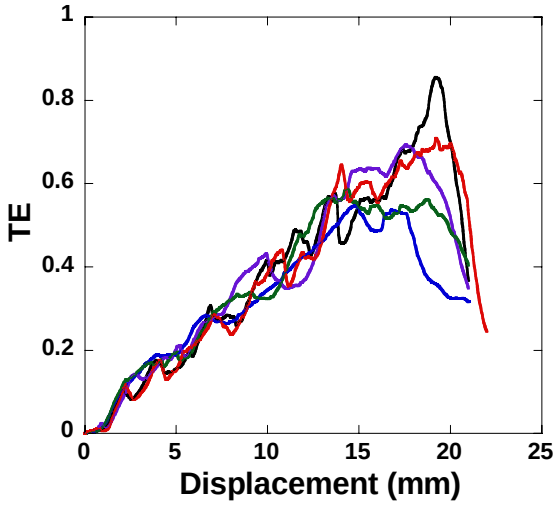

(c)

Figure 4.25. The total efficiency and corresponding stroke efficiency values for the filled tubes (a)3.2 mm (b)4.8 mm and (c)6.4 mm honeycomb filled tubes

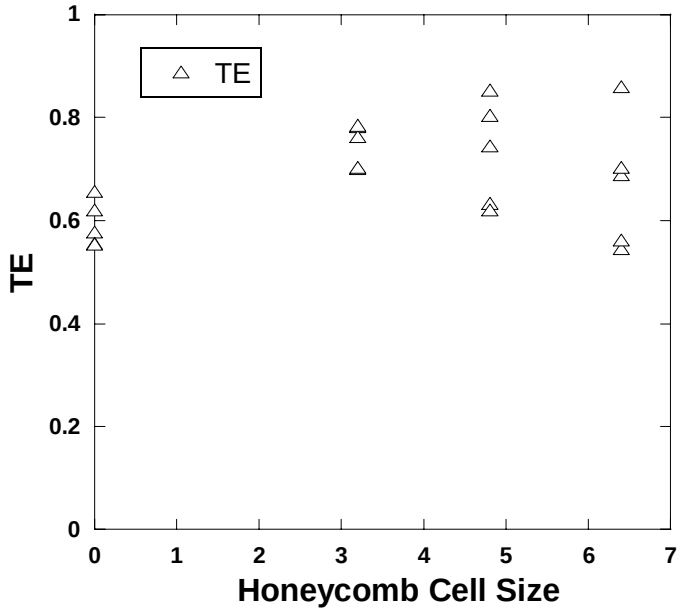

Figure 4.26. Variation of TE with honeycomb cell size at stroke efficiency

4.5. The Interaction Effect

The interaction effects are shown in Figure 4.27.a-c sequentially for 3.2, 4.8 and 6.4 mm honeycomb filled tubes. The interaction effect is found in all honeycomb filled tubes. The value of C in equation. (2.23) is calculated (Appendix D). The C values for 3.2 mm, 4.8 and 6.4 mm honeycomb filled samples are 1.53, 1.32 and 1.48, respectively. The C values based on the double layer honeycomb are sequentially 1.99, 1.54 and 1.83 for 3.2 mm, 4.8 and 6.4 mm honeycomb filled samples, respectively. The average C values, (single layer + double layer)/2 are 1.76, 1.43 and 1.65 for 3.2 mm, 4.8 and 6.4 mm honeycomb filled samples, respectively. The highest interaction effect is found for the smallest cell size honeycomb filling.

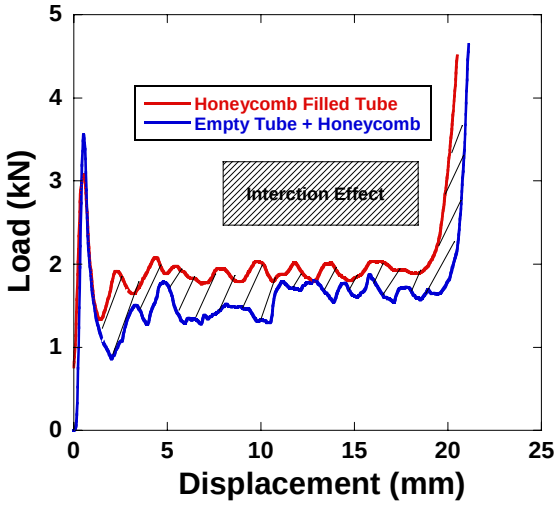

(a)

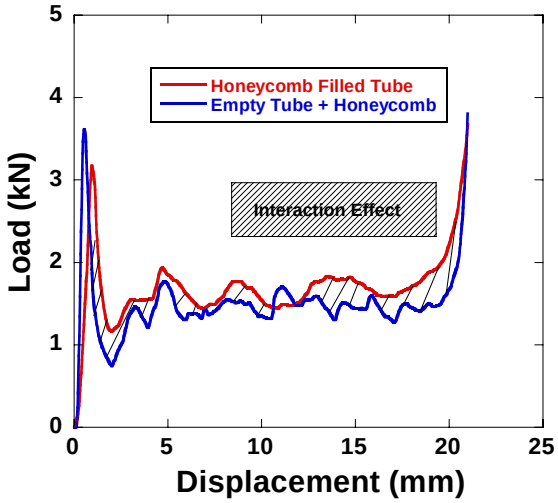

(b)

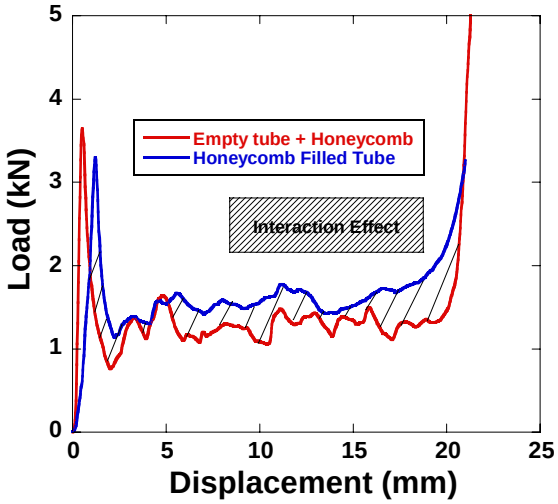

(c)

Figure 4.27. The interaction effect in (a) 3.2 mm cell size (b) 4,8 mm cell size (c) 6.4 mm cell size honeycomb filled tube

The deformed sections of 3.2 mm and 6.4 mm honeycomb filled tubes are shown in Figure 4.28.a and 4.28.b, respectively. Near to the tube folding a highly compressed honeycomb section is clearly seen in these figures. The compressed layer is clearly seen for 3.2 mm honeycomb filled tube sample (Figure 4.28.a).

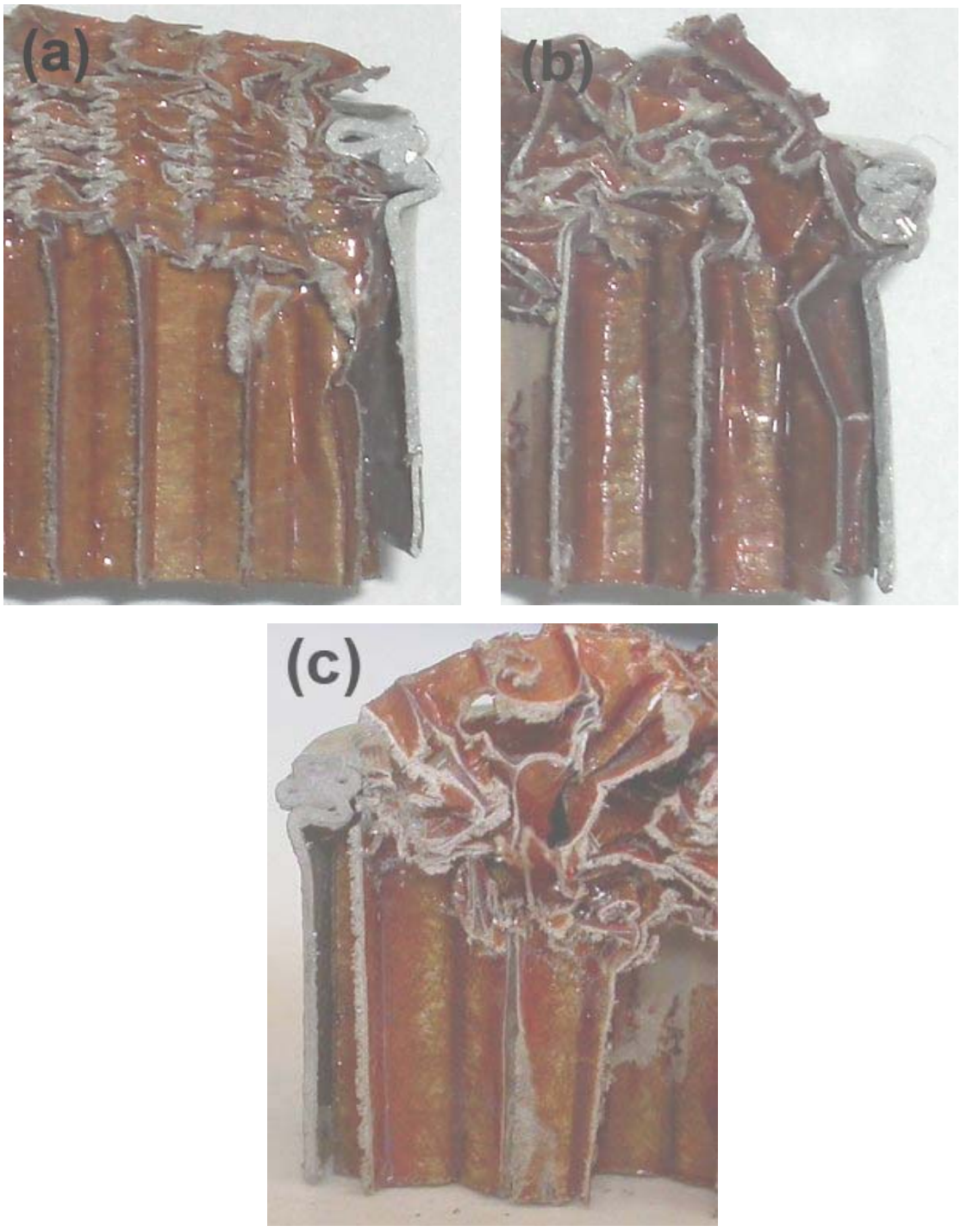

Figure 4.28. Partially compressed honeycombs between tubes: (a) 3.2 mm cell size (b) 6.4 mm cell size and (c) 4.8 mm cell size honeycomb filled tube

CHAPTER 5

NUMERICAL ANALYSIS

5.1. Numerical Modeling of Empty Tube, Honeycomb Filler and Honeycomb Filled Tubes

The numerical models of empty tube and the 6.4 mm cell size honeycombs were simulated. The empty tube model was constructed using LS-DYNA Prepost™ and the honeycomb filled tube (6.4 mm cell size) model was created in Solidworks™ (Solid works 2008 Manual). The meshed geometrical honeycomb model was subsequently exported to LS-DYNA™ software in order to set the boundary conditions and material properties. LS-Prepost™ was used for a post processor for the numerical solutions.

Honeycomb cells and aluminum tube were modeled using Belytschko-Tsay-4 node-thin shell elements. Since the honeycomb material shows anisotropy under compression, a symmetrical model is not applicable; therefore, the specimens were modeled in actual dimensions. The upper and bottom compression test plates were modeled as rigid body with kinematical boundary conditions. The motion of the upper compression plate was determined by an imposed motion (displacement) of a set of nodes in the upper plate. Automatic single surface contact was used between the bottom compression plate and the empty tube. The static and dynamic coefficients of frictions were taken as 0.20 and 0.15, respectively. Material type 024 (LS DYNA user manual), the piecewise linear plasticity, was used during the simulation of both the empty tubes and the honeycomb material. This model is an elasto-plastic material with an stress versus strain curve and strain rate dependency.

In the model, 6x20 elements (6 along the ribbon direction, 20 along the thickness direction) were used in each face of honeycomb sheet and a total of 12 complete hexagonal honeycomb cells were created. For the aluminum tube 40 x 80 elements were used.

In order to understand the mesh dependency behavior of the honeycomb, in empty and honeycomb filled tube, the mesh size was doubled and divided by two, respectively. It must be noted that the larger the element size yielding reasonable accuracy will increase the computational time and cost. By considering the same reason the simulation of the adhesive bonding was neglected.

5.2. The Mesh Optimization

In the finite element analysis number of mesh for a fixed geometry leads to variation in the element size, computational time and accuracy of the numerical results. The optimum mesh size has been established by refining the mesh until the convergence is reached. The mesh size was doubled and divided by two in order to define an optimum mesh size for the simulation.

5.2.1. The Mesh Optimization of Empty Tubes

In Figures 5.1.a, 5.1.b and 5.1.c, the numerical load-displacement curves of empty tube with the number of meshes of 40x40, 40x80 and 50x128 are shown together with experimental load-displacement curves, respectively. As is seen in Figures 5.1.b and 5.1.c, the load-displacement curves of models constructed with 40x80 and 50x128 elements give reasonably well agreements with the experimental load displacement curves, while the load displacement curve of the model constructed with 40x40 (Figure 5.1.a) elements shows much more disagreements with the experimental load-displacement curves in the initial region of the load-displacement curve. For the computational and time efficiency the 40x80 elements were considered as the optimum number of elements for this simulation.

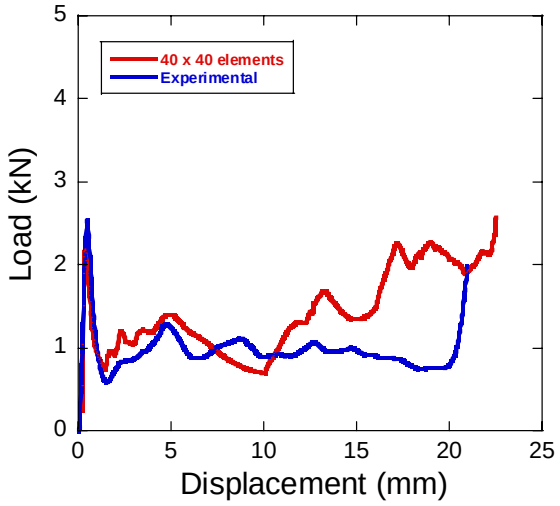

(a)

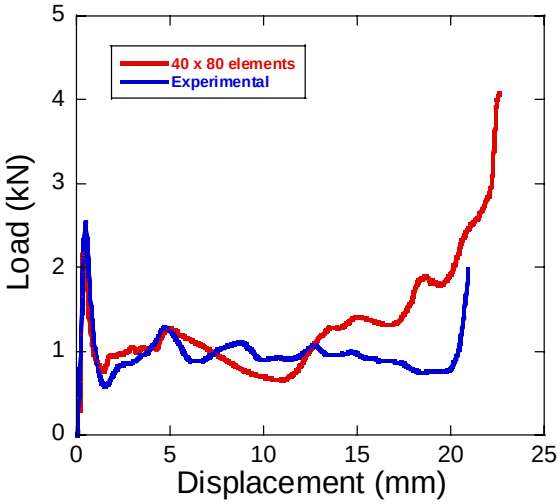

(b)

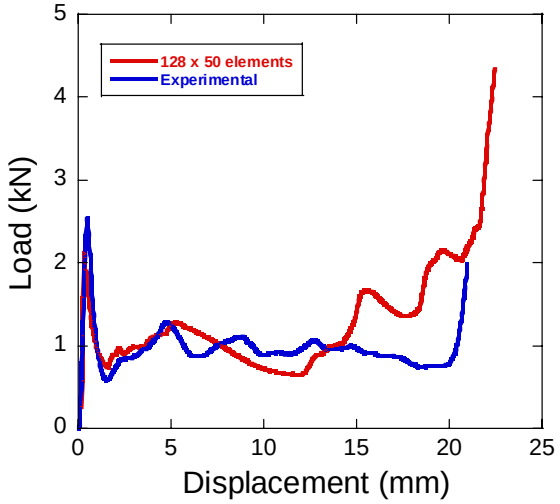

(c)

Figure 5.1. The Numerical and experimental load-displacement curves of empty tubes with (a) 1600, (b) 3200 and (c) 6400 elements

5.2.2. The Mesh Optimization of Honeycomb Filler

Figures 5.2(a), (b) and (c) show the numerical load-displacement curves of 6.4 mm cell size honeycomb with the number of elements of 3x20, 6x20 and 12x20, respectively. On these curves, the experimental load-displacement curves are also shown for comparison. The model with 6x20 and 12x20 give reasonable agreement with the experimental load-displacement curves, while the model with 3x20 elements shows disagreements at low and at high displacements.

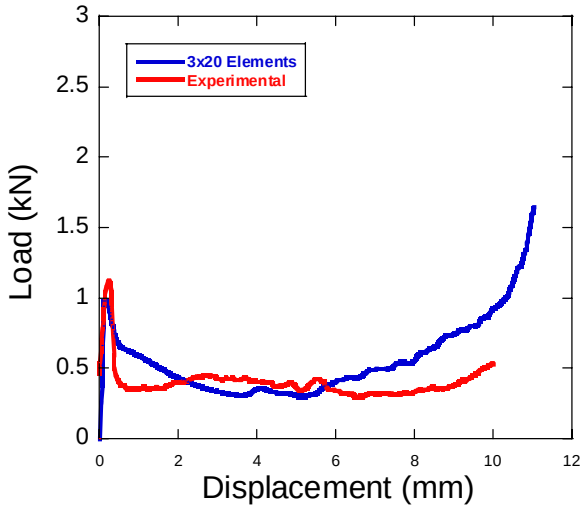

(a)

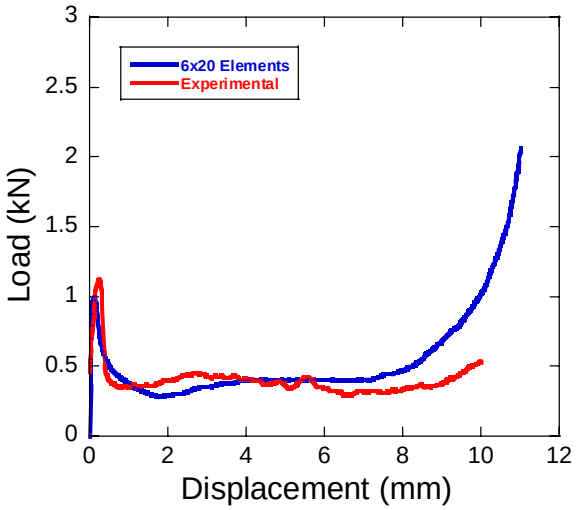

(b)

Figure 5.2. The Numerical and experimental load-displacement curves of honeycomb Filler of 6.4 mm cell size (a) 3x20, (b) 6x20, (c) 12x20 elements (at each wall of the honeycomb)

(cont. on next page)

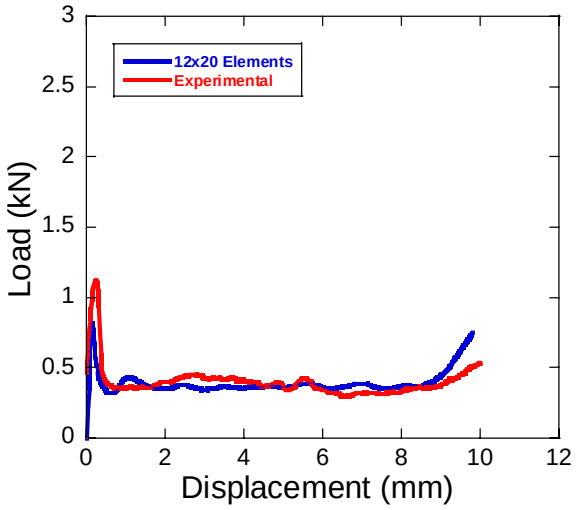

(c)

Figure 5.2. (cont.)The Numerical and experimental load-displacement curves of honeycomb Filler of 6.4 mm cell size (a) 3x20, (b) 6x20, (c) 12x20 elements (at each wall of the honeycomb)

5.2.3. The Mesh Optimization of Honeycomb Filled Tubes

Figures 5.3.a,b and c show sequentially the modeling load-displacement curves of 6.4 mm cell size honeycomb filled tube with number of elements of 40x40-3x20, 40x80-6x20 and 50x128-12x20 On the same curves, the experimental load-displacement curves are also shown for comparison. It is noted in Figure 5.3, the modeling results gives very much similar load-displacement values/curves with those of experiment when the element size is selected 50x128-12x20.

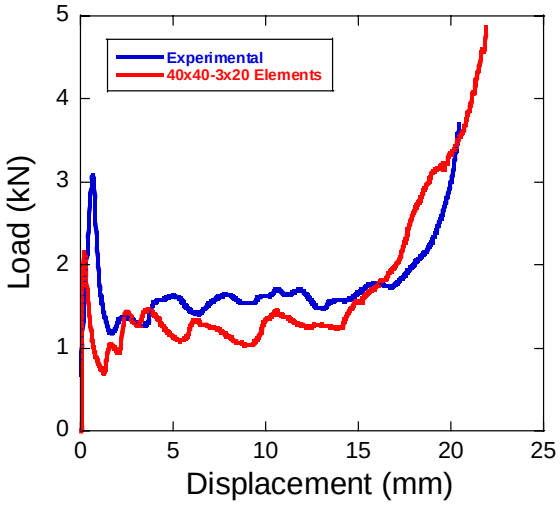

(a)

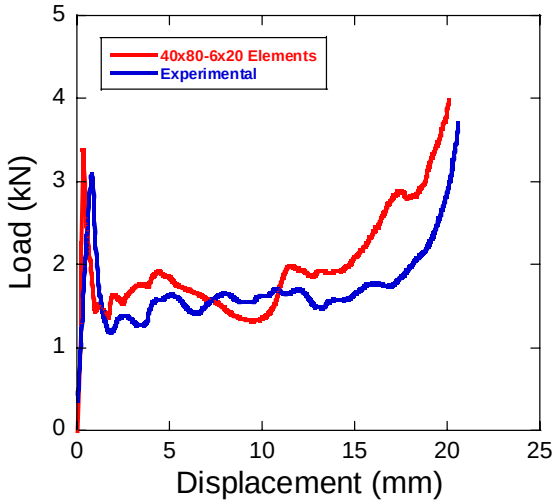

(b)

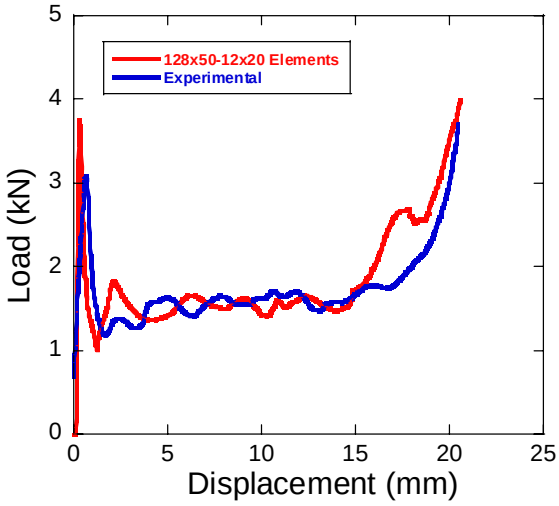

(c)

Figure 5.3. The Numerical and experimental load-displacement curves of honeycomb filled tubes: (a) 40x40-3x20, (b) 40x80-6x20 (c) 50x128-12x20 elements

5.3. The Comparison between Experimental and Numerical Results

Figures 5.4.a and 5.4.b show the numerical and experimental deformed empty tubes at various deformation levels, respectively. In the experiments, the tube deformation starts with axisymmetric mode and then revert into diamond mode which the same with numerically deformed tubes. A total number of 4 and 5 folds were formed numerically and experimentally and the fold lengths were calculated as 4.12 mm and 2.83 mm respectively. Figure 5.5 shows the load displacement curves of experimentally and numerically compressed empty tubes together. The numerical load-displacement curve closely approximates the main characteristics of the experimental load-displacement curves of the empty tube: the load increases initially to a maximum peak load; thereafter, the load decreases to lower values and shows fluctuations as the tube progressively deforms until densification region. The average crushing loads were calculated 1.108 kN and 1.086 kN for experimentally and numerically deformed empty tubes, respectively. The SAE values calculated from simulation and experiment also show very good agreements as shown in Figure 5.6. The SAE values were found experimentally and numerically as 12.270 and 11.181 kJ/kg at the densification point respectively.

(a)

(b)

Figure 5.4. The deformed empty tubes at 0%, 20%, 40%, 60%, 80% strains (left to right); (a) simulation (b) experimental

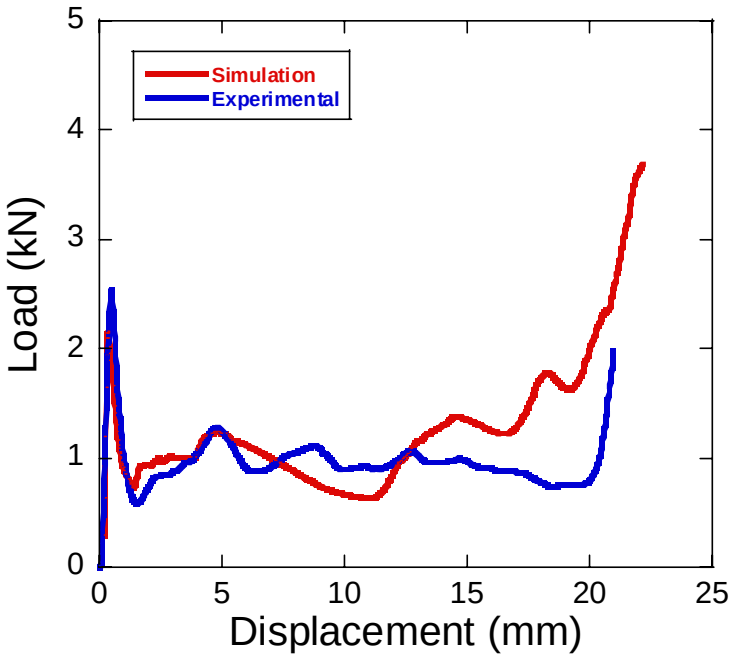

Figure 5.5. The experimental and numerical load displacement curve of empty tube

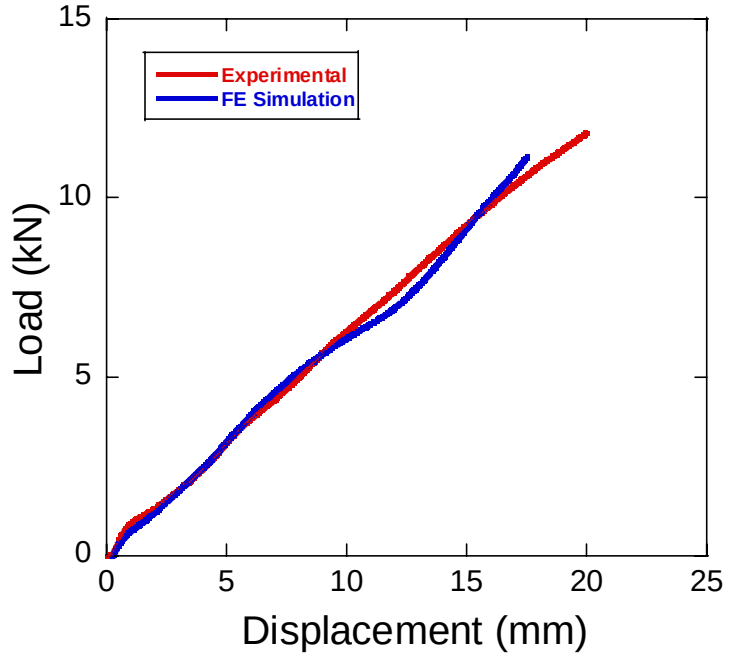

Figure 5.6. The experimental and numerical SAE curve of empty tube

Figure 5.7.a and 5.7.b show sequentially the numerical deformed pictures of single and double layer 6.4 mm cell size honeycomb samples. The deformation mechanism is similar in both sample types. The plastic buckling of cell walls followed by debonding and fracture at the cell interfaces.

The irregular folding of the honeycomb walls and local tears and separations are observed in the numerical simulation, similar to experimentally deformed honeycomb samples. The numerical load displacement and SAE curve of the honeycomb show good agreement with the experimental load-displacement and SAE curve as shown in Figure 5.8 and 5.9 respectively. The SAE values are calculated 11.301 and 12.826 for numerically and experimentally, respectively. The double layer honeycomb, which is originally consisted of two layers glued with an epoxy based bonding material, was simulated as single layer. The modeling of double layer sample will be considered in future.

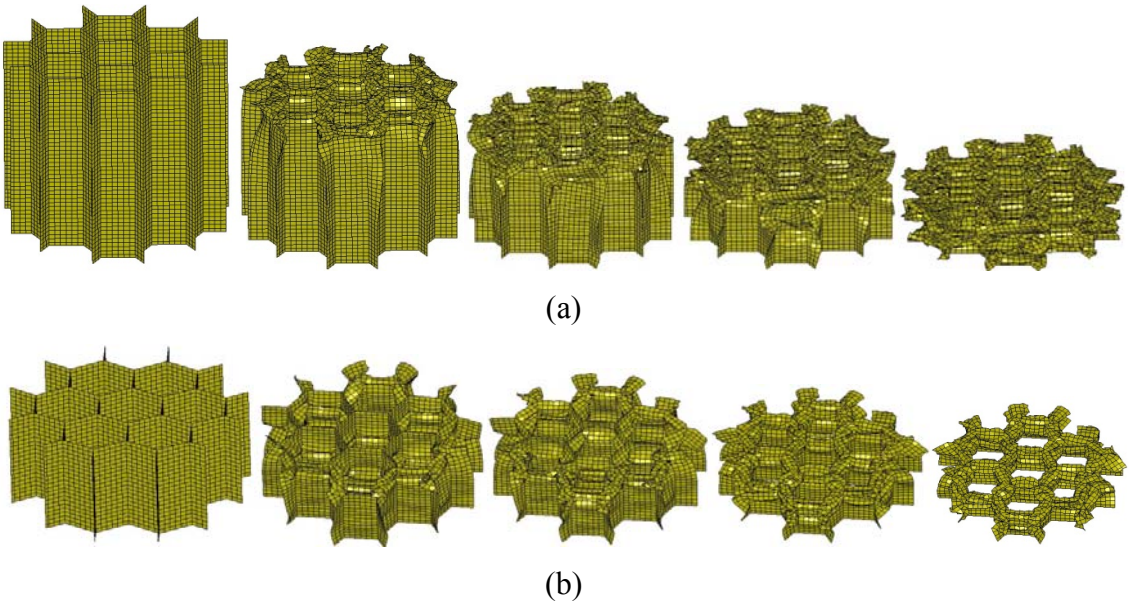

(a)

(b)

Figure 5.7. The numerical deformed of 6.4 mm honeycomb: (a) double layer and (b) single layer, at 0%, 20%, 40%, 60%, 80% strains (left to right)

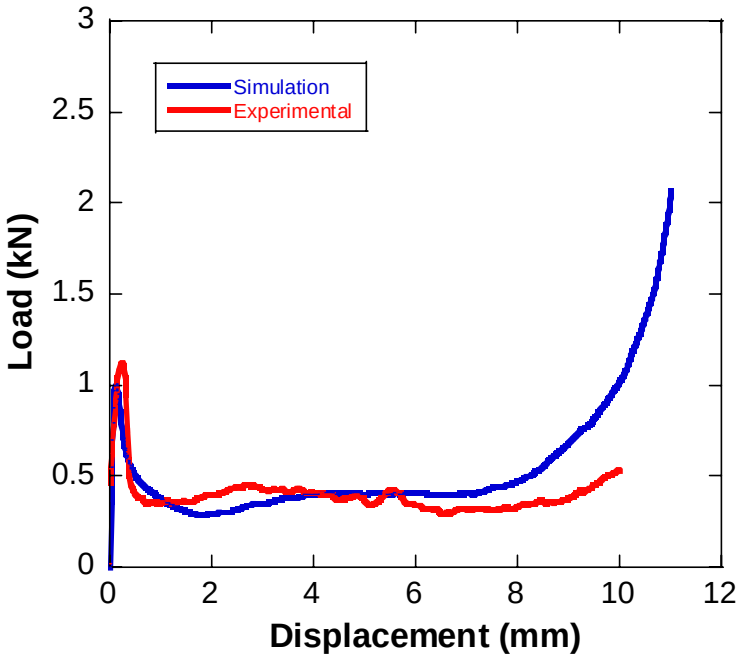

Figure 5.8. The numerical and experimental load-displacement curve of single layer 6.4 mm cell size honeycomb

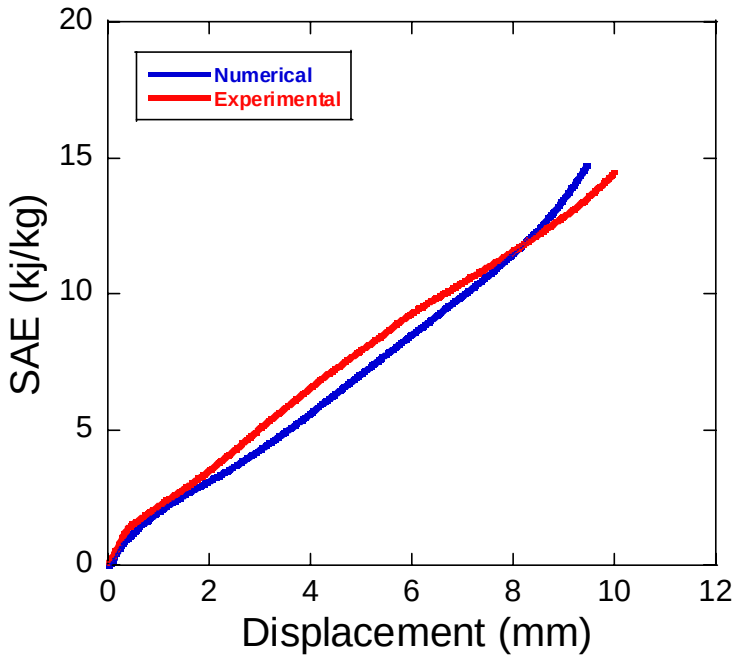

Figure 5.9 . The numerical and experimental SAE curve of single layer 6.4 mm cell size honeycomb

Figures 5.10.a and 5.10.b show sequentially the numerical and experimental deformed filled tubes at various strains, respectively. The numerical simulation shows the mixed mode of deformation of filled tube with progressive folding mechanism, which is also observed in the experiments. The numerical and the experimental load displacement curves (Figure 5.11), further show good agreements except the number of folds. Totally 5 folds formed experimentally and 4 folds formed in the simulation of the filled tubes. The fold length in the simulation is 3.72 mm and 2.95 mm in the experiment. The experimental and numerical average crushing loads are 1.678 kN and 1.723 kN, respectively. Furthermore, the numerical SAE values at the stroke efficiency show well agreements with those experiments (Figure 5.12). The SAE is 12.290 kJ/kg, in the experiment and 11.677 kJ/kg in the simulation. Figures 5.13.a and 5.13.b show the partially deformed 6.4 mm cell size honeycomb filled tubes, triggering the deformation at the glued sections (middle section) and at the free end of the tube, respectively. However, the numerical filler and the tube deformation are generally progressive and triggers from one of the ends of the filled tube (Figure 5.13.c).

As a summary and for easy comparison, the average crushing load, the maximum load, SAE, fold length and number of folds calculated both experimentally and numerically for empty tube, honeycomb and filled tube are listed altogether in Table 1. Despite the small variations generally the numerical model satisfactorily reaches the values of experimental found deformation parameters.

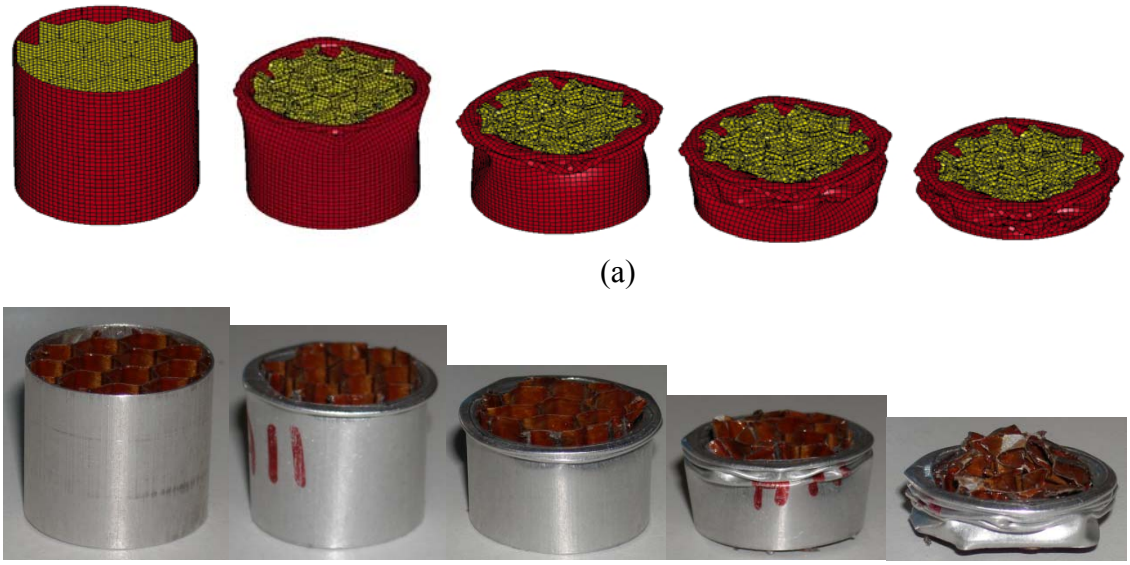

(a)

(b)

Figure 5.10. The deformed filled tubes (a) experimental and (b) numerical, strains 0%, 20%, 40%, 60%, 80%

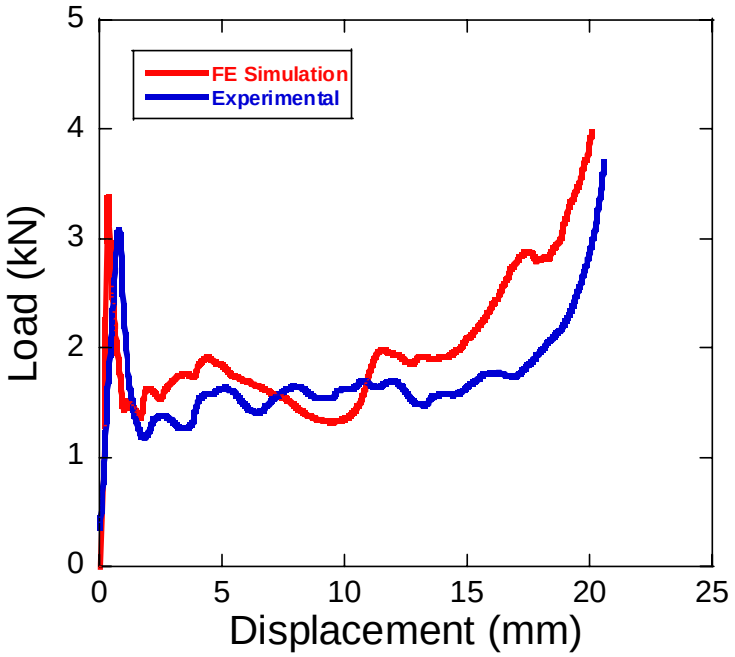

Figure 5.11. The experimental and numerical load displacement curve of 6.4 mm cell size honeycomb filled tube

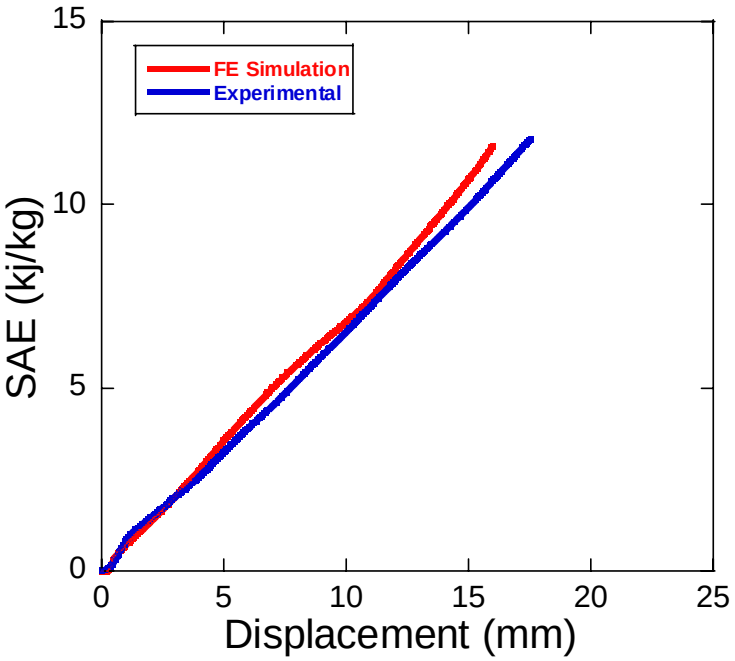

Figure 5.12. The experimental and numerical SAE curve of 6.4 mm cell size honeycomb filled tube

Figure 5.13. Deformed filled tubes, (a) trigger at the mid-section, (b) trigger from the end of the tube and (b) numerical deformation triggering from the tube end

Table 5.1 The experimental and the numerical deformation parameters of empty tube, filler and filled tube

	Pa (kN)	Pmax (kN)	SAE (kj/kg)	Hf (mm)	Number of folds
Empty Tube simulation	1.086	2.150	11.181	4.19	4
Empty Tube experimental	1.108	2.543	12.270	2.883	5
Honeycomb simulation	0.419	0.987	11.301	-	-
Honeycomb experimental	0.370	1.136	12.826	-	-
Filled tube simulation	1.723	4.934	11.677	3.724	4
Filled Tube experimental	1.678	3.673	12.291	2.953	5

5.4. The Effect of Honeycomb Cell Wall Thickness Variation

The experimental measurements show that the honeycomb cell wall thickness varies between 0.09-0.15 mm. In the numerical analysis in order to determine the effect of the honeycomb wall thickness on the crushing mechanism and the average crushing load the cell walls thickness changes as 0.09, 0.12 and 0.15 mm. In Figure 5.14.a the variation of the load-displacement curve with cell wall thicknesses of 6.4 mm cell size honeycomb filler is shown. The peak load and the average crushing load increase with the increasing cell wall thickness. In Figure 5.14.b the numerical load-displacement curves of the filler at various cell wall thicknesses is shown together with experimental load-displacement curve. This figure clearly shows that, 0.13 mm cell wall thickness load-displacement numerical curve nearly matches to the experimental load-displacement curve, when the peak-load and load values are considered. It is also noted that in Figure 5.14.b a small increase in the cell wall thickness results in significant increase in peak and higher average crushing loads values.

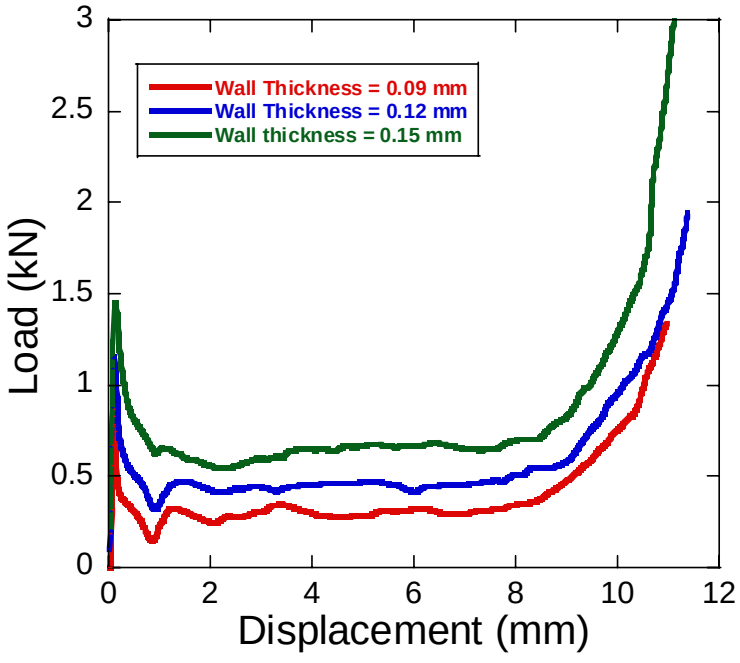

(a)

Figure 5.14. (a) Numerical load-displacement curves of 6.4 mm cell size honeycombs of varying cell thickness and (b) comparison with experimental load-displacement curve

(cont. on next page)

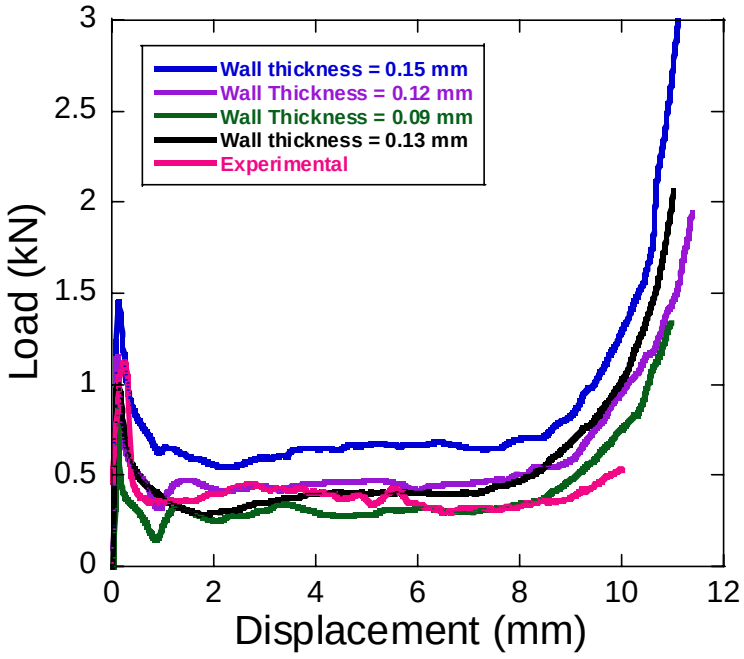

(b)

Figure 5.14. (cont.)(a) Numerical load-displacement curves of 6.4 mm cell size honeycombs of varying cell thickness and (b) comparison with experimental load-displacement curve

The effect of honeycomb cell wall thickness on the filled tubes is also very similar. The values of peak loads and the plateau load increases with increasing wall thickness (Figure 5.15.a). However, in filled tubes the experimental load-displacement curve shows best matches with both 0.13 and 0.12 mm honeycomb cell wall thicknesses as seen in Figure 5.15.b

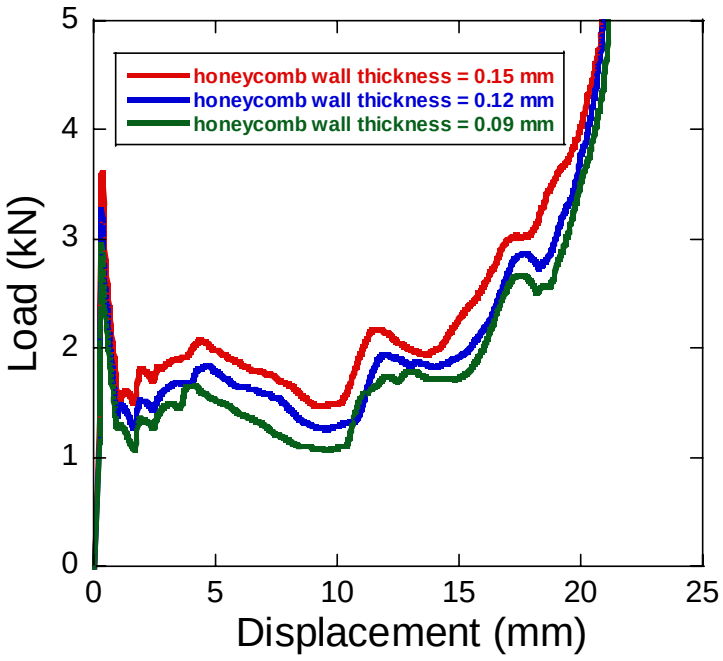

(a)

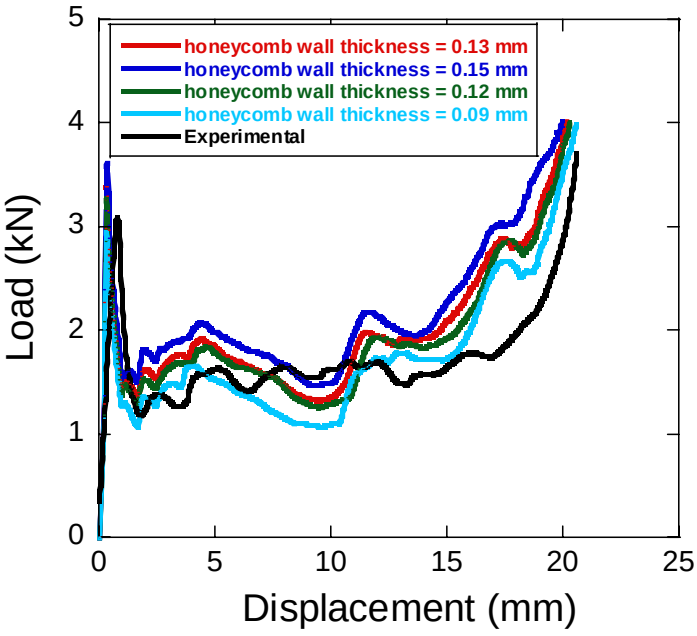

(b)

Figure 5.15. (a) the numerical load-displacement curves of 6.4 mm cell size honeycomb filled tubes of varying honeycomb cell wall thickness and (b) comparison with experimental load-displacement curve

CHAPTER 6

DISCUSSION

6.1. The Average Crushing Loads and Deformation Modes of the Empty Tubes

The average crushing loads of the empty tubes were analyzed for the diamond and concertina mode of deformation in Chapter 4. The results of the analysis are further given in Table 4.2. The empty tube was dominantly deformed in mixed mode of deformation and the analysis showed good correlations with the empirical equations of Abramowicz and Jones (1986), Pugsley et al. (1979), Wierzbicki (1988), and Guillow et al. (2001) developed for the concertina and diamond mode of deformation. The results also show that the experimental average crushing loads show significant differences from the equations of Singace (1996) and Alexander (1960). The difference between the average crushing loads of experiments and empirical equations given in Table 4.2 is in the range of 86-99 %. For diamond mode of deformation the difference is in the range between 51 and 99% and for concertina between 65 and 90%. In addition, the mixed mode of deformation of the empty tubes observed in this study shows a good agreement with the collapse mode of deformation chart of aluminum alloys constructed by Andrews et al. (1983) (Figure 2.4), when the L/D and t/D ratios of the tubes are considered.

The deformation rates show no significant effect on the deformation of the empty tubes. The mixed mode of deformation was observed as the dominant deformation mode in all strain rates used. This is mainly due to the strain rate insensitive mechanical response of aluminum and alloys. The observed variations in the deformation mode within the tube samples tested with the same testing parameters may be related to the existing non-uniformities in the tube samples such as variations in microstructure, tube thickness and surface conditions.

In the numerical analysis, the number of finite element mesh for a fixed geometry is known to lead to variations in the numerical results. The optimum finite element mesh number was determined by refining the mesh until convergence was

reached. The increasing number of elements in the finite element simulation resulted in better agreements with the experimental data.

However in order to keep a reasonable computational efficiency and cost, a compromise should be made. For tested tubes, the model was constructed using 40x80 elements for the highest computational efficiency.

6.2. The Average Crushing Loads and Deformation Modes of Honeycomb and Honeycomb Filled Tubes

When the honeycomb specimens are loaded quasi-statically, they exhibited a peak load, followed by a series of oscillatory crush loads with a nearly constant mean value (Chawla, et .al 2003). The quasi-static crush response of the Nomex® honeycomb also showed the same behavior. The deformation of the cells include the following mechanism: elastic buckling of cell walls followed by a plastic buckling, debonding and fracture at cell interfaces and fracture of the phenolic resin layer. These mechanisms were also previously observed (Aktay, et al. 2007). The resin type of the honeycomb is expected to influence the deformation mode of the honeycombs having the same cell size. This further affects the average crushing loads and the peak loads.

The cell size is one of the most important parameter effective on the load-displacement curves of honeycombs. In this thesis, it was shown both experimentally and numerically that reducing the cell size slightly without changing the density of the honeycomb gave higher crushing forces and a more stable deformation. These were also confirmed previously in a separate study on the effect cell size (Wu and Jiang 1996). 4.8 and 6.4 mm cell size honeycombs tested in accord with this and showed lower mean crushing loads and more non uniform folding mechanisms and brittle fractures at their cell walls. The crushing strengths and mean crushing loads of the honeycombs converged with the theoretical crushing strengths with 76, 98, 93% and the theoretical mean crushing loads with 96, 92 and 97% for 3.2, 4.8 and 6.4 mm cell size honeycombs respectively. In order to asses, the effect of the honeycomb cell wall thickness on the load-displacement curve, the honeycomb cell wall thicknesses of 0.09, 0.12, 0.13 and 0.15 mm were simulated. Since the compressive loads are mainly taken by the vertical edges of honeycombs, the increase cell wall thickness increased significantly both average crushing loads and peak loads.

The mesh size of the numerical simulation is known to be an important factor in computational efficiency. The increasing number of elements results in more approximate results with experimental data, but decreases the computational efficiency. Figures 6.1.a, 6.1.b and 6.1.c show the numerical analysis of 6.4 mm cell size honeycomb with different number of elements. The Nomex® honeycomb deformation mode is global collapse mode which can be observed in Figure 6.1.b. The reduction in element size as shown in Figure 6.1.b results in a change of deformation mode. In Figure 6.1.c the model with the double mesh number is shown and shows a progressive collapse mode which is not observed in experiments. This shows that increasing the number of elements doe not always give the best converging results with those of experiments. Therefore as stated earlier in another study (Aktay, et. Al 2007) the optimum number of meshes must be selected based on the experimental results.

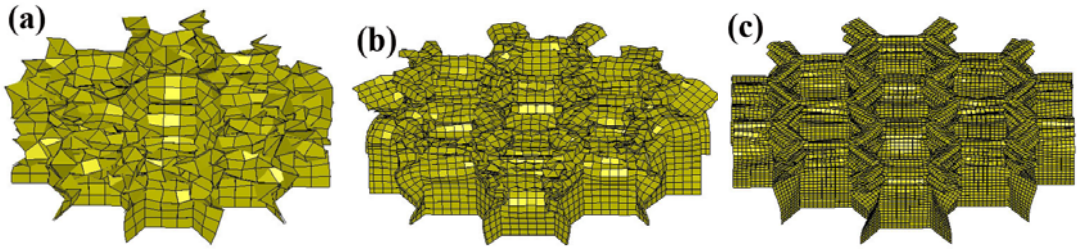

Figure 6.1. The effect of mesh size on the deformation of 6.4 mm cell size Nomex® honeycombs, (a)3x20 (b) 6x20 (c) 12x20 elements on each wall of honeycomb

Tube filling with Nomex® honeycomb resulted in increased peak and average crushing loads and SAE values as compared with empty tube. The lateral strength of honeycomb resists against inward penetration of the tube walls during the crash process, leading to an effect known as interaction effect. This effect is seen in simulations as shown in Figure 6.2. Due to interaction effect, the energy absorption capacity of the filled tubes increased and the tubes deformed in a more stable manner when compared with the empty tubes (Zarei and Kröger 2006). The cell sizes of the honeycomb also affect the specific absorbed energy. In this study, although 6.4 mm and 4.8 mm cell size honeycomb filling had no effect on the deformation mode of the empty tube (mixed/diamond), 3.2 mm cell size honeycomb filling changed the deformation mode

into mixed/concertina mode, showing clearly the effect of filling on the deformation mode of the filled tube.

Due to its progressive folding mechanism and symmetrical deformation, 3.2 mm cell size honeycomb showed the highest interaction effect in this study.

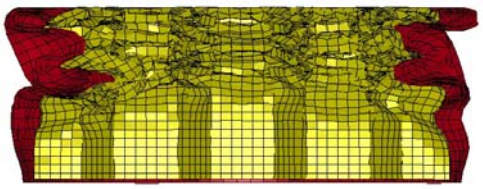

Figure 6.2. The simulation of interaction effect in 6.4 mm cell size honeycomb filled tube

6.3. The Strengthening Effect and Specific Absorbed Energy

The strengthening coefficient of the Nomex® honeycomb filling is determined as 1.53, 1.32 and 1.48 for 3.2, 4.8 and 6.4 mm cell size honeycomb fillings respectively and is given in Appendix C. The use of adhesive can contributed to the specific energy absorption of the tube by two mechanisms; increased load transfer from tube wall to the foam core and peeling of the adhesive. The double layer honeycombs (adding the adhesive effect) give higher strengthening coefficients for the filler honeycombs; 1.99, 1.54, 1.83 for the 3.2, 4.8 and 6.4 mm cell size honeycomb filled tubes respectively. The results may be compared with the previous works on foam filled tubes as 2.8 and 1.8 (Santosa, et al. 2000), 2 and 1.7 (H.Kavi, et al. 2006) for the bonded and unbounded foam fillers, respectively.

The specific energy absorption values of honeycomb filling are further compared with Al-closed cell foam (0.27, 0.35 and 0.42 g/cm^3) filled aluminum tubes (Aktay, et al. 2008). 3.2 mm cell size honeycomb filled aluminum tube was found to show higher SAE than Al-foam filled tubes at % 50 deformations. It also showed higher SAE than 0.27 g/cm^3 foam filling and similar SAE with 0.35 g/cm^3 foam filling at 80% deformation. These show the potentials of honeycomb filling of thin walled tubes in increasing SAE values. However, the strength of honeycomb is relatively low and the strengthening effect dictates honeycomb filling can solely be used in thin walled tubes having the crushing loads comparable with that of honeycomb.

CHAPTER 7

CONCLUSION

The quasi-static crushing behavior of three different cell size, 3.2, 4.8 and 6.4 mm, Nomex® honeycomb filled Al tubes was investigated through compression testing at quasi-static strain rates. The crushing behavior of empty tube and the fillers were also determined in order to asses the effect of filler on the crushing behavior of filled tubes. The deformation of empty tube, 6.4 mm cell size honeycomb filler and 6.4 mm cell size honeycomb filled tube were modeled in LSDYNA™ and ANSYS™. The followings are concluded

1. The experimental and numerical results showed that 6.4 mm and 4.8 mm cell size honeycomb filling had no effect on the deformation mode of empty tube (diamond/mixed), while 3.2 mm cell size honeycomb filling changed the tube deformation mode into mixed/concertina mode of deformation.

2. The honeycomb filling was shown, both experimentally and numerically, to increase crushing load, peak load and SAE values of filled tubes as compared with empty tubes.

3. The interaction effect was observed in all types of honeycomb filled tubes. 3.2 mm cell size honeycomb filling showed the highest average crushing load and SAE values. The strengthening coefficient was also the highest in 3.2 mm honeycomb filled tubes.

4. It was shown that 3.2 mm cell size honeycomb might be an alternative to aluminum foam as filler in tubes as long as the tube crushing load was comparable with honeycomb crushing load.

5. The modeling efforts gave similar deformation mode, crushing loads and SAE values with those of experiments. The modeling was also shown to be a tool to see the interaction between tube and filler.

REFERENCES

Abramowicz W. and N. Jones. 1984. Dynamic and axial crushing of circular tubes. *International Journal of Impact Engineering* 2: 263-281.

Abramowicz W. and N. Jones, 1986. Dynamic progressive buckling of circular and square tubes. *International Journal of Impact Engineering* 4: 243-269.

Aktay L, A.K Toksoy, M. Guden. 2005. Quasi-static axial crushing of extruded polystyrene foam filled thin walled aluminum tubes: Experimental and numerical analysis. *Materials and Design* 27 : 556-565.

Aktay L., A.F Johnson, B.H Kröplin.2007. Numerical modeling of honeycomb core crush behavior. *Engineering Fracture Mechanics* 75: 2616-2630.

Alexander J.M. 1960. An approximate analysis of the collapse of thin cylindrical shells under axial loading. *Quarterly Journal of Mechanics and Applied Mathematics* 13: 10-15.

Aminanda Y. , B Castaine , J-J. Barrou, P. Thevenet, 2005. Experimental Analysis and Modeling of the crushing of honeycomb cores. *Composite materials* 12: 213-227.

Andrews K.R.F , G.L.England, E.Ghani.1983. Classification of the axial collapse of cylindrical tubes under quasi-static loading. *International Journal of Mechanical Sciences* 25: 687-696.

Chawla A. , S. Mukherjee, D.Kumar, T. Nakatani, M. Ueno. 2003. In prediction of crushing behavior of honeycomb structure. *International Journal of Crash* 8: 229-235.

Foo C.C. , G.B Chai, L.K Seah.2007. Mechanical properties of Nomex material and Nomex honeycomb structure. *Composite Stuructures*, 80: 588-594.

Guillow S.R. , G.Lu, R.H. Grzebieta.2001. Quasi-static axial compression of thin walled circular aluminum tubes. *Internationa Journal of Mechanical Sciences* 43: 2103-2123.

Guillow S.R, G. Lu, R.H Grebieta,.2001. Quasi static axial compression of thin walled circular aluminum tubes. *International Journal of Mechanical Sciences* 43: 2103-2123.

Gupta N.K and H. Abbas. 2001. Some considerations in axisymmetric folding of metallic round tubes. *International Journal of Impact Engineering* 25: 331-344.

Hanssen A.G, M. Langseth, O.S Hopperstod,2000. Static crushing of square aluminum extrusions with aluminum foam filler. *International Journal of Impact Engineering* 24: 509-534.

Jones N. and W. Abramowicz. 1985. Static and dynamic axial crushing of circular and square tubes. *Metal Forming and Impact Mechanics* 10: 225-247.

Kavi H, A.K Toksoy, M. Guden. 2006. Predicting energy absorbtion in a foam filled thin walled aluminum tube based on experimentally determined strengthening coefficient. *Materials and Design* 27: 263-269.

LS-DYNA^{TM}. 2003. Keyword User's manual, Livermore Software Technology Corparation. Version 970.

LS-DYNA^{TM}.2003. Theoretical Manual, Livermore Software Technology Corparation. Version 970.

Pugsley A.G and M. Macaulay.1979. The large scale crumpling of thin cylindrical columns. *Quarterly Journal of Mechanics and Applied Mathematics* 13: 1-9.

Pugsley A.G.1983. On the crumpling of thin tubular structures. *Quarterly Journal of Mechanics and Applied Mathematics* 19: 845-856.

Santosa S and T.Wierzbicki.1998. Crash behavior of box columns filled with aluminum honeycomb or foam. *Composite Structures* 68: 343-367.

Santosa S , T.Wierzbicki, A.G Hanssen, M. Langseth, 2000. Experimental and numerical studies of foam filled sections. *International Journal of Impact Engineering* 24: 509-534.

Santosa S, T.Wierzbicki, A.G.Hanssen, M.Langseth,2000. Experimental and numerical studies of foam filled sections. *International Journal of Impact Engineering* 24: 509-534.

Seitzberger M, F.G.Rammerstorfer, H.P.Degischer. 1997. Crushing of axially compressed steel tubes filled with aluminum foam. *Acta Mechanica*, 125: 93-105.

Singace A.A. and H.El Sobky. 1995. On the eccentricity factor in the progressive crushing of tubes. *International Journal of Solid Structures* 32: 3589-3602.

Singace A.A. and H.El Sobky. 1996. Further experimental investigation on the eccentricity factor in the progressive crushing of tubes. *International Journal of Solid Structures* 33: 3517-3538.

Singace A.A. and H.El. Sobky.1997. Behavior of axially crushed corrugated tubes. *International Journey of Mechanical Sciences* 39: 249-268.

Singace A.A and H.El Sobky. 2001.Uniaxial crushing of constrained tubes. *Proc Instn Mech Engnrs* 215: Part C.

Tasdemirci A. 2008. The effect of tube and constraining on the axial crush behavior of aluminum tubes. *Materials and Design*, In Press.

Toksoy A.K and M. Guden.2005. The strengthening effect of polystyrene foam filling in aluminum thin-walled cylindrical tubes. *Thin walled structures* 43: 333-350.

Wierzbicki T. and W.Abramowicz.1983. Axial crushing of multicorner sheet metal columns. *Journal of Applied Mechanics* 50: 727-734.

Zarei H. and M. Kröger, 2008. Optimum honeycomb filled crash absorber design. *Materials and Design* 29: 193-204.

.

APPENDIX A

Mean Crushing Force and Strength of Honeycombs

t = 0.1 mm

σ_0 = 105 MPa

$$P_{m,3.2} = 7.17x105MPa(0.1mm)^{\frac{5}{3}}(3.2mm)^{\frac{1}{3}} = 0.0239(kN/cell)$$

$$P_{m,3.2} = 0.0239kN \times 30 = 0.717kN$$

$$\sigma_{h3.2} = 16.55 \times 105MPa(0.1mm/3.2mm)^{5/3} = 5.38MPa$$

$$P_{m,4.8} = 7.17 \times 105MPa \times (0.1mm)^{\frac{5}{3}} \times (4.8mm)^{\frac{1}{3}} = 0.0273(kN/cell)$$

$$P_{m,4.8} = 0.0273(kN)20 = 0.546kN$$

$$\sigma_{h4.8} = 16.55x105MPa(0.1mm/4.8mm)^{5/3} = 2.7MPa$$

$$P_{m,6.4} = 7.17x105MPa \times (0.1mm)^{\frac{5}{3}}(6.4mm)^{\frac{1}{3}} = 0.0301(kN/cell)$$

$$P_{m,6.4}0.0301(kN)12 = 0.362kN$$

$$\sigma_{h6.4} = 16.55x105MPa(0.1mm/6.4mm)^{5/3} = 1.69MPa$$

APPENDIX B

The Mean Crushing Forces of Empty Tubes

Alexander's approach

Concertina Mode

$$P_a = 6\sigma_0 t(Dt)^{1/2} \tag{2.8}$$

$$P_a = 6\sigma_0 t(Dt)^{1/2}$$

$$P_a = 6 \times 155MPa \times 0.29mm \times (25mm \times 0.29mm)^{1/2}$$

$$P_a = 0.726kN$$

Abramowicz and Jones approach

Concertina Mode

$$P_a = \frac{\sigma_0 \sqrt{Dt} + 3.44t}{0.86 - 0.568\sqrt{t/D}} \tag{2.10}$$

$$P_a = \frac{155MPa\sqrt{25mm \times 0.29mm} + 3.44 \times 0.29mm}{0.86 - 0.568\sqrt{0.29mm/25mm}}$$

$$P_a = 1.008kN$$

Diamond Mode

$$P_a = 86.14(D/t)^{0.33}\sigma_0(t^2/4) \tag{2.11}$$

$$P_a = 86.14 \times (25mm/0.29mm)^{0.33} \times 155MPa \times (0.29mm^2/4)$$

$$P_a = 1.286kN$$

Concertina Mode

$$P_a = \sigma_0 t(6(Dt)^{1/2} + 3.44t) \tag{2.12}$$

$$P_a = 155MPa \times 0.29mm \times (6(25mm \times 0.29mm)^{0.5} + 3.44 \times 0.29mm)$$

$$P_a = 0.804kN$$

Singlace and Elbosky's Approach

Concertina Mode

$$P_a = (\sigma_0 t^2/2\sqrt{3}) \times (22.27 \times \sqrt{D/t} + 5.632) \tag{2.13}$$

$$P_a = (155MPa \times (0.29mm)^2/2\sqrt{3}) \times (22.27 \times \sqrt{25mm/0.29mm} + 5.632)$$

$$P_a = 0.833kN$$

Diamond Mode

The average crushing force ;

$$P_a = \sigma_0 t^2 (7.874(R/t)^{1/2} + 1.408) \quad (2.14)$$

$$P_a = 155MPa \times (0.29mm)^2 \times (7.874 \times (12.5mm/0.29mm)^{0.5} + 1.408)$$

$$P_a = 0.725kN$$

Pugsley and Macaulay's Approach

Diamond Mode

$$P_a = \sigma_0 t(10.05t + 0.38D) \quad (2.16)$$

$$P_a = 155MPa \times 0.29mm \times (10.05 \times 0.29mm + 0.38 \times 25mm)$$

$$P_a = 0.573kN$$

Pugsley's Approach

Diamond Mode

$$P_a = 2.28n^2 \sigma_0 t^2 \quad (2.17)$$

Where the n is the number of diamond folds formed during deformation.

$$P_a = 2.286 \times (6)^2 \times 155MPa \times (0.29mm)^2$$

$$P_a = 1.148kN$$

Wierzbicki's approach

Diamond Mode

$$P_a = 18.15\sigma_0 t^2 (D/t)^{1/3} \tag{2.18}$$

$$P_a = 18.15 \times 155MPa \times (0.29mm)^2 \times (25mm/0.29mm)^{0.33}$$

$$P_a = 1.098kN$$

Concertina Mode

$$P_a = 11.22\sigma_0 t^2 (R/t)^{1/2} \tag{2.19}$$

$$P_a = 11.22 \times 155MPa \times (0.29mm)^2 \times (12.5mm/0.29mm)^{0.5}$$

$$P_a = 1.006kN$$

Concertina Mode

$$P_a = 7.933\sigma_0 t^2 (D/t)^{1/2} \tag{2.20}$$

$$P_a = 7.933 \times 155MPa \times (0.29mm)^2 \times (25mm/0.29mm)^{0.5}$$

$$P_a = 1.007kN$$

Guillow's Approach

The average crushing force ;

$$P_a = \sigma_0 (t^2 / 4) \times 72.3 (D/t)^{0.32} \qquad (2.21)$$

$$P_a = 155MPa(0.29mm^2 / 4) \times 72.3(25mm / 0.29mm)^{0.32}$$

$$P_a = 1.033kN$$

APPENDIX C

The Mean Crushing Force of Nomex Honeycomb Filled Tubes

$$P_{nh} = P_{ae} + C \times P_m \tag{2.23}$$

3.2 mm cell-sized Nomex honeycomb Filled Tube

$P_{nh,3.2} = 1.108kN + C \times 0.692kN$

$2.168kN = 1.108kN + C \times 0.692kN$

$C = 1.53$

Double layer:

$2.168\text{kN} = 1.108\text{kN} + \text{C} \times 0.532\text{kN}$

C=1.99

4.8 mm cell-sized Nomex honeycomb Filled Tube

$P_{nh,4.8} = 1.108kN + C \times 0.503kN$

$1.768kN = 1.108kN + C \times 0.503kN$

$C = 1.32$

Double layer:

$1.768\text{kN} = 1.108\text{kN} + \text{C} \times 0.428\text{kN}$

C=1.54

6.4 mm cell-sized Nomex honeycomb Filled Tube

$P_{nh,6.4} = 1.108kN + C \times 0.37kN$

$1.657kN = 1.108kN + C \times 0.37kN$

$C = 1.48$

Double layer:

$1.657\text{kN} = 1.108\text{kN} + \text{C} \times 0.3\text{kN}$

C=1.83

APPENDIX D

Result Tables

APPENDIX D

Result Tables

Specimen Type	*Specimen Number*	*Strain rate (s^{-1})*	*P_{max} (kN)*	*Pa (kN)*	*SE*	*SAE (%50) [kj/kg]*	*SAE At SE [kj/kg]*	*Specimen weight (g)*	*TE*	*Dc*
6.4 mm cell size	1	$1.64x10^{-2}$	3.0012	1.6321	0.757	6.938	13.012	2.352	0.850	0.748
6.4 mm cell size	2	$1.64x10^{-2}$	3.2608	1.9526	0.688	6.631	11.847	2.372	0.546	0.688
6.4 mm cell size	14	$1.64x10^{-2}$	3.5807	1.6433	0.698	6.185	10.869	2.503	0.689	0.708
6.4 mm cell size	17	$1.64x10^{-2}$	3.7391	1.6774	0.738	6.582	12.391	2.371	0.559	0.590
6.4 mm cell size	19	$1.64x10^{-2}$	3.9316	1.6780	0.787	6.672	13.245	2.328	0.691	0.826
6.4 mm cell size	4*	$1.64x10^{-2}$	3.2391	1.5180	-	3.470	-	2.374	-	-
6.4 mm cell size	5*	$1.64x10^{-2}$	3.7204	1.5405	-	3.337	-	2.345	-	-
6.4 mm cell size	6*	$1.64x10^{-2}$	3.7981	1.5072	-	3.410	-	2.381	-	-
6.4 mm cell size	21*	$1.64x10^{-2}$	4.1055	1.5558	-	3.488	-	2.489	-	-

Specimen Type	*Specimen Number*	*Strain rate (s^{-1})*	*P_{max} (kN)*	*Pa (kN)*	*SE*	*SAE (%50) [kj/kg]*	*SAE At SE [kj/kg]*	*Specimen weight (g)*	*TE*	*Dc*
6.4 mm cell size	7	$6.56x10^{-3}$	3.5031	1.7501	0.721	7.786	13.866	2.300	0.713	0.708
6.4 mm cell size	22	$6.56x10^{-3}$	3.3260	1.5406	0.787	6.630	13.322	2.285	0.788	0.787
6.4 mm cell size	9	$3.28x10^{-3}$	3.4720	1.4826	0.636	6.253	9.677	2.378	0.667	0.728
6.4 mm cell size	20	$3.28x10^{-3}$	4.0496	1.5734	0.711	7.300	11.614	2.380	0.806	0.688

Specimen Type	*Specimen Number*	*Strain rate (s^{-1})*	*P_{max} (kN)*	*Pa (kN)*	*SE*	*SAE (%50) [kj/kg]*	*SAE At SE [kj/kg]*	*Specimen weight (g)*	*TE*	*Dc*
4.8 mm cell size	4	$1.64x10^{-2}$	3.8291	1.6382	0.776	7.564	14.099	2.258	0.795	0.767
4.8 mm cell size	17	$1.64x10^{-2}$	3.9378	1.7346	0.718	6.376	11.645	2.508	0.632	0.629
4.8 mm cell size	18	$1.64x10^{-2}$	3.0993	1.7783	0.711	6.401	11.459	2.590	0.630	0.752
4.8 mm cell size	24	$1.64x10^{-2}$	3.7267	1.5261	0.701	6.364	12.571	2.439	0.744	0.708
4.8 mm cell size	23	$1.64x10^{-2}$	4.0062	2.1334	0.770	7.427	14.099	2.459	0.854	0.826
4.8 mm cell size	2*	$1.64x10^{-2}$	4.3664	1.5565	-	3.491	-	2.407	-	-
4.8 mm cell size	6*	$1.64x10^{-2}$	3.9223	1.9364	-	3.788	-	2.617	-	-
4.8 mm cell size	11*	$1.64x10^{-2}$	4.3291	1.6935	-	3.837	-	2.512	-	-
4.8 mm cell size	22*	$1.64x10^{-2}$	3.8136	1.4771	-	3.238	-	2.312	-	-

Specimen Type	*Specimen Number*	*Strain rate (s^{-1})*	*P_{max} (kN)*	*Pa (kN)*	*SE*	*SAE (%50) [kj/kg]*	*SAE At SE [kj/kg]*	*Specimen weight (g)*	*TE*	*Dc*
4.8 mm cell size	16	$6.56x10^{-3}$	4.1428	2.0698	0.708	7.858	13.866	2.595	0.657	0.669
4.8 mm cell size	8	$6.56x10^{-3}$	3.5652	1.6060	0.754	6.011	12.453	2.390	0.622	0.757
4.8 mm cell size	10	$3.28x10^{-3}$	3.1014	1.6576	0.708	6.678	12.267	2.368	0.725	0.718
4.8 mm cell size	15	$3.28x10^{-3}$	4.4596	2.0251	0.728	6.249	13.198	2.841	0.640	0.734

Specimen Type	*Specimen Number*	*Strain rate (s^{-1})*	*P_{max} (kN)*	*Pa (kN)*	*SE*	*SAE (%50) [kj/kg]*	*SAE At SE [kj/kg]*	*Specimen weight (g)*	*TE*	*Dc*
3.2 mm cell size	3	$1.64x10^{-2}$	4.0310	2.4767	0.751	7.951	14.907	2.654	0.716	0.761
3.2 mm cell size	4	$1.64x10^{-2}$	3.4347	1.9903	0.731	8.183	15.035	2.354	0.768	0.748
3.2 mm cell size	11	$1.64x10^{-2}$	4.3983	2.1367	0.748	7.743	14.720	2.596	0.740	0.764
3.2 mm cell size	22	$1.64x10^{-2}$	3.7049	1.6531	0.774	6.790	14.201	2.429	0.790	0.787
3.2 mm cell size	16	$1.64x10^{-2}$	3.4316	2.0737	0.783	7.275	14.633	2.383	0.778	0.787
3.2 mm cell size	5*	$1.64x10^{-2}$	3.5093	1.5405	-	3.598	-	2.483	-	-
3.2 mm cell size	7*	$1.64x10^{-2}$	4.0496	1.8489	-	3.812	-	2.492	-	-
3.2 mm cell size	8*	$1.64x10^{-2}$	4.3664	2.2250	-	4.335	-	2.632	-	-
3.2 mm cell size	17*	$1.64x10^{-2}$	3.7981	1.5248	-	3.525	-	2.380	-	-

Specimen Type	*Specimen Number*	*Strain rate (s^{-1})*	*P_{max} (kN)*	*Pa (kN)*	*SE*	*SAE (%50) [kj/kg]*	*SAE At SE [kj/kg]*	*Specimen weight (g)*	*TE*	*Dc*
3.2 mm cell size	19	$6.56x10^{-3}$	3.7142	2.0796	0.780	7.610	15.885	2.513	0.593	0.741
3.2 mm cell size	16	$6.56x10^{-3}$	2.9751	1.5403	0.748	6.554	11.863	2.383	0.722	0.754
3.2 mm cell size	15	$3.28x10^{-3}$	3.2639	1.7352	0.780	7.052	14.177	2.402	0762	0.793
3.2 mm cell size	21	$3.28x10^{-3}$	3.8291	1.8086	0.770	7.639	14.565	2.403	0.806	0.777

Specimen Type	*Specimen Number*	*Strain rate (s^{-1})*	*P_{max} (kN)*	*Pa (kN)*	*SE*	*SAE (%50) [kj/kg]*	*SAE At SE [kj/kg]*	*Specimen weight (g)*	*TE*	*Dc*
Empty Tube	1	$1.64x10^{-2}$	2.245	1.2306	0.721	7.490	12.484	1.576	0.573	0.787
Empty Tube	2	$1.64x10^{-2}$	2.692	1.0202	0.767	6.438	11.217	1.640	0.577	0.783
Empty Tube	3	$1.64x10^{-2}$	3.316	1.2706	0.741	7.238	12.422	1.625	0.521	0.820
Empty Tube	4	$1.64x10^{-2}$	3.149	1.0775	0.787	7.425	13.711	1.616	0.545	0.797
Empty Tube	5	$1.64x10^{-2}$	3.027	1.0913	0.777	7.437	12.888	1.636	0.672	0.790
Empty Tube	6	$1.64x10^{-2}$	3.127	0.9680	0.721	6.997	12.080	1.635	0.648	0.728
Empty Tube	7	$1.64x10^{-2}$	2.322	0.5215	0.721	6.696	11.018	1.628	0.526	0.741
Empty Tube	8	$1.64x10^{-2}$	2.968	1.1001	0.767	6.554	12.391	1.640	0.553	0.774

Specimen Type	*Specimen Number*	*Strain rate (s^{-1})*	*P_{max} (kN)*	*Pa (kN)*	*SE*	*SAE (%50) [kj/kg]*	*SAE At SE [kj/kg]*	*Specimen weight (g)*	*TE*	*Dc*
Empty Tube	9	$6.56x10^{-3}$	2.565	0.847	0.761	6.260	10.347	1.614	0.530	0.800
Empty Tube	10	$6.56x10^{-3}$	2.510	0.826	0.787	5.695	10.173	1.622	0.529	0.793
Empty Tube	11	$6.56x10^{-3}$	2.239	0.822	0.741	5.562	9.347	1.644	0.667	0.744
Empty Tube	12	$6.56x10^{-3}$	3.189	0.928	0.783	6.235	11.515	1.574	0.691	0.783
Empty Tube	13	$6.56x10^{-3}$	1.852	0.812	0.761	5.037	8.546	1.616	0.638	0.761
Empty Tube	14	$3.28x10^{-3}$	3.164	0.866	0.833	5.992	10.913	1.689	0.673	0.839
Empty Tube	15	$3.28x10^{-3}$	2.350	0.860	0.705	5.851	9.391	1.621	0.665	0.711